Emplacement of sharp-walled sulphide veins during reactivation of impact-related structures at the Broken Hammer Mine, Sudbury, Ontario

by

Marshall Francis Hall

A thesis submitted in partial fulfillment
of the requirements for the degree of
Master of Science (MSc) in Geology

The Faculty of Graduate Studies,
Laurentian University
Sudbury, Ontario, Canada

THESIS DEFENCE COMMITTEE/COMITÉ DE SOUTENANCE DE THÈSE
Laurentian Université/Université Laurentienne
Faculty of Graduate Studies/Faculté des études supérieures

Title of Thesis Titre de la thèse	Emplacement of sharp-walled sulphide veins during reactivation of impact-related structures at the Broken Hammer Mine, Sudbury, Ontario
Name of Candidate Nom du candidat	Hall, Marshall Francis
Degree Diplôme	Master of Science
Department/Program Département/Programme	Geology
Date of Defence Date de la soutenance	August 26, 2019

APPROVED/APPROUVÉ

Thesis Examiners/Examinateurs de thèse:

Dr. Bruno Lafrance
(Supervisor/Co-directeur de thèse)

Dr. Harold Gibson
(Co-Supervisor/Co-directeur de thèse)

Dr. Attila Pentek
(Committee member/Membre du comité)

Mr. Michael Sweeny
(External Examiner/Examinateur externe)

Approved for the Faculty of Graduate Studies
Approuvé pour la Faculté des études supérieures
Dr. David Lesbarrères
Monsieur David Lesbarrères
Dean, Faculty of Graduate Studies
Doyen, Faculté des études supérieures

ACCESSIBILITY CLAUSE AND PERMISSION TO USE

Abstract

Broken Hammer is a hybrid, Cu-Ni-Platinum Group Element (PGE) footwall deposit in the North Range of the ca. 1.85 Ga Sudbury impact structure. The sulphide vein system and associated low sulphide PGE mineralization were mined as an open pit operation over a 15-month period, providing a unique opportunity to study a complete 90-meter vertical section across a footwall deposit. The deposit is hosted within Archean basement rocks and impact-induced Sudbury breccia, 1.5 km north of the Sudbury Igneous Complex (SIC) – basement contact. The low sulphide mineralization consists of disseminated to blebby chalcopyrite (<5%), minor pyrite, chalcocite, galena, sphalerite and platinum group minerals, associated with Ni-bearing chlorite overprinting alteration patches of epidote, actinolite and quartz. The veins comprise massive chalcopyrite and minor magnetite, chalcocite, millerite, and rare sperrylite, surrounded by thin epidote, actinolite and quartz selvedges. They are grouped into five, steeply-dipping, NE-, SW-, SE-, S- and EW-striking sets, which intersect in a common line controlling the plunge (60°) and trend (220°) of ore shoots. The veins were emplaced along syn-impact fractures that were reactivated multiple times during stabilization of the impact crater floor. Early reactivation of the fractures created pathways for the migration of hydrothermal fluids from which quartz and chlorite precipitated sealing the fractures. Renewed slip and reactivation shattered the quartz-chlorite veins into fragments that were incorporated in massive sulphide veins that crystallized from strongly fractionated sulphide melts or high temperature (400°C-500°C) hydrothermal fluids which migrated outward into the basement rocks from a cooling and crystallizing impact melt sheet represented by the SIC. Hydrothermal fluids syn-genetic with the epidote-actinolite-quartz alteration distributed the PGE into the footwall rocks, or late hydrothermal fluids associated with the Ni-bearing chlorite leached Ni and PGM's from the sulphide veins and re-distributed them within the footwall rocks, forming

the low-sulphide high-PGE mineralization. During post-impact tectonic events, reactivation and slip at temperatures below the brittle-ductile transition for chalcopyrite (<200°C-250°C) produced striations along the vein margins. The Broken Hammer deposit exemplifies how Cu-Ni-PGE footwall deposits formed by the reactivation of syn-impact fractures that provided conduits for the migration of melts and hydrothermal fluids.

Keywords
Sudbury footwall deposit, Broken Hammer, impact cratering, crater modification, crater floor fractures, reactivated syn-impact fractures, Cu-Ni-PGE deposits

Co-Authorship Statement

The thesis is written as a multi-authored scientific paper for submission to a peer-reviewed scientific journal. The candidate is the first author on the paper. The project was originally conceived by Joshua Bailey and Dr. Attila Pentek of Wallbridge Mining and further defined by Dr. Bruno Lafrance, Dr. Harold Gibson and the candidate. The field work, that is, mapping of the mine walls and benches, was carried out by the candidate from July 2014 to October 2015. Samples were collected by the candidate and submitted to a commercial lab (ALS Labs) for crushing and analysis. Willard Desjardin, technologist at the Harquail School of Earth Sciences, did the thin sections used in this thesis from cut pucks provided by the candidate. 3D digital modelling of the Broken Hammer deposit was done by the candidate in consultation with Wallbridge geologists Eilidh Lewis and Dr. Attila Pentek. Drs. Bruno Lafrance and Harold Gibson supervised the project and edited and co-authored the paper but the candidate is responsible for all the data and interpretation presented in the thesis and paper.

Acknowledgements

I would like to start by thanking my advisors Dr. Bruno Lafrance and Dr. Harold Gibson. Without their continued support this thesis would never have seen completion. I thank you for all of the encouragement, guidance and positivity you provided me with and for reading a seemingly endless barrage of thesis drafts. I could not have asked for a better supervisory team and words can never properly express my gratitude.

I would like to thank Mr. Joshua Bailey who helped seed the conception of this project and has been a mentor for many years. I would also like to thank Dr. Attila Pentek who was the other half behind developing the concept of the project and has also been a monumental support and mentor.

Thank you to Marz Kord and Alar Soever, without whom there would have been no funding and no project. I am forever thankful for everything you two provided me with and for all aspects of Wallbridge's support.

I cannot forget the rest of the Wallbridge team. You have all been a great support of me in both this project and my development as a professional over many, many years. Dave Smith and Shannon Baird I could not have gotten to where I am without your training and mentorship. So many of the mapping techniques I implemented in this thesis I know because of you. Natalie MacClean, you are a logistical wizard and so many things would never have come to fruition without your ingenuity, resourcefulness and planning. Peter Andersen your technical support and endless positivity were always welcomed and appreciated.

Thank you to all of my fellow graduate students as well. You guys made the experience so enjoyable and helped me through so many discussions. Evan Hastie and Zsuzsanna Tóth, you two will always be inspirations and I thank you for all the support you leant me through the duration of this thesis. Thomas Ogilvy and Chris Kelly, I will always remember the late nights on the 5th floor of the Willet we helped keep each other on track. There are so many people who have helped support me through this experience and if I was to list them all this section would never end. So, thank you to everyone in the student body of the Laurentian Department of Earth Sciences.

There are two lovely ladies whom I also cannot forget. Roxanne Mehes and Edda Bozzato, you two are so kind, helpful, and welcoming. Every student within the department is lucky to have you two as part of their support system.

Thank you to my wonderful girlfriend Cory Kozmik. I would not be here today and this thesis truly would not be where it is if it weren't for you. I thank you for all your support and understanding. There were many late nights and without your steadfast resolve keeping me on track I don't know what I would have done. You are truly amazing and no master of the English language could string words together to tell you how grateful I am for your support.

Last but certainly not least, I would like to thank my parents. Dad if it weren't for you introducing me to rocks at such a young age and having me trapes through the woods with you I don't know if I ever

would have found this profession. Mom you are the best candidate for sainthood I can imagine. You were there through everything and can't thank you enough.

Thank you to all of you, I truly could not have done this without each and everyone of you. Words will never express my gratitude.

Contents

List of Figures

Chapter 1 – Introduction to Thesis

1.1 Introduction

Footwall deposits of the Sudbury impact structure are enriched in Copper-Nickel-Platinum Group Elements (Cu-Ni-PGE) and as such have become prime exploration targets of mineral exploration companies operating in the Sudbury mining camp. The deposits are composed of chalcopyrite with minor pyrrhotite, pentlandite and chalcocite (Ames et al, 2007). They occur as massive, sharp-walled, Cu-Ni- PGE veins, and as low sulphide PGE mineralized zones. The veins are dominated by chalcopyrite (>90%) and are up to 10's of meters in width and hundreds of meters in length. The low sulphide zones are characterized by less than 5% chalcopyrite as disseminations and stringers containing valuable platinum group minerals (PGM) (Ames et al., 2007).

The formation of these deposits is linked to that of Ni-enriched contact deposits along the contact between the ca. 1850 Ma Sudbury Igneous Complex (SIC), representing an impact melt sheet (Grieve et al., 1991; Mungall et al., 2004), and underlying Archean and Paleoproterozoic basement rocks (Li and Naldrett, 1993). Crystallization of contact deposits may have produced Cu-PGE-rich residual sulphide melts which could have then been injected into fractures within basement rocks to form sharp-walled sulphide veins (Li and Naldrett, 1993; Jago et al., 1994; Morrison et al., 1994). In addition, magmatic-hydrothermal fluids derived from partial melting of the footwall rocks, or exsolved from the cooling SIC, may have leached Cu and PGE from the contact deposits and redeposited these metals into footwall fractures to form sharp-walled sulphide veins (Farrow, 1994; Watkinson 1999; Molnar et al., 2001; Farrow et al., 2005; Hanley et al., 2005; Pentek et al., 2008). The low sulphide PGE(-Cu-Ni) mineralized zones are thought to have formed either from water-free, halogen-PGE rich fluids that were released during the crystallization of the

veins and that mixed with groundwater (Jago et al., 1994), or from magmatic-hydrothermal fluids which brought the metals from the contact environment or leached them out locally from pre-existing sharp-walled veins (Li and Naldrett, 1993; Jago et al., 1994; Morrison et al., 1994; Hanley et al., 2005; 2011; Tuba et al., 2010, 2014).

Notwithstanding the uncertainty on their origin, the sharp-walled sulphide veins occupy fractures and faults that either represent: (1) pre-impact structures that were reactivated during the impact, (2) syn-impact structures that formed during the propagation of shock waves and collapse of the impact crater, or (3) post-impact structures that formed during stabilization of the crater floor. Sharp-walled sulphide veins were exposed at the Broken Hammer Mine in the North Range of the Sudbury impact structure in Sudbury, Ontario. The Broken Hammer deposit was mined as an open pit operation that exposed a complete 90-meter vertical section across a footwall vein system. As such, it provided a unique opportunity to document the 3D architecture of a footwall vein system and determine how the fractures hosting the veins formed.

1.2 Objectives of the Thesis

The main objective of the thesis is to provide a new interpretation for the evolution of the Broken Hammer deposit and the formation of the fractures and faults hosting the sharp-walled sulphide veins.

More specifically, the objectives are to:

1) Characterize the alteration associated with the sharp-walled sulphide veins and low sulphide PGE mineralization,
2) Determine the structural controls on the emplacement of sharp-walled sulphide veins,

3) Establish the relative timing between the emplacements of the sharp-walled sulphide veins, the formation of the fractures hosting the veins, alteration events, and introduction of low sulphide PGE mineralization,
4) Create a 3D model of the Broken Hammer deposit and its vein system,
5) Provide an interpretation for the formation of the Broken Hammer deposit and its modification during subsequent deformation events.

1.3 Methodology

The Broken Hammer open pit was mapped from Summer 2014 through to Fall 2015 as mining progressed. Bench walls and floors were mapped at a scale of 1:2000 to 1:50 using the surveyed mine grid as base map. This data was integrated into a 3D model of the deposit built using the software Leapfrog. Sample sets taken across the five vein sets were collected and submitted to a commercial lab (ALS) for whole rock, major, and trace (including PGE) element analyses to characterize the geochemistry of the veins and their alteration halo. Representative samples of the vein and alteration were examined using the scanning electron microscope at the Central Analytical Facility of Laurentian University for identification of platinum group minerals associated with the veins and alteration.

1.4 Organization of the Thesis

The thesis is written as two chapters. The first chapter introduces the Broken Hammer deposit, the objectives of the study, and methodology. The second chapter is written as a submission to the Canadian Journal of Earth Sciences and is entitled "*Emplacement of sharp-walled sulphide veins at the Broken Hammer Mine, Sudbury, Ontario*". Co-authors on the manuscript are:

- Lafrance, B., Mineral Exploration Research Centre, Harquail School of Earth Sciences, Laurentian University, 935 Ramsey Lake Road, Sudbury, Ontario, P3E-2C6, Canada

- Gibson, H.L., Mineral Exploration Research Centre, Harquail School of Earth Sciences, Laurentian University, 935 Ramsey Lake Road, Sudbury, Ontario, P3E-2C6, Canada

Chapter 2 - Emplacement of sharp-walled sulphide veins at the Broken Hammer Mine, Sudbury, Ontario

2.1 Introduction

Impact craters are one of the most intriguing geological structures on Earth and on other planets and moons of the solar system (Michel and Morbidly, 2013). Commonly classified as simple and complex craters, their shapes (or morphology) range from simple depressions to complex multi-ring basins (Dence, 1964). The formation of large impact structures starts with contact compression (Stage 1) during which the energy of the impacting bolide is transferred to the target rocks, continues with the formation of an impact melt sheet, excavation of the target rocks, and opening of a transient crater (Stage 2), and ends with the modification of the transient crater into its final crater shape as the crater walls subside and the crater center rebounds (Stage 3) (French, 1998). This last stage involves the displacement of kilometer-sized blocks within the first twenty minutes after initial contact (Osinski and Pierazzo, 2013 and references therein) after which the crater remains unstable for thousands of years as it readjusts by slip along new or reactivated basement footwall faults as a way of accommodating magmatic doming or isostatic rebound of the crater floor (Hall et al., 1980; Dombard and Gillis, 2001).

The Sudbury mining camp is located within one of the largest impact structures on Earth (Krogh et al., 1984; Grieve et al., 1991; Deutsch et al, 1995; Krogh et al., 1996; Petrus et al., 2015). The Sudbury impact event occurred 1.85 Ga ago when a 15 km diameter comet (Petrus et al., 2015) collided with Earth and melted large volumes of rocks, forming an impact melt sheet that crystallized as the Sudbury Igneous Complex (SIC). During crystallization and cooling of the SIC, sulphide melts accumulated at its base forming Ni-Cu-PGE (Platinum Group Elements) contact deposits, and were transported in silicate melts that crystallized as offset dikes in the basement footwall rocks, forming Ni-Cu-PGE offset deposits (Ames et al, 2007). Fractionation of the

sulphide melts at the base of the SIC (Li and Naldrett, 1993; Jago et al., 1994; Morrison et al., 1994) and/or leaching of metals from the contact deposits by magmato-hydrothermal fluids (Farrow, 1994; Watkinson 1999; Molnar et al., 2001; Farrow et al., 2005; Hanley et al., 2005; Pentek et al., 2008) produced Cu-PGE-rich sulphide melts and/or metal-rich hydrothermal fluids, which were injected in fractures within the basement rocks forming the footwall deposits. The latter are sought because of their high PGE values. They are subdivided into "sharp-walled veins" composed of massive chalcopyrite and minor platinum group minerals and "low-sulphide PGE-rich" mineralization expressed by narrow sulphide veinlets and disseminations (Farrow et al., 2005).

Fractures and faults played an important role in providing conduits for the transport of melts, fluids and metals from the base of the SIC to the footwall rocks. Several interpretations have been proposed for the formation of the fractures and faults and the emplacement of mineralization. For example, Abel (1981) suggested that fractures formed from compression perpendicular to the SIC-footwall contact whereas Coats and Snajdr (1984) suggested that the veins were emplaced along tensile and conjugate fractures. Stout (2009) further suggested that this shortening event occurred during crater modification. These studies did not, however, address the relative chronology of the veins, fractures, and footwall vein alteration, nor did they consider the post-impact effects of orogenic far field stresses on the formation of fractures and the emplacement of the sulphide veins.

Broken Hammer is a footwall deposit in the North Range of the Sudbury impact structure owned by Wallbridge Mining Company Ltd. (Wallbridge) and was mined by Wallbridge as an open pit operation from July 2014 to October 2015. Mapping and sampling of the deposit were done continuously during mining, providing the unique opportunity for a full three-dimensional

(3D) characterization of a footwall ore system from surface to a vertical depth of roughly 90 meters, the depth at which the sulphide veins ended and mining ceased. In this manuscript we describe the structural evolution and controls on the formation of fractures and emplacement of sharp-walled sulphide veins in basement footwall rocks of the Sudbury impact structure. To achieve this, we: (1) describe the 3D geometry of the sharp-walled footwall veins and associated low sulphide mineralization, (2) present a structural interpretation for the emplacement of the veins, and (3) examine metal values with increasing distance from the sulphide veins to determine if there is a spatial connection, such as a gradation in metal content, between sharp walled veins and low sulphide mineralization.

2.2 Geology of the Sudbury impact structure and footwall deposits

The Sudbury impact structure is located at the junction between the Archean Superior Province, the Paleoproterozoic Southern Province, and the Mesoproterozoic Grenville Province. The Sudbury Igneous Complex (SIC) occupies what is interpreted to be the centre of the structure and is exposed on three ranges, namely the South Range, North Range, and East Range (Fig. 1), which form a rim around a basin defined by the Whitewater Group (Rousell, 1975). The latter consists of fall-back impact breccias, plume collapse deposits and pyroclastic flows of the Onaping Formation (Ames et al. 2002), which were deposited above the SIC immediately after the impact, and are overlain by post-impact carbonaceous argillite of the Onwatin Formation and turbiditic sandstone of the Chelmsford Formation (Rousell, 1975).

In the North Range, the basement rocks beneath the SIC consist of the ca. 2.71 Ga Levack Gneiss Complex (Krogh et al., 1984) and granitoids of the ca. 2.64 Ga Cartier Batholith (Meldrum et al., 1997), which are intruded by younger diabase dikes of the ca. 2.47-2.45 Ga Matachewan dike swarm (Heaman, 1997) and ca. 2.2 Ga Nipissing dike swarm (Corfu & Andrews, 1986).

During the Sudbury event, these rocks were locally brecciated and pulverized into a pseudotachylitic breccia, called Sudbury breccia, which forms meter to hundred meter wide irregular bodies containing variably rounded clasts of the basement rocks surrounded by a fine-grained to aphanitic, black to dark grey matrix (Dietz and Butler, 1964; Dressler, 1984; Müller-Mohr, 1992; Thompson and Spray, 1994, 1996; Spray and Thompson, 1995; Rousell et al., 2003; Spray et al., 2004; Lafrance et al., 2008).

Several post-impact orogenic events affected the Sudbury impact structure and folded the structure into a doubly-plunging syncline (Roussell, 1975). The northern limb of the structure and SIC-basement contact are moderately dipping (30°-50°S) in the North Range, and its southern limb and SIC-basement contact are moderately-dipping (50°N) to overturned (80°S) in the South Range (Fig. 1), where they are offset by crosscutting, reverse, north-directed faults of the South Range shear zone system (Rousell, 1975; Szabo and Hall, 2006; Dreuse et al., 2010). Deformation of the structure may have began immediately after impact, during the waning stage (1.85 Ga – 1.83 Ga) of the Penokean Orogeny (Young, 2015), as suggested by ca. 1.849 Ga and ca. 1.82 Ga U-Pb titanite ages in South Range shear zones overprinting the Garson and Thayer-Lindsley deposits (Fig. 1; Bailey et al., 2004; Mukwakwami et al. 2014), and continued much later during the ca. 1.75 Ga – 1.70 Ga Yavapai orogeny, as indicated by the presence of metamorphic U-Pb monazite ages and crystallization U-Pb zircon ages in the South Range and Southern Province (Piercey et al. 2007; Raharimahefa et al., 2014). Six kilometers south of Sudbury, the Grenvillian orogenic front juxtaposes the Grenville Province against the Southern Province but the effects of the Grenvillian orogeny on the SIC and its deposits appear to be limited to reactivation and minor offset of ca. 1.24 Ga Sudbury diabase dikes along South Range shear zones (Tschirhart and Morris,

2012) and minor modification of contact deposits, as indicated by boudinaged Sudbury dikes in massive sulphide bodies of the Garson deposit (Mukwakwami et al., 2012).

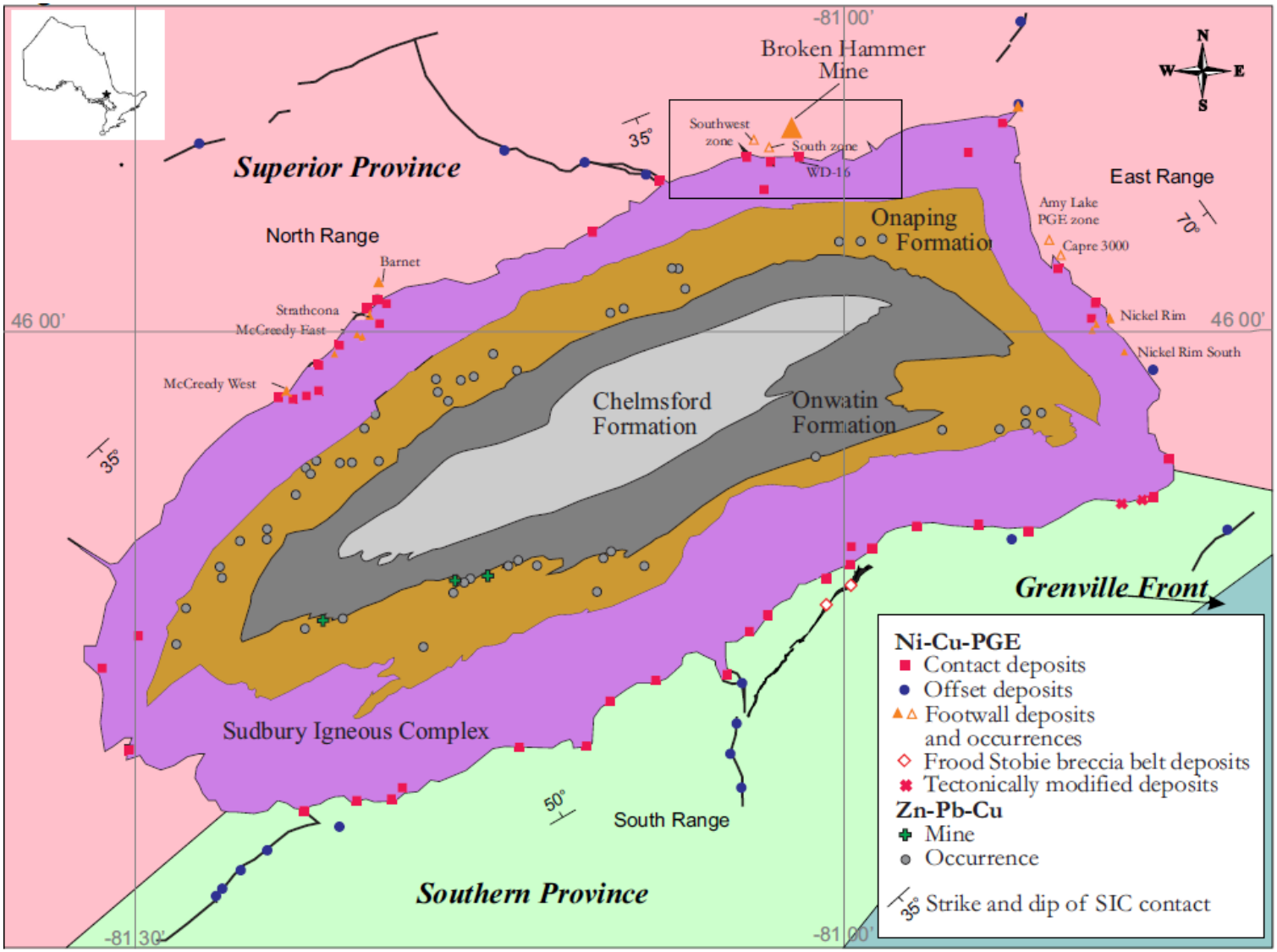

Figure 1: Simplified geological map of the Sudbury impact structure. Average strikes and dips of the SIC-basement contact are from Szabo and Halls (2008). Inset of Ontario showing location (star) of the Sudbury impact structure. Map modified after Ames et al. (2005)

Footwall deposits have been found up to ~1km from the SIC-basement contact typically in close spatial association with zones of metamorphosed Sudbury breccia (Morrison et al., 1994) although some exceptions such as McCreedy Deep do occur where black aphanitic Sudbury breccia host footwall mineralization (Mike Sweeny, personal comms). Metamorphosed Sudbury breccia has a recrystallized, fine-grained, grey matrix that differs from the black and aphanitic matrix of unmetamorphosed Sudbury breccia located farther away from the SIC contact (Ames et al., 2007) Adjacent basement rocks to metamorphosed Sudbury breccia contain leucocratic patches and veins, called footwall granophyre's, which formed either by partial melting of the basement rocks during cooling of the SIC (Pentek et al., 2011) or by differentiation of SIC silicate melts and injection of these differentiated residual melts in the basement rocks during crystallization of the SIC (Hanley et al., 2011).

Most footwall deposits are hybrid deposits with both sharp-walled vein and low-sulphide mineralization (Farrow et al., 2005; Ames et al., 2007). Sharp-walled sulphide veins may be up to several meters in thickness and occur as complex vein networks consisting of massive chalcopyrite ± cubanite, with minor pyrrhotite, pentlandite, millerite, and magnetite (Farrow and Lightfoot, 2002). Massive sulphide veins are interpreted to have formed through the differentiation of an immiscible sulphide liquid that pooled at the base of the SIC, with the differentiated Cu (Ni)-PGE-rich melt injected into the footwall rocks to form veins (Li and Naldrett, 1993; Jago et al., 1994; Morrison et al., 1994), or by leaching of metals from contact deposits by magmato-hydrothermal fluids which then infiltrated fractures in the footwall rocks to form veins (Farrow, 1994; Watkinson 1999; Molnar et al., 2001; Farrow et al., 2005; Hanley et al., 2005; Pentek et al., 2008). The formation of low sulphide mineralization is generally attributed solely to hydrothermal processes (Pentek et al., 2008; Nelles et al., 2010; Hanley et al., 2011). Sharp-walled veins are surrounded

by thin selvages of amphibole, biotite and epidote, which together with quartz become more abundant at the termination of the veins. Low-sulphide, high-PGE mineralization occurs as mm-sized disseminations, cm-sized patches, and sulphide stringers that may be adjacent to, or occur tens to hundreds of meters away from massive sulphide vein-type mineralization. Sulphide minerals represent <5% of the rock and are dominated by chalcopyrite with minor millerite (Farrow et al., 2005; Pentek et al., 2008; Hanley et al., 2011; Tuba et al., 2014).

2.2.1 Previous work at the Broken Hammer deposit

The Broken Hammer deposit is located in Archean Levack gneisses of the North Range within 1.5 km of the SIC-basement contact (Figs. 1, 2). It was exposed at surface and was described by Pentek et al. (2008, 2011, 2013) and Tuba et al. (2014) prior to mining. It is interpreted as a hybrid footwall deposit consisting of sharp-walled veins and low-sulphide mineralization (Pentek et al., 2008). The sharp-walled sulphide veins range in thickness from <1 cm to 1 m and are dominated by chalcopyrite with up to 10% magnetite, <3% chalcocite and millerite, and rare sperrylite. Vein margins are locally sheared and consist of thin selvedges (<10 cm) of epidote, quartz and actinolite, with these gangue minerals dominating over sulphide minerals at the tips of the veins (Pentek et al., 2008). Low-sulphide mineralization locally occurs within the immediate wallrocks of sharp-walled veins, but is more typically localized along lithological contacts where it is associated with strong chlorite, epidote, and actinolite alteration. Low-sulphide mineralization consists of hairline fractures with chalcopyrite, unconnected blebs of chalcopyrite which range in size from 1mm to >1cm, and irregular, elongate, patches of chalcopyrite, epidote and actinolite replacing the matrix of quartz monzonite (centimeters in size) and Sudbury breccia (tens of centimeters in size) (Pentek et al., 2008). For both sharp-walled veins and low sulphide mineralization, PGM's typically occur as discrete grains within sulphides and along silicate/sulphide grain boundaries (Pentek et al., 2008).

The formation of the sulphide veins and low sulphide mineralization are both attributed to a high salinity (up to 50 wt% NaCl equivalent) and high temperature (400-500°C) magmatic-hydrothermal fluid that was released during partial melting of the footwall rocks beneath the SIC contact and mixed with mobilized regional groundwater (Molnar et al., 2001; Pentek et al., 2008, 2013; Tuba et al., 2014). The fluid leached metals from primary contact deposits and deposited these metals into the footwall to form the Broken Hammer massive sulphide veins and low sulphide mineralization (*ibid*).

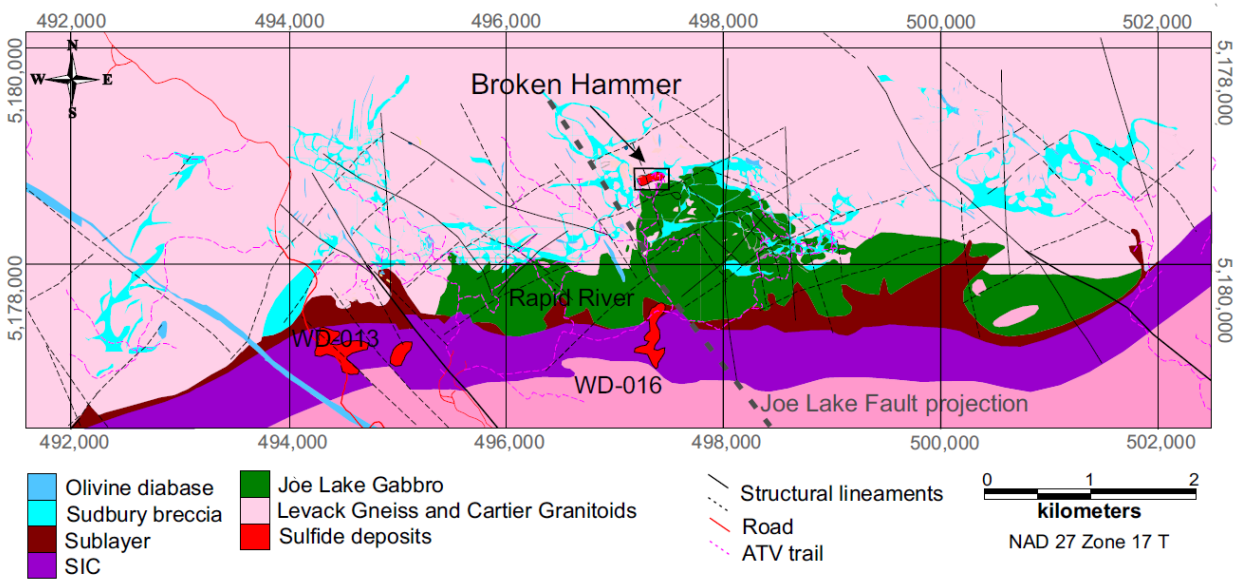

Figure 2: Regional geology map of the Broken Hammer area, showing the location of the Broken Hammer deposit ~1.5km north of the SIC-basement contact. WD-16 and Rapid River are Ni-Cu contact deposits at the base of the SIC. Geology is from maps by Wallbridge Mining

2.3 Methodology

The Broken Hammer open pit consists of a western pit and a smaller eastern pit, roughly 150 m and 60 m in diameter and 100 m and 25 m in depth, respectively. Mapping of the western pit was done continuously as mining progressed from summer to winter. Bench floors and blast faces were mapped in detail at scales of 1:50 to 1:2000 using surveyed markers and chains. In areas where mapping was impeded by mining activities, copper assay values from production drill

holes and diamond drill logs were used to locate and trace the veins. The geology of the deposit and the orientation of the veins were modeled in 3D using Leapfrog Geo (Seequent). Parts of the eastern pit were mined by the start of the study so its geology and vein orientations were modelled using available information from diamond drill logs and previous surface and wall maps. They are not discussed in detail within this work. Veins in the West Pit were modelled from mapping and structural data collected in this thesis and individual vein models are included in Appendix A. They are named after their location in the East or West Pit and a numeric label was added based on the sequence in which they were modelled. The East Pit contained 8 major veins (labelled E Vn 001-007) and the West Pit contained 14 major veins (labelled W Vn 001-014).

Because of its homogeneous composition, the matrix of Sudbury breccia was preferentially sampled to assess the alteration mineralogy and geochemistry adjacent to sharp-walled sulphide veins. Samples were collected at intervals of 10 cm to up to 2 m from the vein margins for total distances of up to 4 m (See Appendix B for sample locations and an example of samples marked for cutting). One hundred-ninety samples were collected at all mine levels from ten sample sets (transects) across five sharp-walled sulphide veins, including 6 samples collected from a low sulphide mineralized zone and 7 samples collected over a 1.5 m vertical section across the Chisel Creek Fault.

To maintain consistency with Wallbridge's database and operating procedure, known certified reference standards and quartz blanks were inserted after every 18th samples. The samples were sent to ALS laboratories in Vancouver, British Columbia, for analysis. Samples underwent a four-acid digestion and were analyzed using inductively coupled plasma mass spectrometry (ICP-MS) instrumentation. Precision of major elements (Ca, Fe, K, Mg, Na, S and Ti) and rare earth elements (Ce, La, Sc, Y) is <5% in all cases except near detection limits. Precision for trace

elements (Bi, Co, Ga, Ge, Nb, Rb, Sb, Sc, and Zr) and base metals (Ag, Cu, Ni, Sn, Ti, Zn) are <10% except where approaching or exceeding detection limits. Ore grade samples exceeding ICP-MS detection limits for Au, Pt, and Pd were further analyzed by inductively coupled plasma atomic emission spectrometry (ICP-AES). Precision for these elements is <5% except for analyses near the detection limit. Accuracy of standards were calculated to be <3% for Pt and Pd; <2% for Co and Cu, and <1% for Ni. Gold was the only element to fail the assay accuracy threshold of 5%, however these values are listed as provisional for the selected analysis package and were not used for data verification.

Mineral chemical analyses were carried out using an Oxford S-Sight energy dispersive detector mounted on the JEOL 6400 scanning electron microscope (SEM) at Laurentian University, using a 15-kV accelerating voltage, a 1.005 nA beam current, acquisition count times of 20 sec or more, and a working distance of 15 mm. Standardization was done using well characterized jadeite, diopside, orthoclase, corundum, quartz, chalcopyrite, and pyrophanite standards.

2.4 Results

2.4.1 Rock units hosting the Broken Hammer deposit

The main rock units exposed in the open pit are quartz monzonitic and dioritic gneisses of the Levack gneiss complex, the Joe Lake gabbro, late granitic sheets and granitic pegmatites, Matachewan diabase dikes, and Sudbury breccia (Fig. 3). Quartz monzonitic gneiss is the dominant rock type. It is white to light pinkish grey on fresh surface, medium- to coarse-grained (1-5mm grain size), with a locally strong gneissic foliation defined by quartz- and feldspar-rich felsic bands (≤ 50 cm in width) alternating with up to 20 cm thick mafic bands composed of amphibole and feldspar (Fig. 3A). Quartzo-feldspathic granitic sheets up to 3 m in width are

parallel to the gneissic banding. Dioritic gneiss is grey on fresh surface, medium- to coarse-grained (1-5 mm grain size), with a gneissic foliation defined by quartz- and feldspar-rich felsic bands alternating with biotite- and amphibole-rich mafic bands. In both units, the gneissic foliation generally strikes NW and dips steeply to the NE. The Joe Lake gabbro is blue to black on fresh surface, medium- to coarse-grained (1-5mm), and massive to weakly foliated. It consists of amphibole after pyroxene (65%) and plagioclase (35%) and was exposed along the southern wall of the deposit as a massive irregular body and in the gneissic units as thick (>3 m) layers parallel to the gneissic foliation.

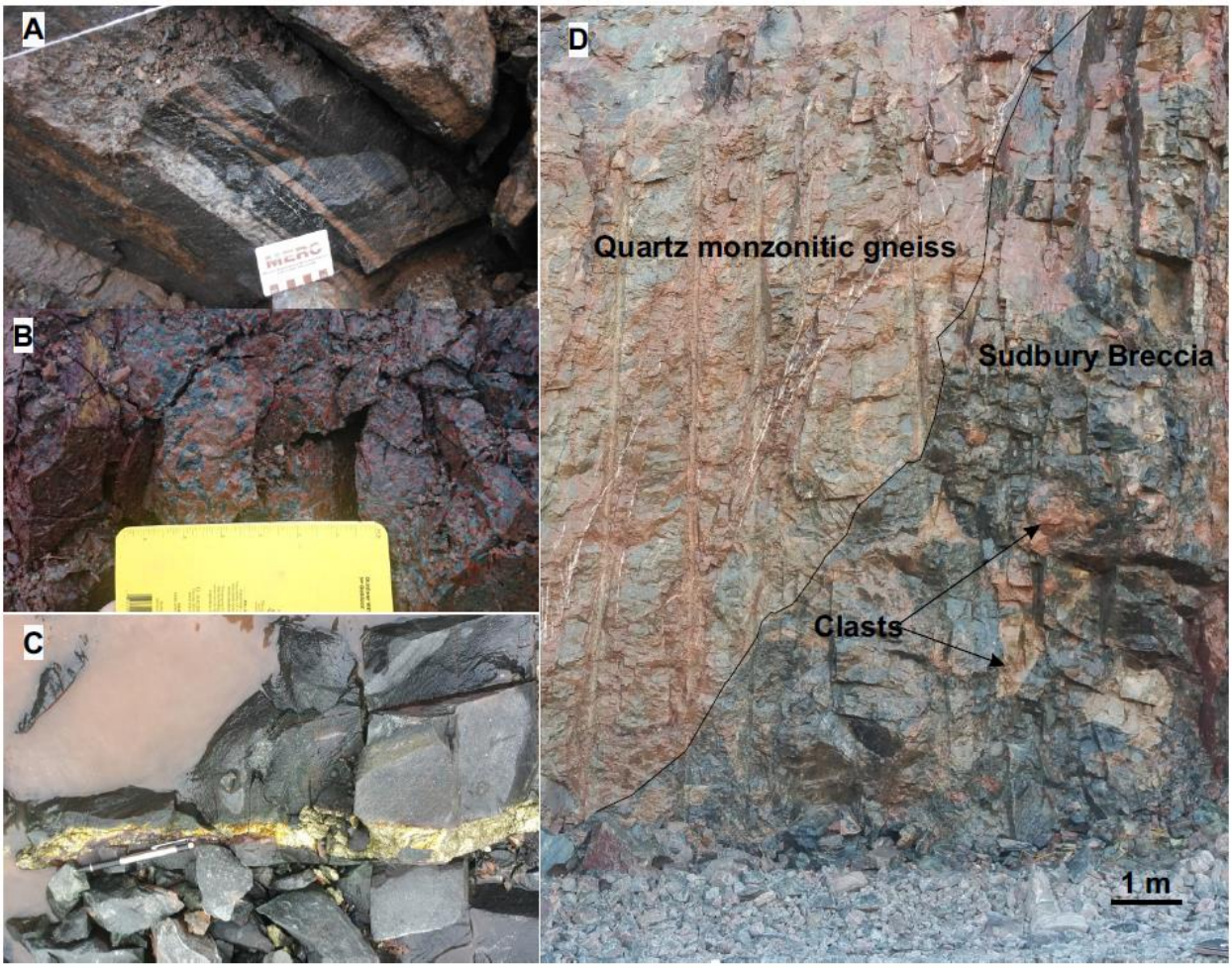

Figure 3: Field photographs of rock units at the Broken Hammer deposit: A) Quartz monzonitic gneiss. Photo card (9 cm in length) for scale. B) Granitic pegmatite with coarse quartz and feldspar intergrowths. Notebook (18 cm in length) for scale. C) Fine-grained Matachewan diabase dike cut by a massive chalcopyrite sharp-walled vein. Pencil (10 cm in length) for scale. D) Sudbury breccia in contact with massive quartz monzonitic gneiss.

Late granitic pegmatites possibly related to the Cartier Batholith (Pentek et al., 2008) cut across the Levack gneisses and Joe Lake gabbro units. They are pink to white, coarse-grained (1-8cm), and consist almost entirely of intergrown quartz and potassium feldspar with graphitic textures (Fig. 3B). Late Matachewan diabase dikes cut across the gneissic units and Joe Lake gabbro. The dikes are EW-striking, greenish blue on fresh surface, fine- to medium-grained (0.1-1mm), and composed mostly of amphibole and plagioclase (Fig 3C). All the units described above, including the late Matachewan dikes and pegmatites, have been brecciated and occur as clasts within Sudbury breccia.

Sudbury breccia occurs as irregular, elongate bodies, striking ENE/WSW to NE/SW (Fig. 4) subparallel to the SIC-basement contact (Fig. 2). Thicknesses range from 10's of meters near surface and upper pit levels to <1 m at lower pit levels. Blocks or clasts within the breccia are up to 10 m in size, randomly oriented, and representative of the basement rocks exposed in the open pit (Fig 3D). Several clasts have rounded diffuse margins that grade into the surrounding, thermally recrystallized, fine-grained, grey matrix of the breccia. Small black amphibole needles are present within the breccia matrix.

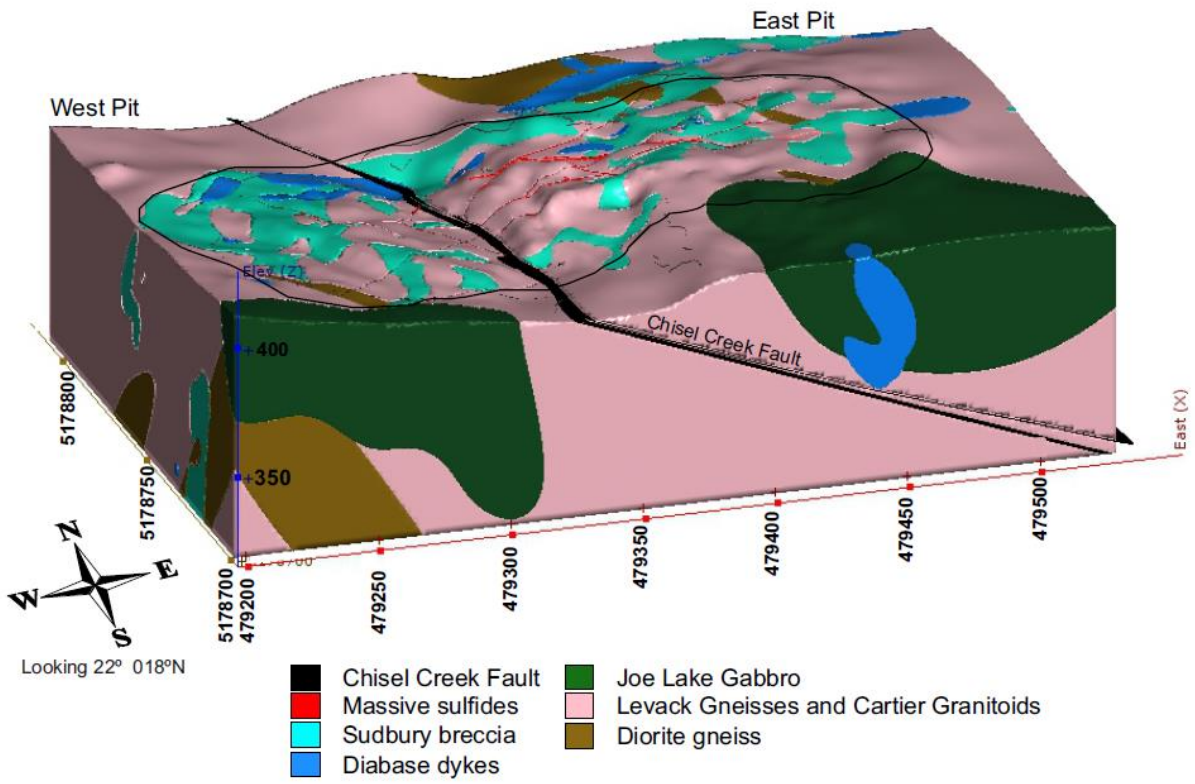

Figure 4: Simplified 3D geologic model of the Broken Hammer area prior to mining. Note that dioritic gneiss has been separated from the Levack Gneiss grouping.

2.4.2 Mineralization

Sharp-walled sulphide veins: The sharp-walled sulphide veins cut across all rock units including Sudbury breccia (Fig. 5A). They vary from <1cm to >1m wide over distances of 5-10m with average widths of roughly 20 cm. Abrupt width variations (>50cm) typically occur where the veins change orientations to follow intersecting structural anisotropies, such as other veins, fractures, and lithological contacts. Structural anisotropies within Sudbury breccia further control the location of the veins which typically follow contacts between the breccia matrix and blocks of the basement rocks. Where the veins cut across blocks, they are typically straight with sharp walls but as they pass into the breccia matrix they either persist unchanged or split into smaller veins with diffuse walls (Fig. 5B). Overlapping, parallel, sharp-walled veins are linked by bridging smaller veins cutting across the matrix of Sudbury breccia (Fig. 5C).

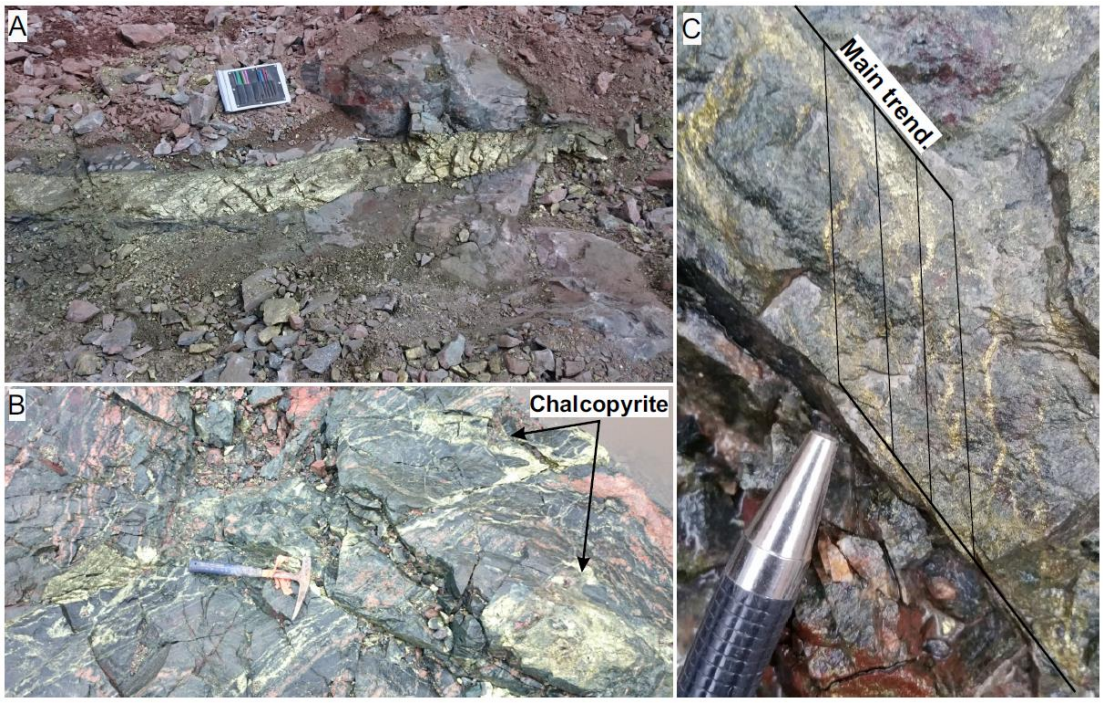

Figure 5: Field photographs of sharp-walled massive sulphide veins and low-sulphide mineralization: A) Massive sharp-walled sulphide vein cutting across dioritic gneiss. Map board is 28 cm in length. B) Wispy chalcopyrite veins in Sudbury breccia. Hammer is 30 cm in length. C) Centimeter scale example "ladder-like" bridging of chalcopyrite veins. Note the trend of the main vein. Tip of pencil is 2 cm in length.

Sharp-walled veins are typically steeply-dipping to vertical (60-90°) and they decrease in dip from 45° to horizontal along jogs (Appendix C). They are divided by orientation into five groups: (1) NE-striking and SE-dipping veins, (2) SW-striking and NW-dipping veins, (3) SE-striking and SW-dipping veins, (4) S-striking and W-dipping veins, and (5) EW-striking and S- and N-dipping veins (Fig. 6). Their variation in orientation with increasing depth in the pit is shown in Appendix D. The main veins within each group can be traced across the open pit whereas other, typically thinner, parallel veins, called connector veins, terminate against other veins or form isolated veins that taper off at both ends. The five orientation groups have a common line of intersection that plunges roughly 60º towards 220º (Fig. 6) and coincides with the trend and plunge of thicker chalcopyrite ore shoots.

Although the veins are similar in composition regardless of orientation, a few differences exist amongst the five orientation groups in the West pit. SW-striking veins are typically the widest and contain more sperrylite crystals. Their strike may change by as much as 90° along jogs parallel to other vein groups. Conversely, the NE-striking veins, which have opposite dips, display the least variations in orientation. Variations in orientation and width also occur along SE-striking and EW-striking veins. SE-striking veins tend to be wider along S-striking jogs, and EW-striking veins, which have an average width of ~2 cm, attain widths of up to 60 cm along dip-parallel bends or jogs. In the East pit, a SE-striking (~120°) and SW-dipping vein, called the Big Boy vein, is by far the largest vein with thicknesses of up to 1.5 m.

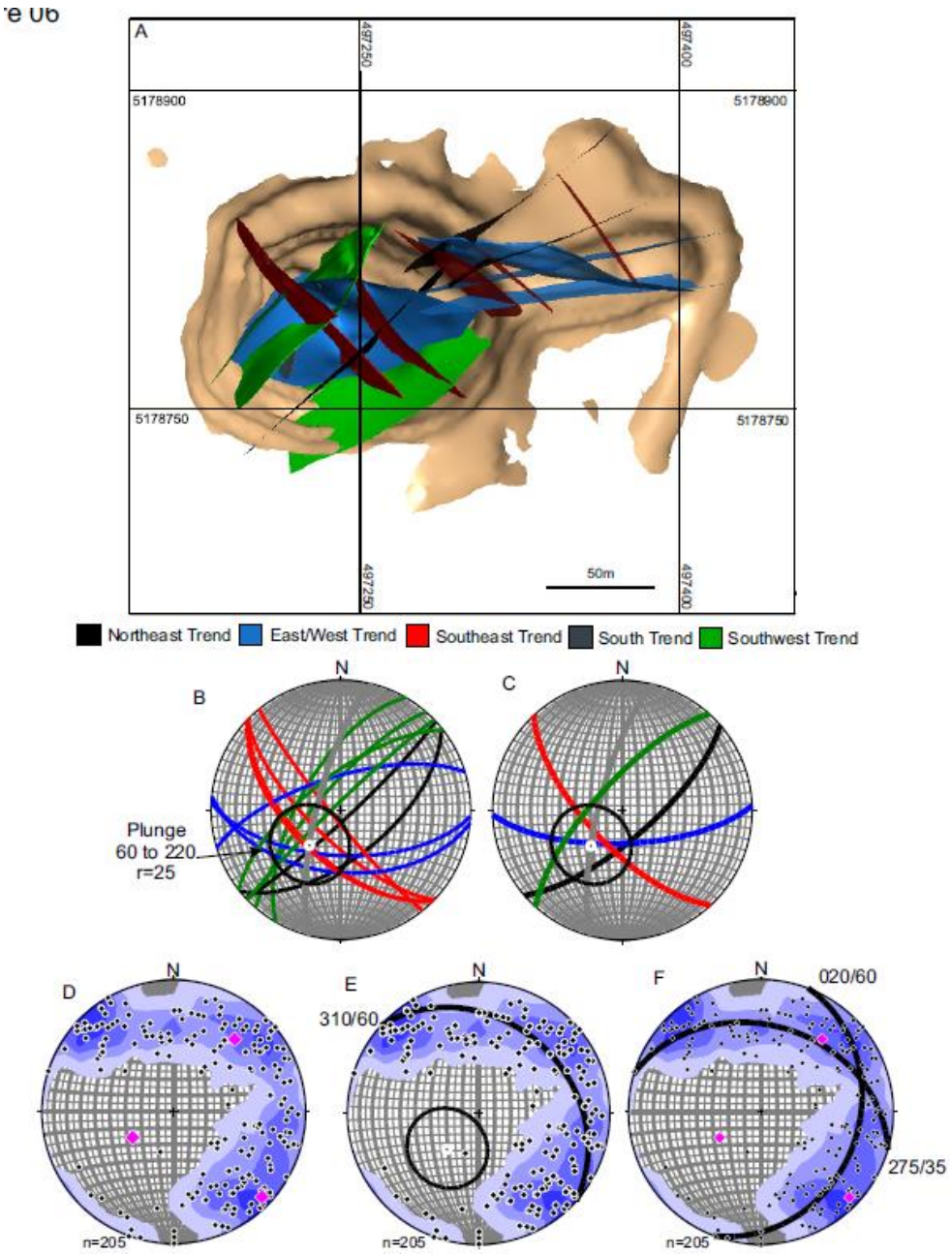

Figure 6: Sharp-walled massive sulphide veins at the Broken Hammer open pit mine: A) 3D model of the sharp-walled sulphide veins from all of Broken Hammer. Vein group sets are represented by different colors. NAD27 UTM coordinate system. B) Lower hemisphere stereonet diagram showing the orientation of the massive sulphide veins shown in Fig. 6A and from the West Pit only. Veins intersect within a small circle with a radius (r) = 25°. The center of the circle represents the average orientation of the common intersection line (plunge of 60° towards 220°) between all vein sets. C) Lower hemisphere stereonet diagram showing average vein group orientations. D) Lower hemisphere stereonet diagram showing contoured poles to all vein measurement from the western pit. Eigenvectors represented by pink diamonds. E) Lower hemisphere stereonet diagram showing best fit great circle for all vein measurements. F) Lower hemisphere stereonet diagram showing two best fit great circles. Number of measurements at bottom left of stereonet plots. Great circles labeled with their strike and dip.

Sharp-walled sulphide veins are composed almost exclusively of chalcopyrite. The latter makes up 90% to nearly 100% of the veins with the remaining (<10%) consisting of magnetite, millerite, pentlandite, chalcocite, rare platinum group minerals (PGM), and hydrothermal minerals such as quartz and epidote. The PGMs occur as inclusions in chalcopyrite and as discrete grains along grain boundaries of sulphide– silicate alteration minerals (described below). They include sperrylite ($PtAs_2$), michenerite ((Pd,Pt)BiTe), merenskyite ($Pd(Te,Bi)_2$), malyshevite ($CuPdBiS_3$) and hessite (Ag_2Te) as well as additional minerals described by Pentek et al., (2008). Sperrylite contains almost all the platinum in the rock. They form large euhedral crystals, up to 3cm in size (Figs. 7A-C), which are transected by chalcopyrite-filled microfractures and surrounded by other Pd-bearing PGMs. The large sperrylite grain in Figure 7B contains inclusions of gold and a Pt-Pd bismuthide, which is the only observed PGM composed of both Pt and Pd. The sharp-walled sulphide veins are enveloped by alteration selvedges of coarse-grained (<5 mm) epidote, quartz, and actinolite-tremolite up to 10 cm wide. The relative proportion of alteration silicate minerals to sulphide minerals increases towards the vein tips or terminations, which are entirely filled by the silicate minerals. Epidote or actinolite dominates in mafic host rocks and epidote is the main alteration mineral in felsic host rocks. No alteration selvedge is observed along sulphide veins that cross granitic pegmatites. Alteration silicate minerals are commonly intergrown and occur as inclusions in each other. Actinolite-tremolite forms euhedral, acicular grains (10 μm in length), locally replacing metamorphic hornblende. Epidote forms subhedral to euhedral, stubby to slender, prismatic grains (<5 μm in length), containing rare earth elements Ce, Cd, and La. Locally, patches or pockets of euhedral prismatic epidote grains, with short axes of ~0.75 mm and long axes of ~5 mm, are intergrown with chalcopyrite along the vein margins (Fig. 7D). Quartz-chlorite fragments are also present along the vein margins as trains of rounded inclusions (1-10 cm in size) (Fig. 8).

The fragments comprise massive white quartz separated by thin (~1mm) black chlorite laminae. A ridge-and-groove slickenline lineation along chlorite laminae is accentuated by chalcopyrite infilling the grooves defining the lineation.

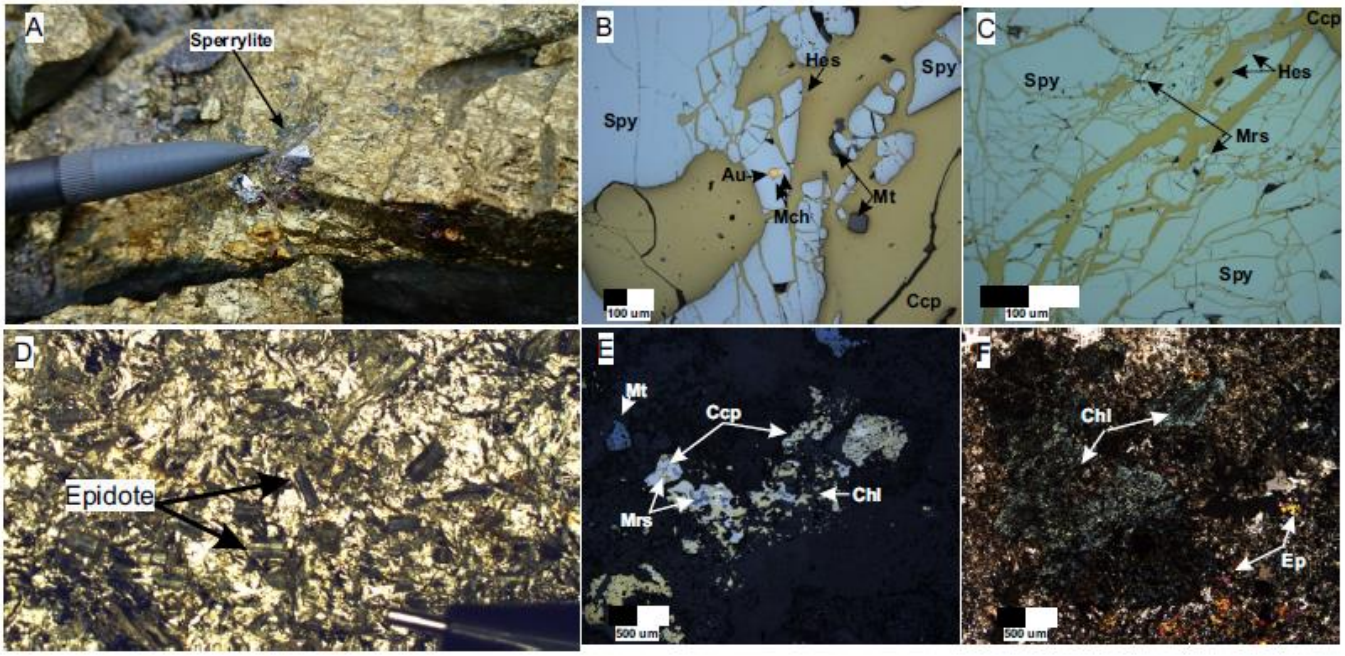

Figure 7: Photographs of mineralization and associated alteration. A) Euhedral sperrylite grain ~1cm in size enclosed in massive chalcopyrite sharp-walled vein. Tip of pencil is 0.5 cm in length. B) Reflected light photomicrograph of a large sperrylite grain with gold inclusion in contact with Pt/Pd bismuth-telluride inclusion. Fractures in sperrylite grain are filled with chalcopyrite which contains a euhedral magnetite inclusion. C) Reflected light photomicrograph of sperrylite grain in Figure 7B showing fractures filled by chalcopyrite and PGM. D) Euhedral green epidote crystals within massive chalcopyrite sharp-walled veins. Tip of pencil is 0.5 cm in length. E) Reflected light photomicrograph of Ni-bearing chlorite with inclusions of chalcopyrite and PGM. D) Cross-polarized photomicrograph of Ni-bearing chlorite associated with chalcopyrite and epidote. Cap = chalcopyrite; Chl = chlorite; Hes = hessite; Mch = michenerite; Mrs = merenskyite; Mt = magnetite; Spy = sperrylite.

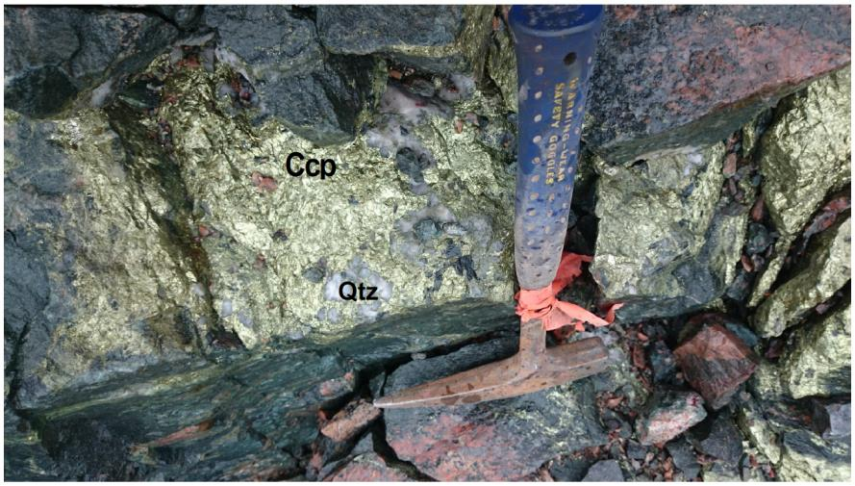

Figure 8: Field photograph of rounded quartz clasts within massive chalcopyrite sharp-walled vein. Hammer is 30 cm in length. Ccp = chalcopyrite; Qzt = quartz

A dark blue to green chlorite overprints epidote and actinolite in the alteration selvedges of the sulphide veins (7E, F). The chlorite is similar to that associated with low sulphide mineralization (described below) and range in composition from nimite ($(Ni, Mg, Fe^{2+})_5Al(Si_3Al)O_{10}(OH)_8$; Fig. 9) within 20 cm of sulphide veins to clinochlore ($(Mg, Fe^{2+})_5Al_2Si_3O_{10}(OH)_8$) farther away from the veins. Disseminated to blebby chalcopyrite (<1mm in size) occur as inclusions within the chlorite grains and these inclusions themselves contain rare PGM inclusions, including palladium bismuthines, palladium tellurides, and sperrylite (Fig. 7E, F).

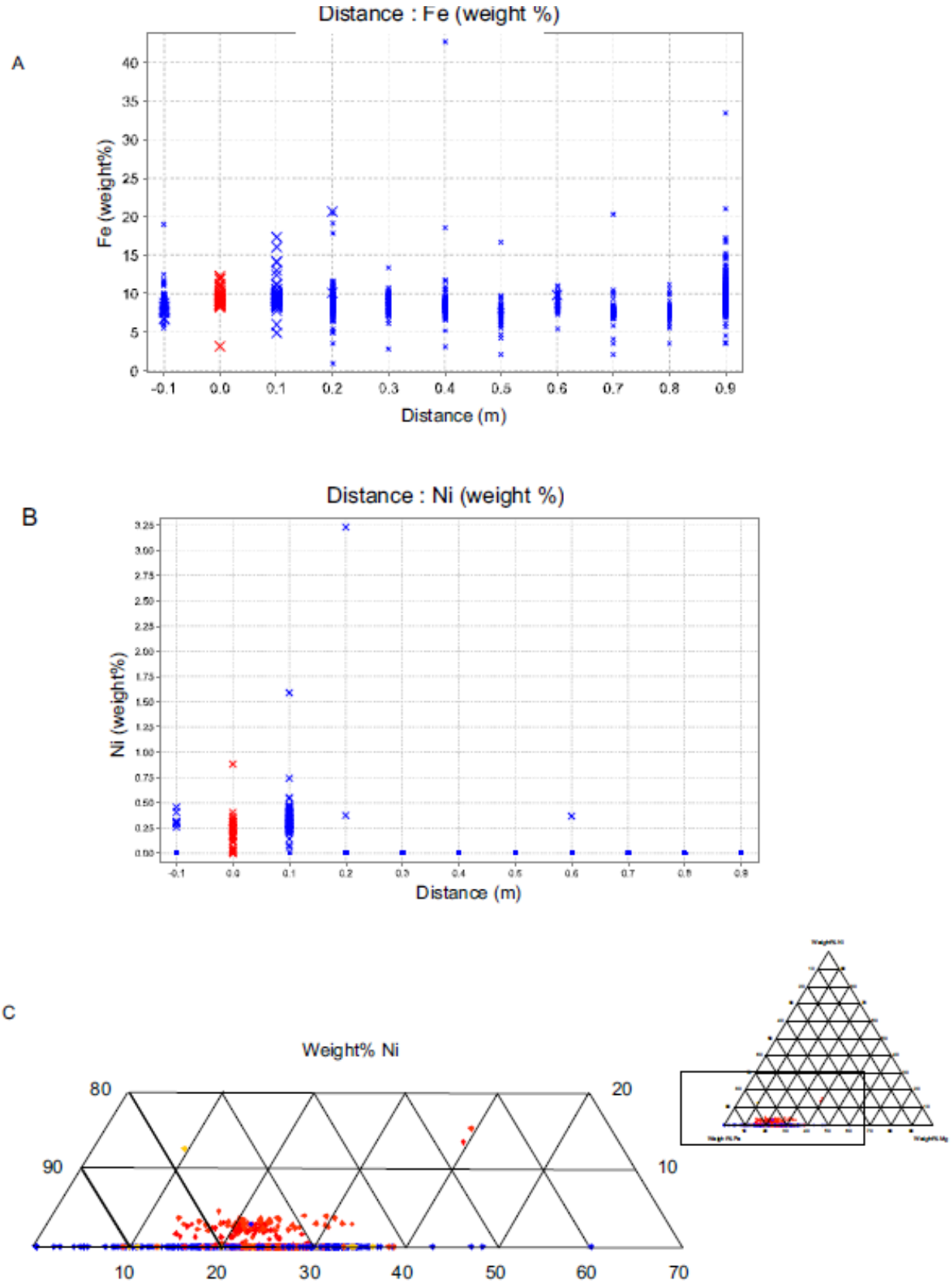

Figure 9: Geochemical plots of chlorites in the hanging wall of sulfide vein set 3. A) Binary plot of weight% Fe in chlorite versus distance in meters from sulfide veins. B) Binary plot of weight% Ni in chlorite versus distance in meters from sulfide veins. C) Ternary Fe-Ni-Mg plot in weight %. 798 analyses. Orange, red, blue circles represent analyses from semi-massive sulfide, massive sulfide, country rocks, respectively.

Low-sulphide mineralization: Low sulphide mineralized zones occur as sulphide stringers and disseminated blebs within zones of pervasive, fine-grained, chlorite alteration. The sulphides make up less than 5% of the rock (Fig. 10). Their mineralogy is similar to that of the sharp-walled veins and consists mainly of chalcopyrite with minor pyrite and trace chalcocite, galena, sphalerite, and PGM. This alteration is more common in mafic host rocks, such as the dioritic gneiss, diabase, gabbro, or the matrix of Sudbury breccia, where it imparts a bluish-green colouration to the rock and overprint irregular-shaped alteration patches of epidote, actinolite and quartz. These patches are similar in mineralogy to the selvedges and terminations of the sharp-walled sulphide veins.

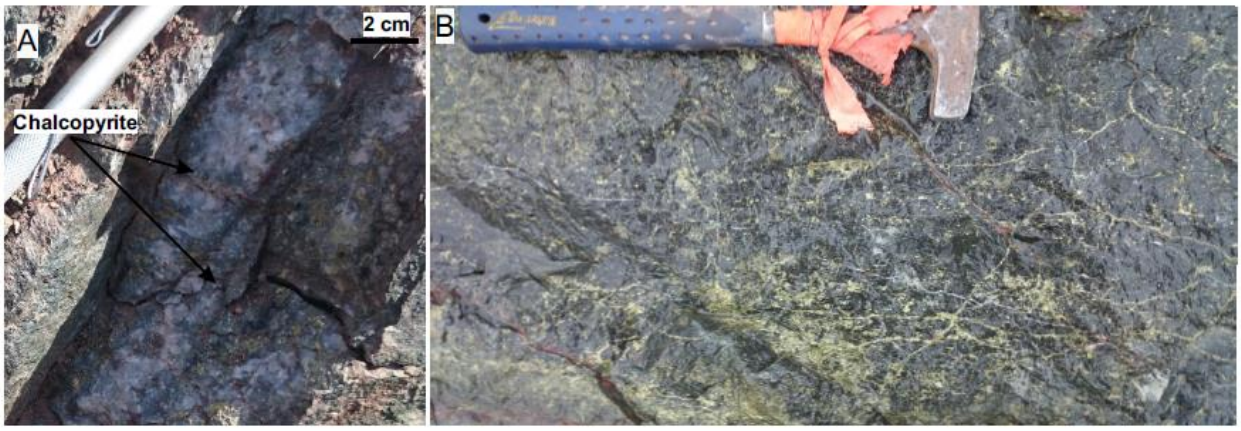

Figure 10: Field photographs of sulphide mineralization. A) Low sulphide mineralization consisting of wispy chalcopyrite veinlets and disseminated chalcopyrite in altered Matachewan diabase dike. Hammer is 30 cm in length. B) Low sulphide disseminated chalcopyrite associated with quartz mineralization and patchy chlorite.

2.4.3 Late structures

Late brittle faults and quartz-chlorite breccia veins cut across the sharp-walled sulphide veins. In the western pit, steeply-dipping brittle faults have strongly hematized and chloritized core zones (<5 cm width) composed of green to red gouge, which are surrounded by <1m wide damage zones characterized by strong fracturing. The faults generally strike NE and dip SE with the exception of one fault, which is SE-striking and SW-dipping, and a second fault which is SW-striking and NW-dipping (Fig. 11).

The quartz-chlorite breccia veins are typically NNW-striking (330-350°) and steeply-dipping (NE). Few, shallowly- to moderately-plunging, slickenlines imprint the vein walls. The breccia veins are typically <10 cm wide but may attain widths of up to 30 cm. They consist of milky white quartz and fine-grained olive-green chlorite locally stained by hematite (Fig. 11). They are filled mainly by chlorite in mafic host rocks (diabase, gabbro, dioritic gneiss) and by quartz in felsic host rocks (quartz monzonitic gneiss, granitic sheets). Quartz and chlorite surrounds jigsaw-fit, angular, altered fragments of the vein wall rocks, suggesting no or negligible displacements parallel to the vein walls. Wider veins have vuggy centers with comb textures defined by rhombohedral quartz crystal terminations. Chlorite and hematite alteration surround the veins and may extend for a few meters into the host rocks.

The Chisel Creek Fault is a shallowly-dipping (30°), NW-striking brittle fault (320°), which separates the smaller eastern pit from the western pit. It is expressed as a 10cm to 3m wide fracture zone of oxidized reddish-brown, rubbly to heavily fractured, broken rock fragments (Fig. 11). It truncates the steeply dipping faults and appears to offset a brecciated diabase dyke, suggesting reverse movement along the fault.

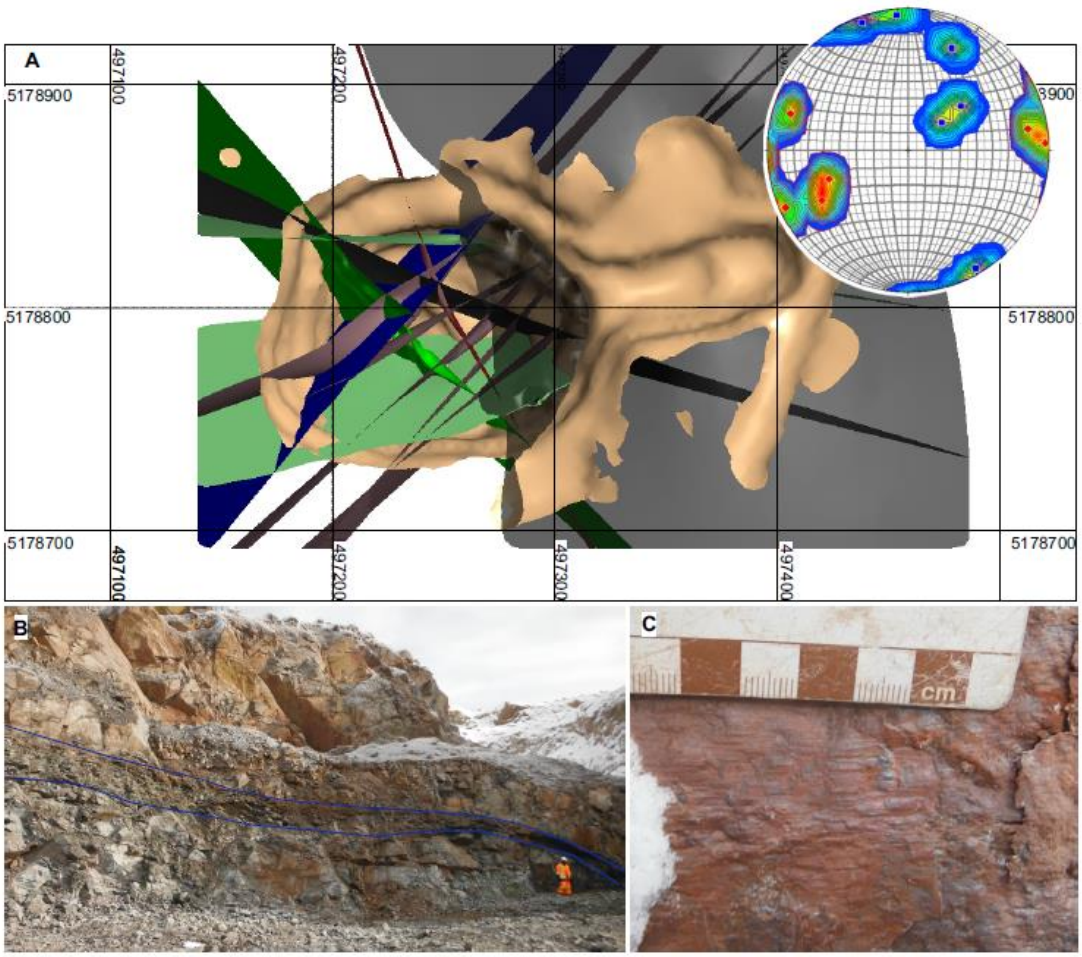

Figure 11: Late brittle faults in the western pit of the Broken Hammer mine. A) 3D model of the faults with lower hemisphere projection stereonet of the poles to the faults. B) Field photograph of the Chisel Creek fault delineated by the blue line along vertical open pit wall. Person for scale. C) Field photograph of shallowly plunging slickenlines along late steeply-dipping brittle fault. Photo card (9 cm) for scale.

2.4.4 Whole Rock Geochemistry

Samples were collected every ~10 cm along 1 m to 4 m transects across 5 sharp-walled sulphide veins and their host rocks. Figure 12A shows the distribution of rock types along 5 of 10 transects and plots metal concentrations (vertical axes) against their distance from the center of the massive sulphide veins (horizontal axis) (See Appendix E for all transect and sample data). Although those diagrams are useful to show the high metal concentrations in sulphide veins relative to their host rocks, their vertical scales are skewed by the high metal concentration in the sulphide veins. This mask the variations in metal concentrations in the host rocks surrounding the veins. The same data

are plotted in Figure 12B without the metal concentrations in the veins. This decreases the range of metal concentrations, changes the scales of the vertical axes, and thus better displays the variations in metal concentrations in the host rocks.

Metal concentrations are highest in the sulphide veins, where they range from 0.5 – 7 ppm Au, 0.1 – 90 ppm Pt, 10 – 50 ppm Pd, 2-100 ppm Ag, 8 – 30 wt % Cu, and 0.08 – 10 wt % Ni. Metal concentrations are elevated in the alteration selvedges surrounding the veins but they drop abruptly to background values within 25 cm of the sulphide vein contacts. Spikes in metal concentrations, characterized by up to 5 ppm Au, 2.5 ppm Pt, 9 ppm Pd, 10 ppm Ag, 1 wt % Cu, 0.5 wt % Ni, are present regardless of rock types in the sampled ~4 m transects across the veins and their host rocks, and are also likely present at greater distances from the veins.

Spot samples from the low sulphide mineralization are compared to wall rock mineralization adjacent to sharp-walled vein plots in Figure 12 B. From this figure it is apparent that the metal tenor variations of the low sulphide mineralization sampled are comparable to the anomalous metal tenor of samples from country rock within 2m of the sharp-walled veins.

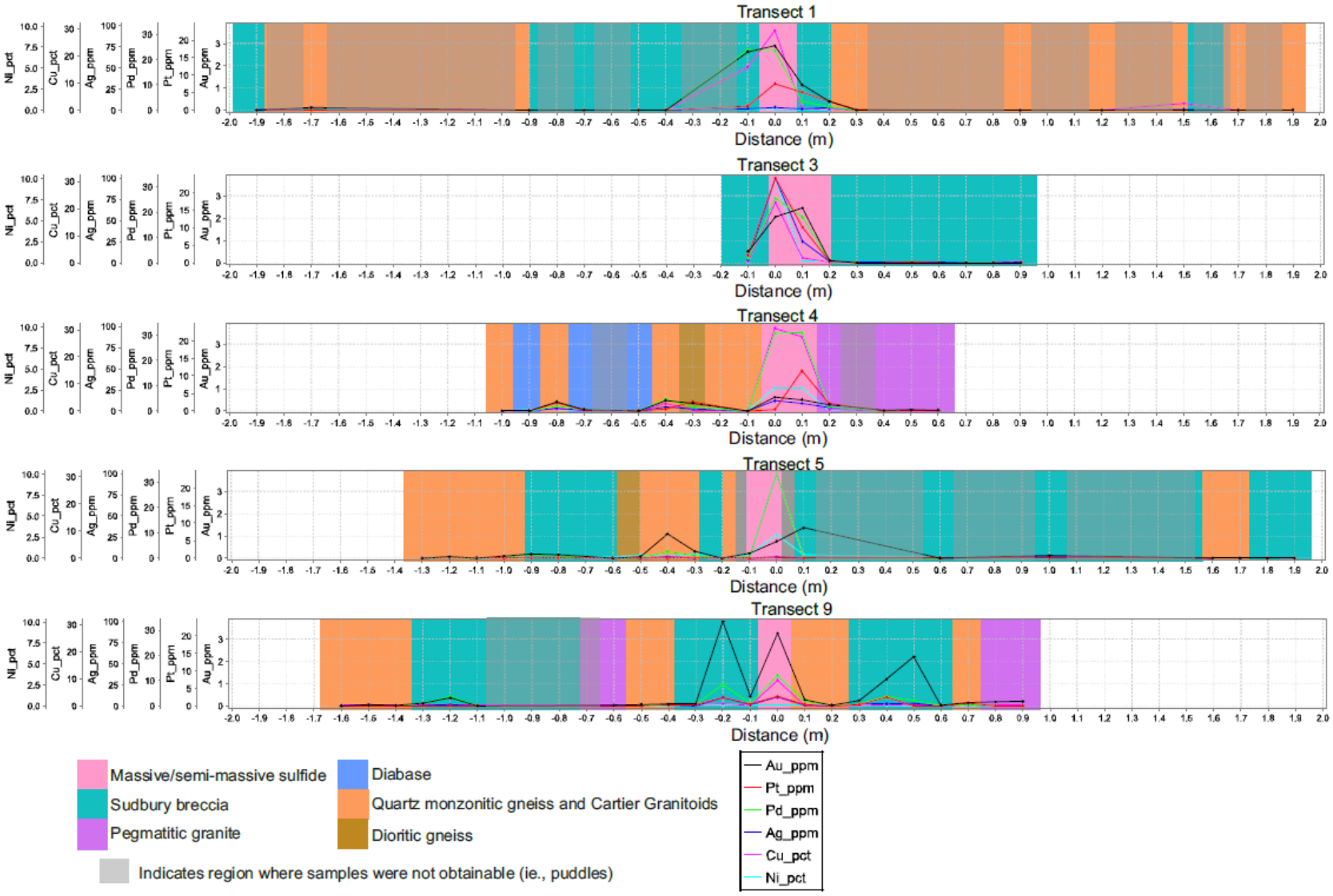
Transect 1
Transect 3
Transect 4
Transect 5
Transect 9
Ni_pct
Cu_pct
Ag_ppm
Pd_ppm
Pt_ppm
Au_ppm
Distance (m)
Massive/semi-massive sulfide
Sudbury breccia
Pegmatitic granite
Diabase
Quartz monzonitic gneiss and Cartier Granitoids
Dioritic gneiss
Indicates region where samples were not obtainable (ie., puddles)
Au_ppm
Pt_ppm
Pd_ppm
Ag_ppm
Cu_pct
Ni_pct

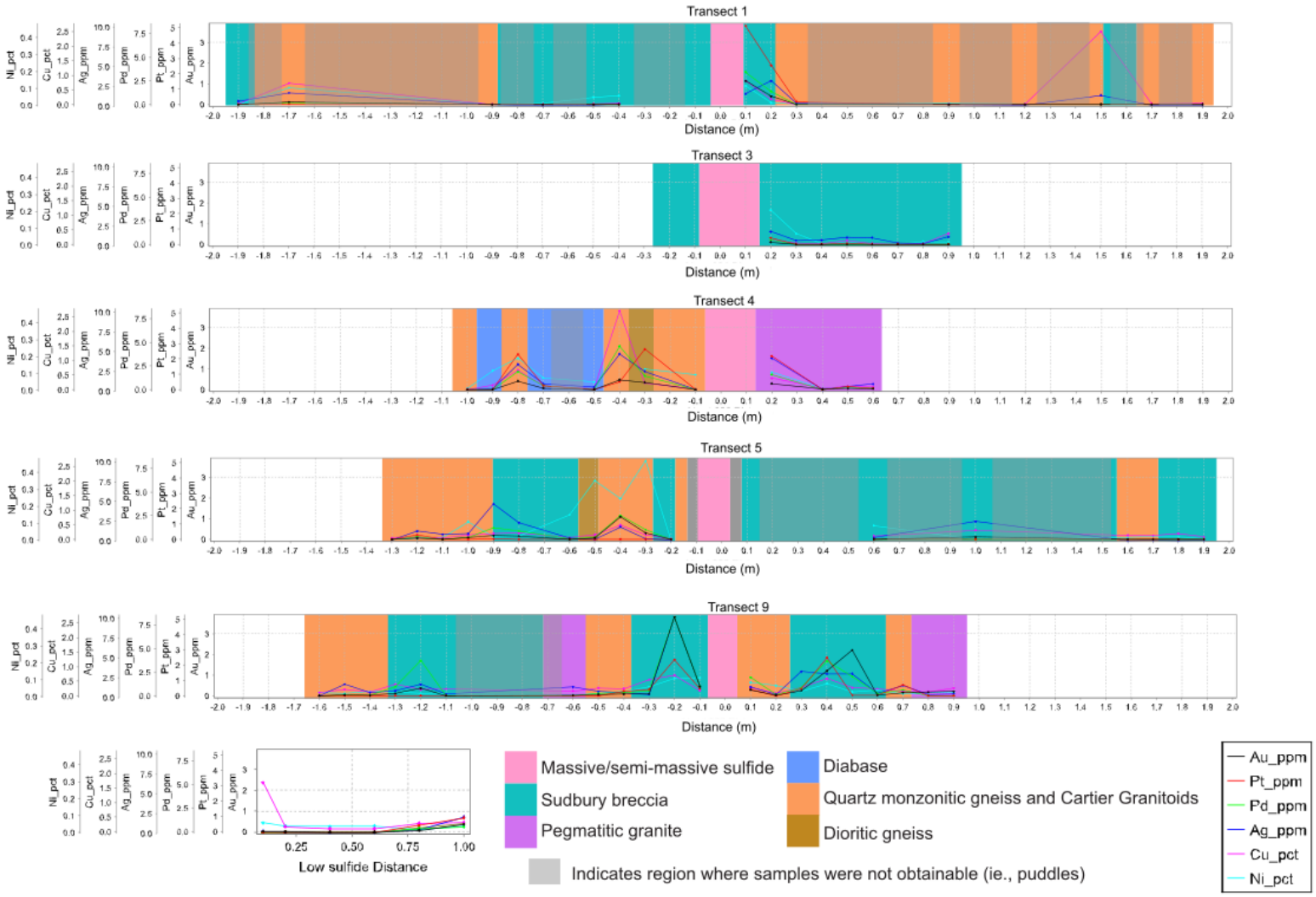

Figure 12: Plots of Ni, Ci, Ag, Pd, Pt, Au concentrations with distance in meter from massive sulphide vein sets 1,3,4,5 and 9 with metal concentration superposed on rock type: A) Displays metal concentrations with massive sulphide veins included. B) Excludes metal concentration in sulphide veins and also presents values for low sulphide mineralization with imposed distance values.

Palladium concentrations in the sharp-walled veins and their host rocks are less variable than Pt concentrations. This variability is also observed in more than 6,400 drill core samples submitted prior to mining. Platinum concentrations typically range between <1 to 10 ppm with peaks of 750-1000 ppm in samples collected in the lower pit levels, whereas Pd concentrations consistently range between 2 and 35 ppm. No vertical metal zonation is observed, but Pt/Pd ratios are higher in low-sulphide high-PGE mineralized zones (Pt/Pd ≈ 1.3) than in the sharp-walled sulphide veins (Pt/Pd ≈ 0.53). The more extreme variations in Pt concentrations is likely a nugget effect as Pt is mostly held in sperrylite and rare (Pt, Pd) bismuth tellurides (Pentek et al., 2008). Nickel concentration patterns differ slightly from those of the other metals. They remain elevated over distances of 0.75 meter from sulphide vein contacts, and peak Ni concentrations in the host rocks do not correspond to peaks in other metals.

Oxidation along the Chisel Creek Fault suggests that the fault acted as a conduit for the infiltration of fluids. Samples collected across the faults yielded negligible metal values, suggesting that the fault played no role in the remobilization of metals.

2.5 Discussion

2.5.1 Emplacement of the sharp-walled sulphide veins

Sharp-walled sulphide veins and low sulphide mineralization in the footwall environment at Sudbury are interpreted to have formed by magmatic or hydrothermal processes or a combination of the two (Naldrett et al., 1982; Li and Naldrett, 1993; Jago et al., 1994; Mungall and Brenan, 2003; Molnar et al., 2001; Pentek et al., 2008) The sharp-walled veins at the Broken Hammer deposit are divided into five groups based on orientation. Apart from slight differences in their widths along jogs and bends, they are similar in sulphide and hydrous silicate mineral

composition, suggesting that the veins were emplaced during a single event although the fractures hosting them may have formed during more than one event. Fractures may represent pre-existing faults that were reactivated during the emplacement of the veins, or neoformed faults that formed during the emplacement of the veins. Their formation and reactivation are discussed below.

Two prominent fault systems, the Onaping and Murray fault systems, existed before the Sudbury impact event (Spray et al., 2004). The Onaping Fault System comprises NNW-trending faults that offset the SIC by less than 0.5 km in the North Range but were likely active in the Paleoproterozoic before the impact as they displace magnetic units beneath the SIC and South Range without corresponding offset of the overlying SIC (Spray et al., 2004). The Murray Fault System consists of ENE-trending, listric, normal faults that formed during rifting of the southern margin of the Archean Superior craton and deposition of the 2.45 Ga to 2.2 Ga Huronian Supergroup as a rift-drift to passive continental margin sequence (Bennett et al., 1991; Young et al., 2001). Outliers of Huronian sedimentary rock located north of the SIC, were deposited in and are now preserved by, paleo rift valleys that transected the Superior craton (Roussell and Long, 1998; Long, 2004; Riller, 2005). This suggests that faults related to this extension event affected basement rocks over a distance of at least 40 km from the Superior-Southern Province boundary. Pre-impact fractures at other terrestrial craters were reactivated during the cratering process (Osinski and Spray, 2005; Kenkmann et al., 2014) and at Meteor Crater in Arizona, they even controlled the shape of the crater (Kumar and Kring, 2008). At Sudbury, these earlier extensional faults may have been reactivated during impact (Spray et al., 2004), but fractures or faults belonging to this fault system have not been recognized at Broken Hammer and surrounding rocks. Near Broken Hammer, the Joe Lake fault is expressed by a NNW-trending topographic lineament similar in orientation to the Onaping fault system (Spray et al, 2004) and was also intersected in

drill holes. The SIC terminates against the fault so the fault may have been present prior to the impact and was reactivated during and after the impact but conclusive evidence on the slip movement history of the fault is lacking.

At Sudbury, post-impact faulting in the basement rocks below the impact melt sheet (SIC) may be due to isostatic readjustment (Wichman and Schultz, 1993) or differential loading of the crater floor. The latter is caused by variations in the thicknesses of the impact melt sheet (Coleman, 1905) and overlying fall-back breccias, pyroclastic flows and sedimentary rocks of the Whitewater Group. The formation of new faults and the reactivation of pre- or syn-impact faults by differential overburden loading have been suggested by Tsikalas and Faleide (2007) for the Bosumtwi (Ghana) and Mjølnir (Barents Sea, Norway) craters, which are buried under thick sequences of sedimentary rocks. If new faults were to have formed by post-impact loading, Anderson's (1951) theory of faulting predicts that the faults would be inclined at ~30° to the maximum principal stress axis (σ_1) and would contain the intermediate principal stress axis (σ_2). σ_1, which represents the weight of the overlying rocks, would be vertical and σ_2 and σ_3 would be horizontal. As Andersonian faulting is a plane-strain deformation (Aydin and Reches, 1982), the orientation of the faults would not be affected by σ_2 and conjugate fault sets would intersect parallel to the σ_2 direction. Three-dimensional strain conditions are more common in nature and under these conditions, multiple fault sets form during a single deformation event (Oertel, 1965; Reches and Dietrich, 1983). Symmetrical orthorhombic fault patterns are produced if the principal stresses and strains are coaxial, resulting in fault intersections that are oblique, albeit close in orientation, to σ_2 (Reches, 1978, 1983; Aydin and Reches, 1982; Reches and Dietrich, 1983; Blenkinsop, 2008). For more general deformations, conjugate fault intersections would be oblique to σ_2 while others would contain it (Blenkinsop, 2008).

On stereonet plots, the great circles representing the main vein orientations at Broken Hammer intersect within a small circle with a radius of 25° (Fig. 6). The center of the circle represents the average orientation of the vein intersection lines (60° towards 220°), which also represents the mean orientation of σ_2 if the veins occupy fractures that formed during a single deformation event. The SIC-basement contact can be restored to its original horizontal orientation by a rotation of 30° around an east-west horizontal axis, i.e. the dip and strike of the SIC-basement contact in the North Range. Rotation of the veins by the same angle rotates their average intersection line and σ_2 to a plunge of 48° towards 200°. The rotated veins are subvertical and shallowly to moderately dipping. Their dips and the deviation of σ_2 and σ_1 from horizontal and vertical, respectively, are inconsistent with the formation of the faults during post-impact vertical loading and readjustment of the crater floor.

The post-impact Penokean and Yavapai orogenies deformed the Sudbury impact structure into a north-verging and doubly-plunging synclinorium which is offset along its south limb by reverse faults and shear zones of the South Range shear zone system. Although the effects of those orogenies are less pronounced in the North Range and north limb of the Sudbury structure, the tilting of SIC-basement contacts to its present 30°-35° southerly dip was presumably accompanied by the formation of fractures and faults in the Archean basement rocks. The onset of these orogenic events was preceded by the post impact burial of the Sudbury structure under sedimentary rocks of the Whitewater Group. The deposition of laminated carbonaceous mudstone of the ~600-m-thick Onwatin Formation and turbiditic sandstone of the >850-m-thick Chelmsford Formation lasted 0.6 to 600 Ma assuming modern depositional rates of 0.001 – 0.060 m/Ka for the Onwatin Formation (Long, 2004; Mukwakwami et al., 2014). As these formations conformably overlie the

Sudbury structure and were deformed during these orogenies, this suggests that tectonic reworking and deformation of the Sudbury structure began at least 0.6 Ma after the impact.

Sulphide melts segregated and accumulated at the base of the SIC as the SIC cooled from its initial temperature of 1800°C to its solidus temperature of ~1100°C. Numerical modeling by Prevec and Cawthorne (2002) suggests that cooling of the SIC to its solidus temperature took 97,000 years by conductive heat loss and 56,000 years by convective heat loss, assuming an initial temperature of 300°C for the basement rocks. Using different parameters (i.e. higher basement rock temperatures), Ionov and Deutsch (1999) calculated a longer time interval of 350,000 years to 500,000 years for conductive cooling of the SIC to its solidus temperature. Thermomechanical erosion and assimilation of the footwall basement rocks (Prevec and Cawthorn 2002) and phreatomagmatic explosive volcanism due to interaction of the impact melt sheet with infiltrating seawater from a basin above the melt sheet and the Onaping Formation (Ames et al. 2002; Grieve et al. 2010) increased heat loss both at the base and top of the impact melt sheet resulting in faster cooling rates for the impact melt sheet. As deformation of the SIC began at least 0.6 Ma after the impact, sulphides had accumulated at the base of the SIC and were injected in footwall fractures less than 350,000 years to 500,000 years after the impact and therefore before the deformation of the SIC and formation of related fractures in the basement rocks.

Large impacts produce large volumes of highly fractured rocks and breccias within damage zones that extend for several km below the crater floor (Ahrens et al., 2002). In projectile impact experiments, four types of fractures form during impact: concentric fractures roughly parallel to the impact cavity, radial fractures extending away from the impact cavity, conical fractures dipping away from the impact cavity, and near-surface spall fractures (Polanskey and Ahrens, 1990; Ai and Ahrens, 2004). These reproduce fractures patterns observed around bowl-shaped, terrestrial,

simple craters with diameters of less than 4 km. For example, the basaltic flow rocks surrounding the Lonar crater, India, are crossed by concentric fractures, conjugate radial fractures, conical fractures, and flow-parallel shallowly-dipping fractures (Kumar, 2005). For larger complex crater, the outward excavation flow during the growth of the transient crater causes shear and tensile fracturing, and the reversal of the flow during the modification of the crater reactivates these fractures and causes new fracturing (Collins et al., 2004). During crater modification, the centre of the crater is uplifted along converging thrust faults, forming a central uplift that rises above the crater floor as the rim of the crater collapses along listric normal faults (Kenkmann, 2003; Kenkmann et al., 2005; Osinski and Spray, 2005). The inward and downward displacement of fault blocks during rim collapse produces radial transpression ridges or positive flower structures consisting of oblique-slip and reverse faults (Kenkmann and von Dalwigk, 2000). Additional fractures form during downward collapse of the central uplift (Kenkmann et al., 2014).

The multiple fractures that form and are reactivated during impact provide conduits for the downward injection of impact and sulphide melts. Paleostress conditions for the formation of new faults and the reactivation of pre-existing inherited faults can be typically determined from measurements of fault slip directions and shear senses (Angelier 1984, 1994).

In this study, slickenlines representing the fault slip directions have been measured along a few vein margins but as they overprint the veins (discussed below), the paleostress conditions could not be determined using paleostress inversion methods and simple geometrical considerations are used to constrain how the veins were emplaced. The orientation of all measured veins is shown in Figure 6. The distribution of their poles can be approximated by a great circle (Fig. 6E) whose pole plunges 60° towards 220° parallel to the common intersection line between the veins, and a closer fit is obtained with two great circles (Fig. 6F) whose poles plunge 60°

towards 290° and 55° towards 185°. Restoration of the SIC-basement contact to the horizontal rotates the poles to the great circles to shallow to moderate plunges and the veins to shallow to steep dips. This suggests that fractures with shallow to steep dips were reactivated and dilated during post-impact isostatic stabilization of the crater floor as metal-rich magmatic-hydrothermal fluids flowed along the fractures and deposited the sulphide veins, or downward migrating sulphide melts from the base of the SIC wedged their way and forced the opening of the fractures due to their higher density relative to the surrounding basement rocks.

At other footwall deposits in the North and East Ranges of the Sudbury structure, sharp-walled veins are subparallel to the SIC contact (Ames et al, 2007), strike NE and dip to the SE at the Morrison deposit (Nelles, 2012), and strike SE and dip to the SW and NW at the Capre deposit (Tremareva, 2017). NE- and SE-striking veins are present at the Broken Hammer deposit but contact-parallel veins are scarce. The latter were likely emplaced in concentric fractures that formed during the excavation or modification stages of the impact. The concentric fractures were connected to the SIC by more steeply dipping fractures and were forced open either by high-pressure hydrothermal fluids or by hydrostatic pressures exerted by the denser sulphide melts filling the more steeply dipping fractures (see Appendix F for schematic emplacement model).

Subsequent bulk shortening during post-impact orogenic events resulted in the formation of steeply dipping and shallowly dipping faults including the Chisel Creek Fault, the emplacement of quartz breccia veins, and the formation of slickenlines along sulphide veins. As the veins are not otherwise ductilely deformed, this suggests that these brittle structures formed below the brittle-ductile transition temperatures (~250°C-300°C) of chalcopyrite (Kelly and Clark, 1975; Cox et al., 1981; Cox, 1987; Marshall and Gilligan, 1987, 1993).

2.5.2 Geochemical variations and alteration history at Broken Hammer

The high PGE concentrations in the sulphide veins and their abrupt drop within 25 cm in the vein wallrocks suggest that the addition of metals in the footwall basement rocks is linked to the emplacement of the sulphide veins. The low-sulphide high-PGE mineralization has been interpreted to have formed: 1) by late magmatic PGE-rich fluids that were released during the crystallization of the sharp-walled sulphide veins and deposited PGM in the footwall environment (Li and Naldrett, 1993), with possible redistribution of the PGE by subsequent hydrothermal events (Jago et al., 1994; Mungall and Brenan, 2013); 2) by mixed magmatic and external hydrothermal fluids, or the latter only, which leached the PGEs and other metals from the magmatic sulphide veins and deposited the metals in the footwall rocks to form the low-sulphide high-PGE mineralization (Li and Naldrett, 1993; Morrison et al., 1994; Hanley et al., 2005, 2011; Dare et al., 2010, Tuba et al., 2014).

Both models involve hydrothermal distribution and/or re-distribution during or after the emplacement of the sharp-walled sulphide veins. At Broken Hammer, the presence of clasts or fragments of quartz-chlorite within the massive sulphide veins suggests that hydrothermal fluids migrated along and sealed these fractures prior to the emplacement of the sulphide veins. Hydrothermal fluids exsolved from the crystallizing sulphide melts, or directly involved in the transport in solution of the metals and formation of the sulphide veins, may have deposited epidote, actinolite and quartz within the wall rocks and along the selvedges and terminations of the sulphide veins. Alternatively, the presence of euhedral epidote crystals encased within the massive sulphide veins and the similarity in the mineralogy of the vein selvedges and epidote-actinolite -quartz alteration patches in the footwall rocks, suggest that the emplacement of the sulphide veins may have been preceded by the migration of high-temperature fluids which altered the footwall rocks, deposited epidote, actinolite, and quartz along the margins and tips of

the fractures, and entrained and incorporated these minerals within the veins during their crystallization. Chalcopyrite and PGM, which are associated with epidote-actinolite-quartz in the sulphide vein selvedges and with alteration patches in the footwall rocks, may have been deposited by those high-temperature fluids, or were leached from the sulphide veins and transported in the footwall environment by subsequent hydrothermal fluids during chloritisation of the footwall rocks and the formation of the late Ni-rich chlorite proximal to sulphide veins. Thus, the low sulphide zones may have formed either from a high-temperature fluid that preceded the emplacement of the sulphide veins and infiltrated the footwall rocks, or from late hydrothermal remobilisation of these metals from the sulphide veins to the footwall rocks during pervasive chloritisation of the footwall rocks.

2.6 Conclusions

The main sets of sharp-walled sulphide veins at the Broken Hammer deposit typically dip steeply with strike orientations within the NE and SW quadrants, with the exception of one vein set striking SE. They define a common intersection line that plunges 60º towards 220º, parallel to the trend and plunge of mineralization. The veins were emplaced in fractures that formed during the impact and were reactivated during post-impact stabilization of the crater floor prior to regional orogenesis. The reactivated fractures acted as conduits for the migration of hydrothermal fluids and were sealed by quartz and chlorite that were later incorporated as clasts in the sulphide veins. Reactivation and/or dilation of the fractures allowed for emplacement of the sulphide veins which was syn-genetic with the epidote-actinolite-quartz alteration association. Low-sulphide high-PGE mineralization in the footwall rocks was either syn-genetic with this alteration or formed later as subsequent hydrothermal fluids leached Ni and PGM's from the sulphide veins and distributed them within the footwall during the formation of Ni-bearing chlorite. During post-impact tectonic

events, the vein-hosting fractures were reactivated at least once more at lower temperatures (<250°C) as evidenced by slickenlines along the vein margins and offsetting of mineralization.

2.7 References

Abel, M., (1981) The structure of the Strathcona Mine copper zone; *Canadian Institute of Mining and Metallurgy*, **Bulletin 74**, p 89-97

Ahrens, T., Xia, K., & Coker, D., (2002), Depth of cracking beneath impact craters: New constraint for impact velocity, *AIP Conference Proceedings*, **volume 620 no 1**, p 1393-1396

Ai, H., & Ahrens, T., (2004), Dynamic tensile strength of terrestrial rocks and application to impact cratering, *Meteoritics & Planetary Science*, **volume 39 no 2**, p 233-246

Ames, D., Golightly, J., Lightfoot, P., Gibson, H., (2002) Vitric compositions in the Onaping Formation and their relationship to the Sudbury Igneous Complex, Sudbury structure, *Economic Geology*, **Volume 97 no 7**, p 1541-1562

Ames, D., Davidson, A., Buckle, J., & Card, K., (2005) Geology, Sudbury bedrock compilation, Ontario, *Geological Survey of Canada*, **Open File Report 4570(2)**

Ames, D., & Farrow, C., (2007) Metallogeny of the Sudbury mining camp, Ontario, *Mineral Deposits of Canada: A Synthesis of Major Deposit-Types, District Metallogeny, the Evolution of Geological Provinces, and Exploration Methods: Geological Association of Canada, Mineral Deposits Division*, **Special publication No 5**, p 329-350

Anderson, E., (1951), The dynamics of faulting and dyke formation with applications to Britain, *Hafner Pub Co*

Angelier, J., (1984), Tectonic analysis of fault slip data sets, *Journal of Geophysical Research: Solid Earth*, **volume 89 B7**, p 5835-5848

Angelier, J., (1994), Fault slip analysis and paleostress reconstruction, *Continental deformation*, p 53-100

Aydin, A., & Reches, Z., (1982), Number and orientation of fault sets in the field and in experiments, *Geology*, **volume 10 no 2**, p 107-112

Bennett, G., Dressler, O., and Robertson, A., (1991), The Huronian Supergroup and associated intrusive rocks, *Geology Ontario, edited by P.C., Thurston, R. H., Williams, R. H. Sutcliffe, and G. M. Stott*, **Ontario Geological Survey Special Volume 4**, p 549-591

Bailey, J., Lafrance, B., McDonald, A., Federowich, J., Kamo, S., Archibald, D., (2004) Mazatzal-Labradorian-age (1.7-1.6 Ga) ductile deformation of the South Range Sudbury impact structure at the Thayer Lindsley Mine, Ontario, *Canadian Journal of Earth Sciences*, **Volume 41**, p 1491-1505

Bleeker, W., Kamo, S., Ames, D., Davis, D., (2015) New field observations and U-Pb ages in the Sudbury area: toward a detailed cross-section through the deformed Sudbury Structure: *Geological Survey of Canada*, **Open File 7856, Targeted geoscience initiative 4: Canadian Nickel-Copper-Platinum Group Elements-Chromium Ore Systems – Fertility, Pathfinders, New and Revised Models**, p 151-166

Blenkinsop, T., (2008), Relationships between faults, extension fractures and veins, and stress, *Journal of Structural Geology*, **volume 30 no 5**, p 622-632

Coats, C., & Snajdr, P., (1984) Ore deposits of the North Range, Onaping-Levack area, Sudbury, *Ontario Geological Survey*, **Special Volume 1**, p 327-346

Coleman, A.P., (1905). The Sudbury Nickel Field. Ontario Bureau of Mines, Annual Report for 1905, Volume 14, Part 3, 188pp.

Collins, G., Melosh, H., & Ivanov, B., (2004), Modelling damage and deformation in impact simulations, *Meteoritics & Planetary Science*, **volume 39 no 2**, p 217-231

Corfu, F., Andrews, A., (1986) A U-Pb age for mineralized Nipissing diabase, Gowganda, Ontario, *Canadian Journal of Earth Sciences*, **Volume 23**, p 107-109

Cox, S., Etheridge, M., & Hobbs, B., The experimental ductile deformation of polycrystalline and single crystal pyrite, *Economic Geology*, **volume 76 no 8**, p 2105-2117

Cox, S., (1987), Flow mechanisms in sulphide minerals, *Ore Geology Reviews*, **volume 2 no 1-3**, p 133-171

Dare, S., Barnes, S., Prichard, H., & Fisher, P., (2010), Chalcophile and platinum-group element (PGE) concentrations in the sulphide minerals from the McCreedy East deposit, Sudbury, Canada, and the origin of PGE in pyrite, *Mineralium Deposita*, **volume 46 no 4**, p 381-407

Dare, S., Barnes, S., Prichard, H., & Fisher, P., (2014), Mineralogy and geochemistry of Cu-rich ores from the McCreedy East Ni-Cu-PGE deposit (Sudbury, Canada): Implications for the behaviour of platinum group and chalcophile elements at the end of crystallization of a sulphide liquid, *Economic Geology*, **volume 109 no 2**, p 343-366

Dence. M. R., 1964, A comparative structural and petrographic study of probable Canadian meteorite craters, Meteorics, V. 2, p. 249-270

Deutsch, A., Grieve, R., Avermann, M., Bischoff, L., Brockmeyer, P., Buhl, D., Lakomy, R., Muller-Mohr, V., Ostermann, M., Stoffler, D., (1995), The Sudbury structure (Ontario, Canada): a tectonically deformed multi-ring impact basin, *Geol Rundsch*, **Volume 84**, p 697-709

Dietz, R.S., Butler, L.W., 1964. Shatter-cone orientation at Sudbury, Canada. Nature 204, 280-281.

Dressler, B.O., 1984. The effects of the Sudbury event and the intrusion of the Sudbury Igneous Complex on the footwall rocks of the Sudbury structure. In: Pye, E.G., Naldrett, A.J., Giblin, P.E. (Eds.), The geology and ore deposits of the Sudbury Structure. Ontario Geological Survey Special Volume 1, pp. 97-136.

Dombard, A., and Gillis, J., (2001) Testing the viability of topographic relaxation as a mechanism for the formation of lunar floor-fractured craters, *Journal of Geophysical Research*, Volume 106, p 27901-27909

Dreuse, R., Doman, D., Santimano, T., Riller, U., (2010), Crater floor topography and impact melt sheet geometry of the Sudbury impact structure, Canada, *Terra Nova*, **volume 22 no 6**, p 436-469

Farrow, C., Watkinson, D., and Jones, P., (1994), Fluid inclusions in sulphides from north and south range Cu-Ni-PGE deposits, Sudbury structure, Ontario, *Economic Geology*, **volume 89 no 3**, p 647-655

Farrow, C., Lightfoot, P., (2002), Geology, geochemistry, and mineralogy of the Worthington offset dike: A genetic model for offset dike mineralization in the Sudbury Igneous Complex, *Economic Geology*, **volume 97 no 7**, p 1419-1446

Farrow, C., Everest, J., King, D., Jolette, C., (2005) Sudbury Cu-(Ni)-PGE systems: Refining the classification using McCreedy West mine and Podolsky project case studies: *Mungall JE (ed) Exploration for deposits of platinum-group elements*, **MAC short course series 35**, 163-180

French, B.M., (1998) Traces of Catastrophe: A Handbook of Shock-Metamorphic Effects in Terrestrial Meteorite Structures. *Lunar Planetary Institute* **LPI Contribution No 954**

Grieve, R., Stoffler, D., Deutsch, A., (1991) The Sudbury structure: Controversial or misunderstood, *Journal of Geophysical Research: Planets)* **Volume 96**, Issue E5, p 22753-22764

Grieve, R., Ames, D., Morgan, J., Artemieva, N., (2010) The evolution of the Onaping Formation at the Sudbury impact structure, *Meteorics & Planetary Science*, **Volume 45**, p. 759-782

Hall, J., Solomon, S., Head, J., (1980) Lunar floor-fractured craters: The relative importance of isostatic relaxation and uplift by volcanic intrusion, *Lunar and Planetary Science* Volume 11, p 385-387

Hanley, J., Mungall, J., Pettke, T., Spooner, E., & Bray, C., (2005), Ore metal redistribution by hydrocarbonbrine and hydrocarbon-halide melt phases, North Range footwall of the Sudbury Igneous Complex, *Mineralium Deposita*, **volume 40 no 3**, p 237-256

Hanley, J., Ames, D., Barnes, J., Sharp, Z., Guillong, M., (2011) Interaction of magmatic fluids and silicate

melt residues with saline groundwater in the footwall of the Sudbury Igneous Complex, Ontario, Canada: new evidence from bulk rock geochemistry, fluid inclusions and stable isotopes: *Chemical Geology*, **Volume 281**, p 1-25

Heaman, L., (1997) Global mafic magmatism at 2.45 Ga: Remnants of an ancient large igneous province?: *Geology*, **Volume 24**, p 299-302

Ivanov, B., & Deutsh, (2009), Numerical modeling of the largest terrestrial meteorite craters, *Solar System Research*, v 39.P 381-409

Jago, B., Morrison, G., Little, T., (1994), Metal zonation patterns and microtextural evidence for alkali- and halogen-rich fluids in the genesis of the Victor Deep and McCreedy East footwall copper orebodies, Sudbury Igneous Complex, *Ontario Geological Survey*, **Special volume 5**, p 65-75

Kelly, W., & Clark, B., (1975), Sulphide deformation studies; III, Experimental deformation of chalcopyrite to 2,000 bars and 500 degrees C, *Economic Geology*, **volume 70 no 3**, p 431-453

Kenkmann, T., & Von Dalwigk, I., (2000), Radial transpression ridges: A new structural feature of complex craters, *Meteoritics & Planetary Science*, **volume 35 no 6**, p 1189-1201

Kenkmann, T., (2003), Dike formation, cataclastic flow, and rock fluidization during impact cratering: An example from the Upheaval Dome structure, Utah, *Earth and Planetary Science Letters*, **volume 214 no 1-2**, p 43-58

Kenkmann, T., Jahn, A., Scherler, D., & Ivanov, B., (2005), Structure and formation of a central uplift: A case study at the Upheaval Dome impact crater, Utah, *Large meteorite impacts III*, p 85-115

Kenkman, T., Poelchau, M., & Wulf, G., (2014), Structural geology of impact craters, *Journal of Structural Geology*, **volume 62**, p 156-182

Krogh, T., Davis, D., Corfu, F., (1984) Precise U-Pd zircon baddeleyite ages for the Sudbury area, *Ontario Geological Survey*, **Special Volume 1**, p 431-446

Krogh, T., Kamo, S., Bohor, B., (1996) Shock metamorphosed zircons with correlated U-Pb discordance and melt rocks with concordant protolith ages indicate an impact origin for the Sudbury structure, *Geophysical Monograph-American Geophysical Union*, **95**, p 343-354

Kumar, P., (2005), Structural effects of meteorite impact on basalt: Evidence from Lonar crater, India, *Journal of Geophysical Research: Solid Earth*, **volume 110 B12**

Kumar, P., & Kring, D., (2008), Impact fracturing and structural modification of sedimentary rocks at Meteor Crater, Arizona, *Journal of Geophysical Research: Planets*, **volume 113 no E9**

Lafrance, B., Legault, D., Ames, D., (2008) The formation of the Sudbury breccia in the North Range of the Sudbury impact structure: *Precambrian Research*, **Volume 165**, p 107-119

Li, C., & Naldrett, A., (1993), High chlorine alteration minerals and calcium-rich brines in fluid inclusions from the Strathcona deep copper zone, Sudbury, Ontario, *Economic Geology*, **volume 88 no 7**, p 1780-1796

Long, D., (2004) The tectonostratigraphic evolution of the Huronian basement and the subsequent basin fill: Geological constraints on impact models of the Sudbury event: *Precambrian Research*, **Volume 129**, p 203-233

Marshall, B., & Gilligan, L., (1987), An introduction to remobilization information from ore-body geometry and experimental considerations, *Ore Geology Reviews*, **volume 2 no 1-3**, p 87-131

Marshall, B., & Gilligan, L., (1993), Remobilization, syn-tectonic processes and massive sulphide deposits, *Ore Geology Reviews*, **volume 8 no 1-2**, p 39-64

Meldrum, A., Abdel-Rahmen, A., Martin, R., Wodicka, N., (1997) The nature, age and petrogenesis of the Cartier batholith, northern flank of the Sudbury structure, Ontario, Canada: *Precambrian Res*, **Volume 82**, p 265-285

Michel, P., and Morbidelli, A., 2013 Population of impactors and the impact cratering rate in the inner Solar System, in Osinski, G., and Pierazzo, E., ed., Impact cratering processes and products, 1st ed.: West Sussex, Blackwell Publishing, p. 60-75

Molnar, F., Watkinson, D., & Everest, J., (1999), Fluid inclusion characteristics of hydrothermal Cu-Ni-PGE veins in granitic and metavolcanics rocks at the contact of the Little Stobie deposit, Sudbury, Canada, *Chemical Geology*, **154(1-4)**, p 279-301

Molnar, F., Watkinson, D., Jones, P., (2001), Multiple hydrothermal processes in footwall units of the North Range, Sudbury Igneous Complex, Canada, and implications for the genesis of vein-type Cu-Ni-PGE deposits, *Economic Geology*, **volume 96 no 7**, p 1645-1670

Morrison, G., Jago, B., White, T., (1994), Footwall mineralization of the Sudbury Igneous Complex, in Lightfoot, P., and Naldrett, A., *Proceedings of the Sudbury-Noril'sk Symposium, Ontario Geological Survey*, **Special volume 5**, p 119-132

Mukwakwami, J., Lafrance, B., Lesher, M. C., 2012. Back-thrusting and overturning of the southern margin of the 1.85 Ga Sudbury Igneous Complex at the Garson mine, Sudbury, Ontario. Precambrian Research **196-197**: 81-105.

Mukwakwami, J., Lafrance, B., Lesher, M. C., Tinkham, D.K., Rayner, N.M., Ames, D.E., 2014. Deformation, metamorphism and mobilization of Ni-Cu-PGE sulphide ores at Garson Mine, Sudbury. Mineralium Deposita **49**, 175-198**.**

Müller-Mohr, V., 1992. Breccias in the basement of a deeply eroded impact structure, Sudbury, Canada. Tectonophysics 216, 219-226.

Mungall, J., and Brennan, J., (2003), Experimental evidence for the chalcophile behaviour of the halogens, *Canadian Metallurgist*, **volume 41**, p 207-220

Naldrett, A., Innes, D., Sowa, J., & Gorton, M., (1982), Compositional variations within and between five Sudbury ore deposits, *Economic Geology*, **volume 77 no 6**, p 1519-1534

Nelles, E., Lesher, M., Lafrance, B., (2010), Mineralogy and textures of Cu-PGE orebodies. *SEG Conference*, Keystone, USA

Nelles, E., (2012), Genesis of Cu-PGE-rich footwall-type mineralization in the Morrison deposit, Sudbury, *Unpublished M. Sc (Doctoral dissertation, thesis)*, **Laurentian University**

Oertel, G., (1965), The mechanism of faulting in clay experiments, *Tectonophysics*, **volume 5 no 5**, p 343-393

Osinski, G., and Spray, J., (2005) Tectonics of complex crater formation as revealed by the Haughton Impact structure, Devon Island, Canadian High Arctic: *Meteoritics & Planetary Science*, **Volume 40**, p 1813-1834

Osinski, G., and Pierazzo, E., 2013 Impact cratering: processes and products, in Osinski, G., and Pierazzo, E., ed., Impact cratering processes and products, 1st ed.: West Sussex, Blackwell Publishing, p. 60-75

Pentek, A., Molnar, F., (2008) Footwall-type Cu-Ni-PGE Mineralization in the Broken Hammer area, Wisner Township, North Range, Sudbury structure: *Society of Economic Geologists*, **Volume 103**, p 1003-1028

Pentek, A., Molnar, F., Watkinson, D., Jones, P., Mogessie, A., (2011), Partial melting and melt segregation in footwall units within the contact aureole of the Sudbury Igneous Complex (North and East Ranges, Sudbury structure), with implications for their relationship to footwall Cu-Ni-PGE mineralization, *International Geology Review*, **volume 53 no 2**, p 291-325

Pentek, A., Molnar, F., Tuba, G., Watkinson, D., Jones, P., (2013), The significance of partial melting processes in hydrothermal low sulphide Cu-Ni-PGE mineralization within the footwall of the Sudbury Igneous Complex, Ontario, Canada, *Economic Geology*, **volume 108 no 1**, p 59-78

Petrus, J., Ames, D., Balz, K., (2015), On track of the elusive Sudbury impact: Geochemical evidence for a chondrite or comet bolide, *Terra Nova*, **Volume 27.1**, p 9-20

Prevec, S., and Cawthorn, G., (2002) Thermal evolution and interaction between impact melt sheet and footwall: A genetic model for the contact sublayer of the Sudbury Igneous Complex, Canada: *Journal of Geophysical Research*, **Volume 107**, p 1-14

Piercey P., Schneider, D., Holm, D., (2007), Geochronology of Proterozoic metamorphism in the deformed Southern Province, northern Lake Huron region, Canada, *Precambrian Research*, **volume 157 no 1-4**, p 127-143

Polanskey, C., & Ahrens, T., (1990), Impact spallation experiments: Fracture patterns and spall velocities, *Icarus*, **volume 87 no 1**, p 140-155

Raharimahefa, T., Lafrance, B., Tinkham, D., (2014), New structural, metamorphic, and U-Pb geochronological constraints on the Blezardian Orogeny and Yavapai Orogeny in the Southern Province, Sudbury, Canada, *Canadian Journal of Earth Sciences*, **volume 51 no 8**, p 750-774

Reches, Z., (1978), Analysis of faulting in three-dimensional strain field, *Tectonophysics*, **volume 47 no 1-2**, p 109-129

Reches, Z., (1983), Faulting of rocks in three-dimensional strain fields II. Theoretical analysis, *Tectonophysics*, **volume 95 no 1-2**, p 133-156

Reches, Z., & Dieterich, J., (1983), Faulting of rocks in three-dimensional strain fields I. Failure of rocks in polyaxial, servo-control experiments, *Tectonophysics*, **volume 95 no 1-2**, p 111-132

Riller, U., (2005) Structural characteristics of the Sudbury impact structure, Canada: Impact-induced versus orogenic deformation – A review: *Meteoritics & Planetary Science*, **Volume 109**, p 841-854

Rousell, D., (1975), The origin of foliation and lineation in the Onaping Formation and the deformation of the Sudbury Basin, *Canadian Journal of Earth Sciences*, **volume 12 no 8**, p 1379-1395

Rousell, D., & Long, D., (1998), Are outliers of the Huronian Supergroup preserved in structures associated with the collapse of the Sudbury Impact Crater?, *The Journal of Geology*, **volume 106 no 4**, p 407-420

Rousell, D., Fedorowich, J., Dressler, B., (2003), Sudbury breccia (Canada): A product of the 1850 Ma Sudbury event and host to footwall Cu-Ni-PGE deposits, *Earth-Science Reviews*, **volume 60 no 3-4**, p 147-174

Spray, J., Butler, H., Thompson, L., (2004) Tectonic influences on the morphometry of the Sudbury impact structure: Implications for terrestrial cratering and modeling, *Meteoritics & Planetary Science*, **Volume 39**, p 287-301

Spray, J., and Thompson, L., (1995), Friction melt distribution in a multi-ring impact basin, *Nature*, **volume 373 no 6510**, p 130

Stout, A., (2009), Geology, mineralogy, and geochemistry of the McCreedy East 153 Cu-Ni-PGE Deposit, Sudbury, Ontario, *Unpublished M. Sc (Doctoral dissertation, Thesis),* **Utrecht University**, p 1-39

Szabo, E., Halls, H., (2006). Deformation of the Sudbury structure: Paleomagnetic evidence from the Sudbury Breccia: *Precambrian Research*, **Volume 150**, p 27-48

Tschirhart, P. and Morris W.A., (2012). Grenville age deformation of the Sudbury impact structure: evidence from magnetic modeling of the Sudbury diabase dike swarm. *Terra Nova* **24**: 213-220

Thompson, L., and Spray, J., (1994), Pseudotachylytic rock distribution and genesis within the Sudbury impact structure, *Special Papers-Geological Society of America*, p 272-275

Thompson, L., and Spray, J., (1996), Pseudotachylyte petrogenesis: constraints from the Sudbury impact structure, *Contributions to Mineralogy and Petrology*, **volume 125 no 4**, p 359-374

Tsikalas, F., & Faleide, J., (2007), Post-impact structural crater modification due to sediment loading: An overlooked process, *Meteoritics & Planetary Science*, **volume 42 no 11**, p 2013-2029

Tremareva, V., (2017), 3D-visualization and structural evolution of Cu-Ni-PGE-rich sulphide veins of the Capre Footwall deposit, East Range, Sudbury, *Unpublished M. S.c (Doctoral dissertation, Thesis)*, **Technical University Bergakademie Freiberg**

Tuba, G., Molnar, F., Watkinson, D., Jones, P., Mogessie, A., (2010) Hydrothermal vein and alteration assemblages associated with low-sulphide footwall Cu-Ni-PGE mineralization and regional hydrothermal processes, North and East Ranges, Sudbury structure, Canada: *Society of Economic Geologists*, **Special Publication 15**, p 573-598

Tuba, G., Molnar, F., Ames, D., Pentek, A., Watkinson, D., Jones, P., (2014) Multi-stage hydrothermal processes involved in "low-sulphide" Cu(-Ni)-PGE mineralization in the footwall of the Sudbury Igneous Complex (Canada): Amy Lake PGE zone, East Range: *Miner Deposita*, **Volume 49**, p 7-47

Watkinson, D., (1999), Platinum-group element enrichment in Cu-Ni-rich sulphides from footwall deposits,

Sudbury Igneous Complex, Canada, *Chronique de la Recherche miniere*, **volume 67 no 535**, p 29-44

Wichmann, R., & Schultz, P., (1993), Floor-fractured crater models of the Sudbury Structure, Canada: Implications for initial crater size and crater modification, *Meteoritics*, **volume 28 no 2**, p 222-231

Young, G., Long, D., Fedo, C., Nesbitt, H., (2001) Paleoproterozoic Huronian Basin: Product of a Wilson Cycle punctuated by glaciations and meteorite impact: *Sedimentary Geology*, **Volume 141**, p 233-254

Young, G., (2015) Did prolonged two-stage fragmentation of the supercontinent Kenorland lead to arrested orogenesis on the southern margin of the Superior province? *Geoscience Frontiers*, **volume 15 no 6**, p 419-435

Appendix A – Stereographic Plots and Models of Individual Veins

All stereonets are plotted on an equal area net with contouring completed using the Kamb method with a significance value of 3. Stereonets are shown to highlight variation in strike and dip of the mineralized veins.

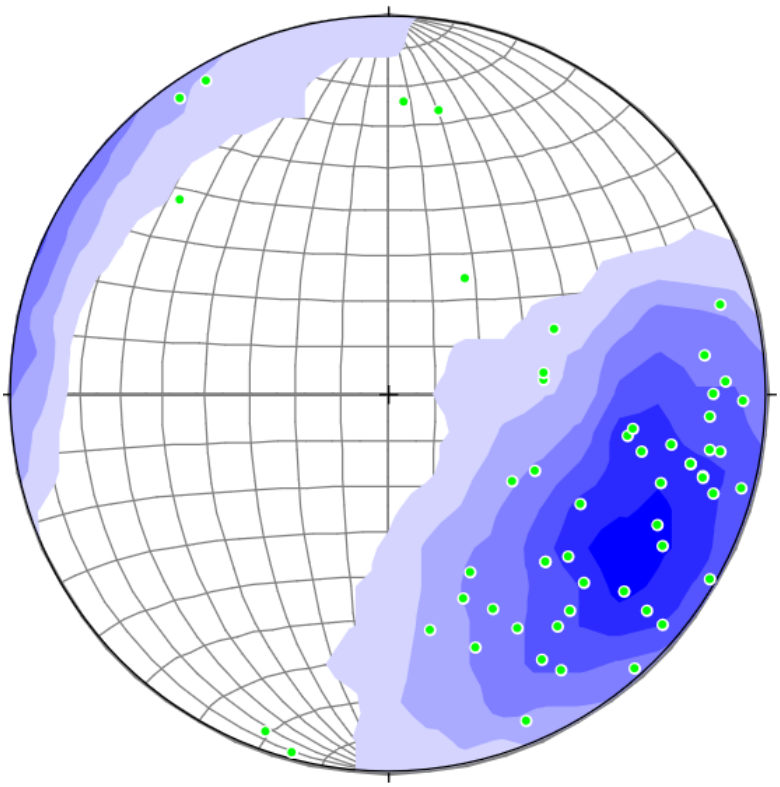

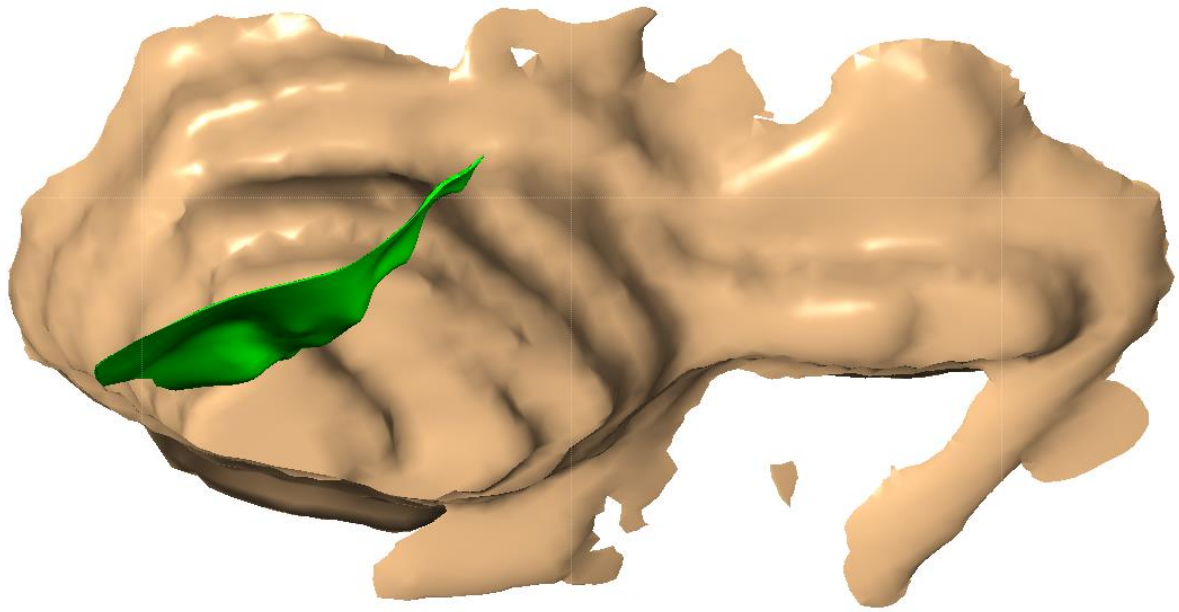

West vein 01 is by far the most examined of the veins at Broken Hammer and exhibits strong deviations in strike and dip. Located in the NW corner of the deposit.

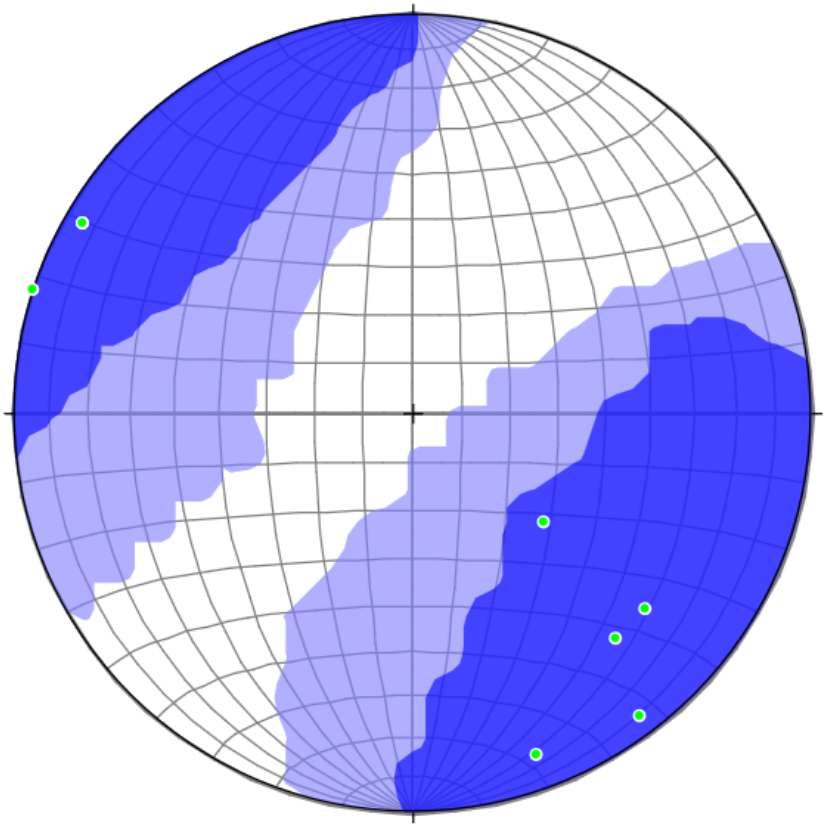

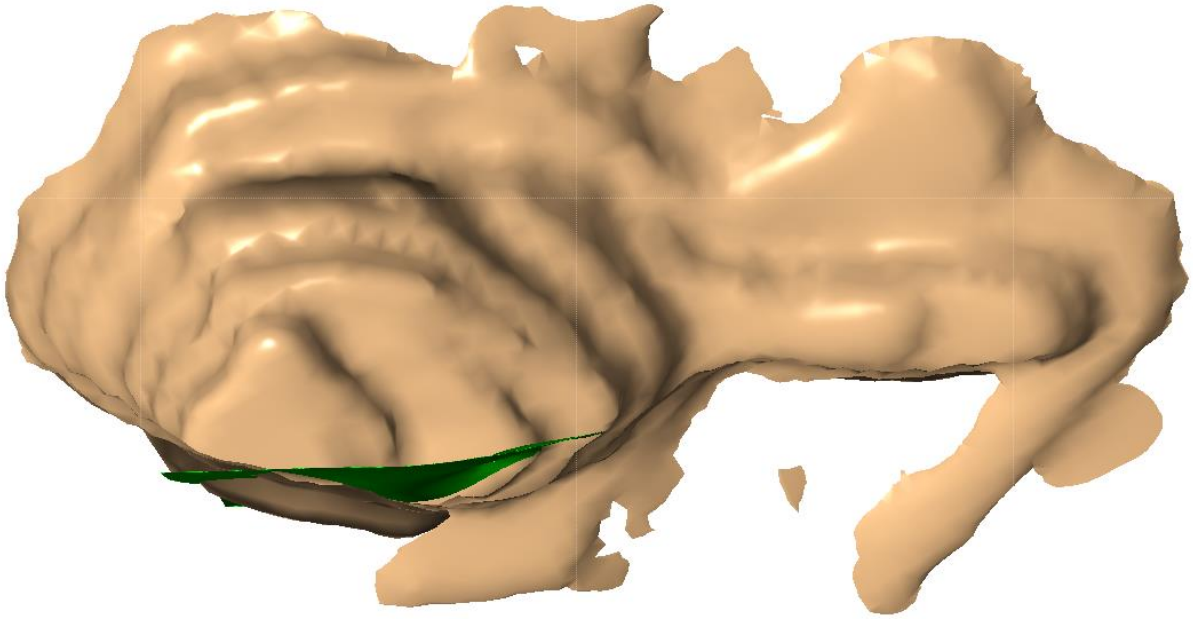

West vein 02 is sub-parallel to west vein 01 and seems to be a bounding structure that south of which there is no mineralization.

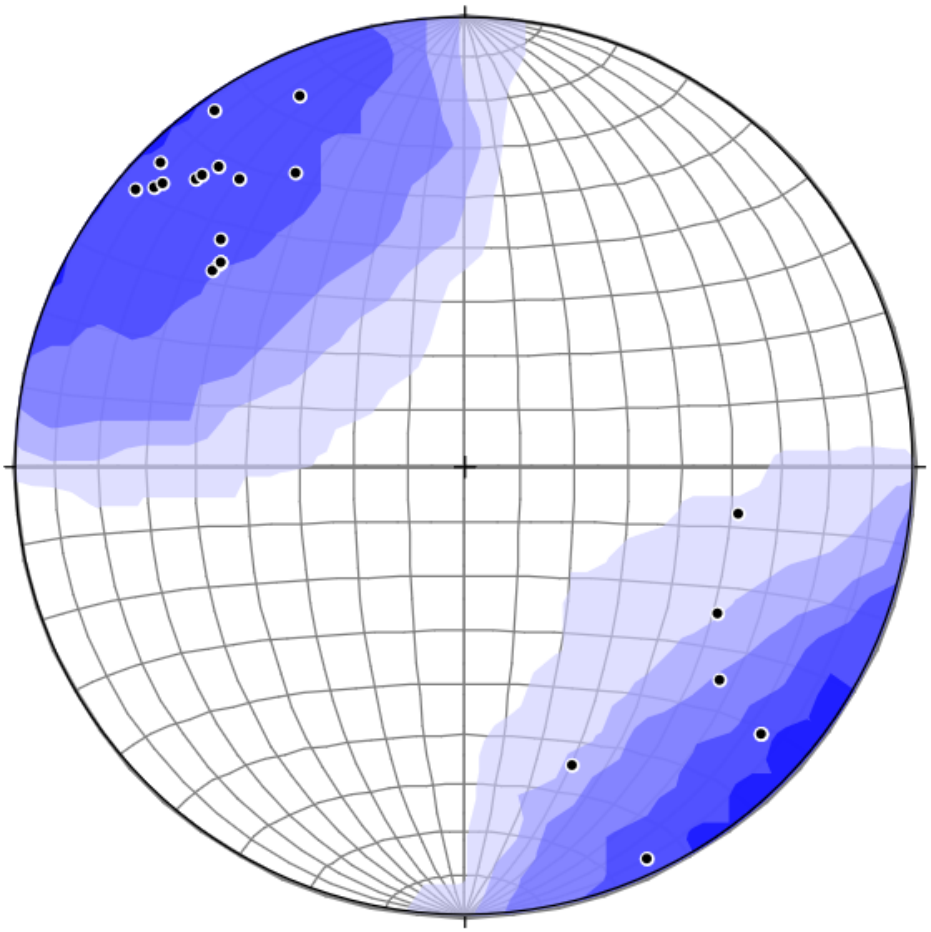

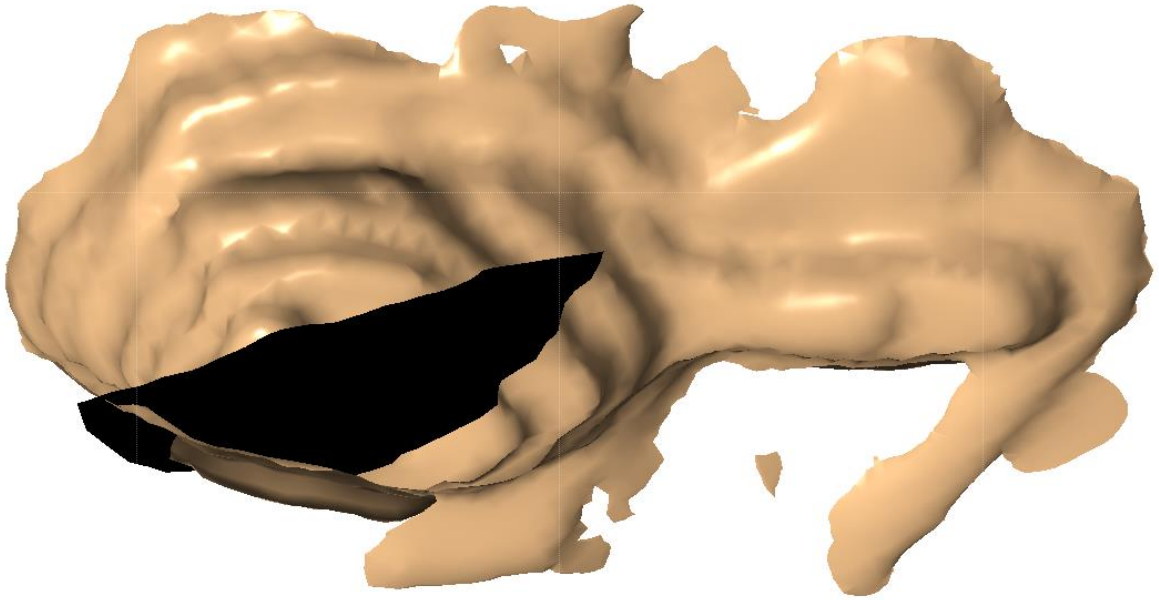

West vein 03 is a thin but highly consistent vein that could be traced across the deposit.

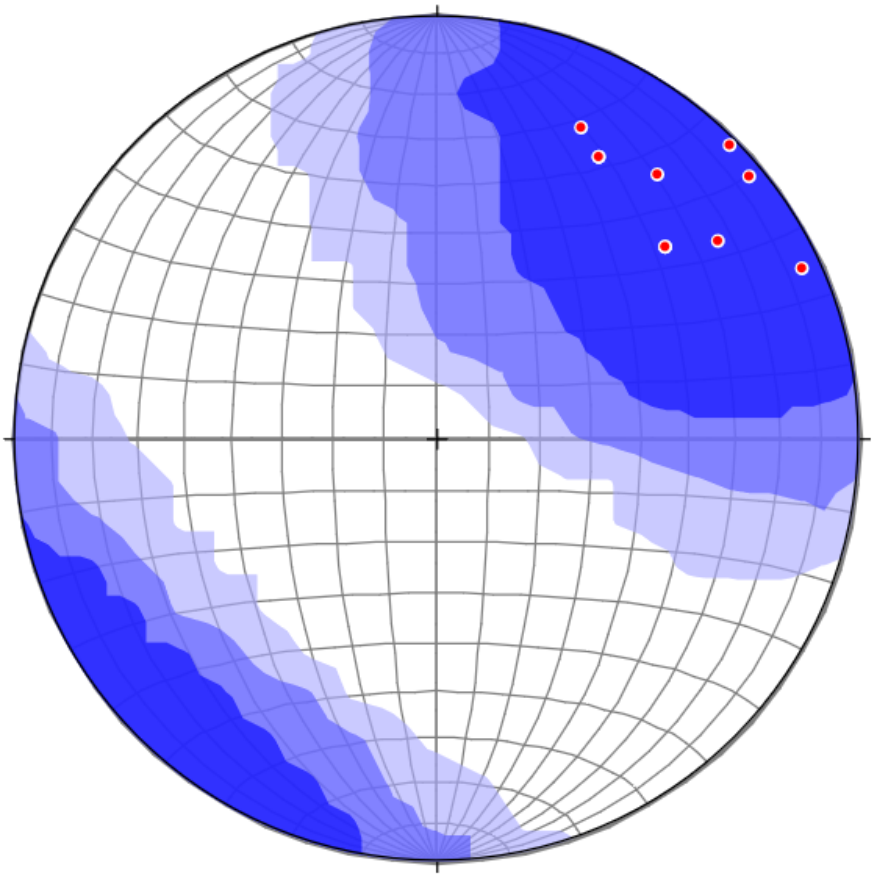

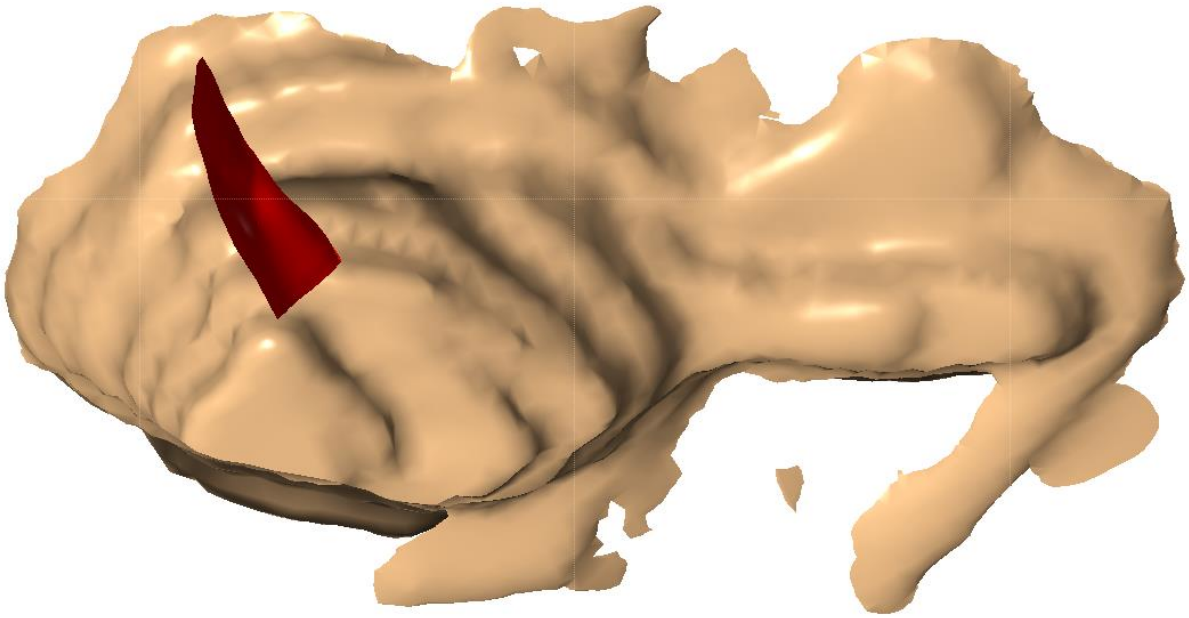

West vein 04 is a small SE trending vein located in the NW corner of the deposit.

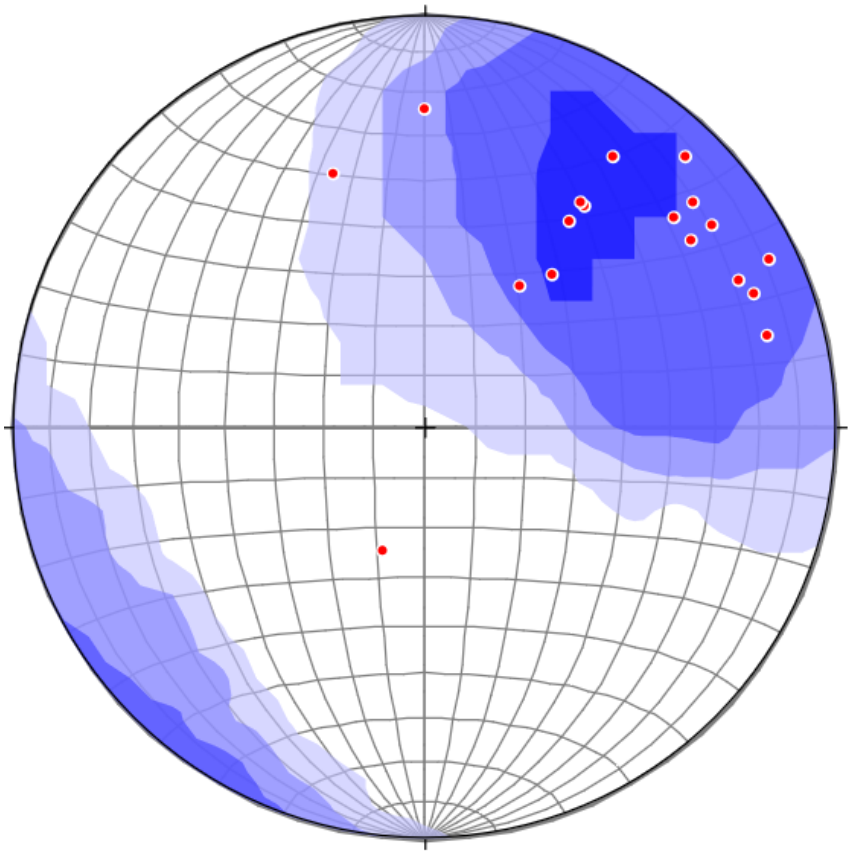

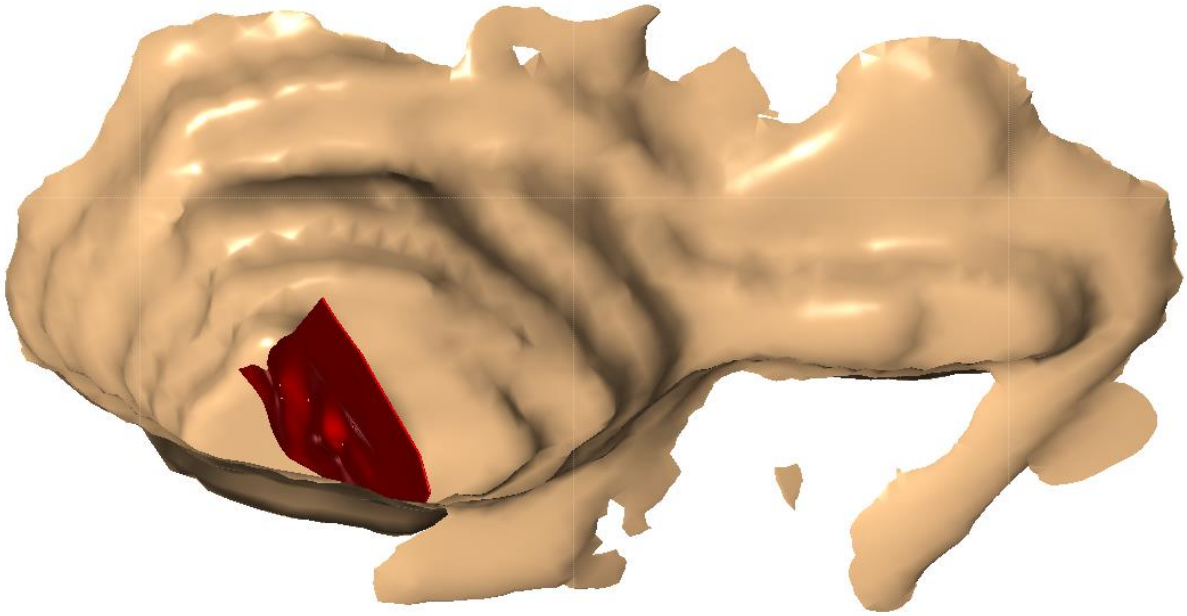

West vein 05 is a highly consistent SE trending vein located near the center of the deposit.

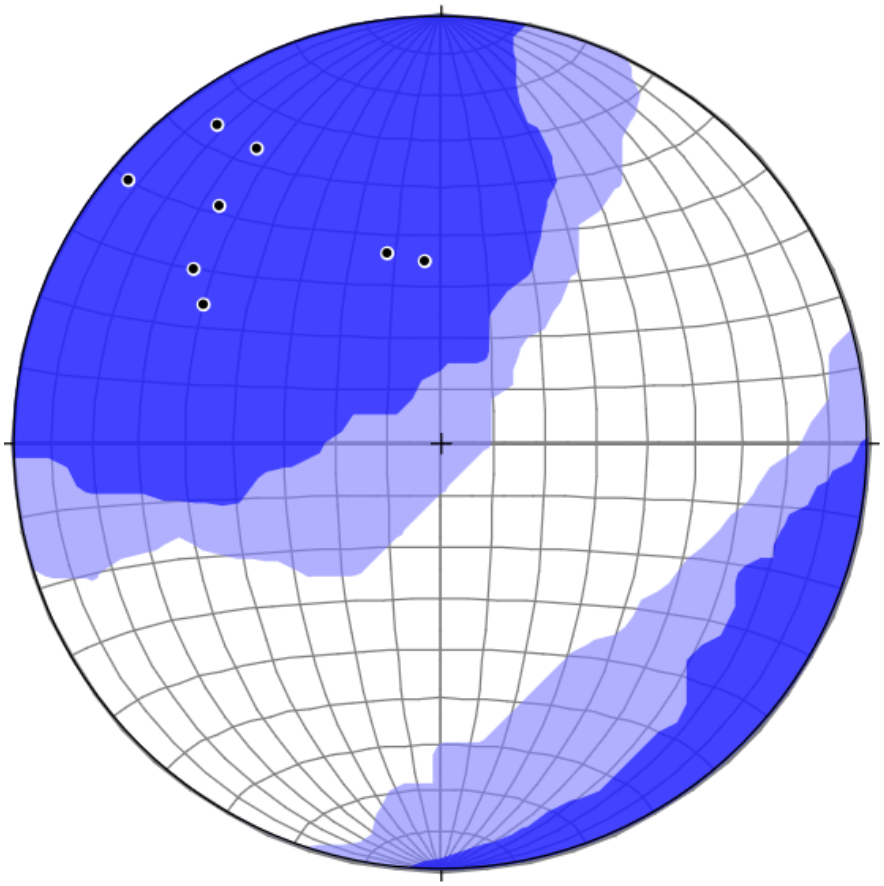

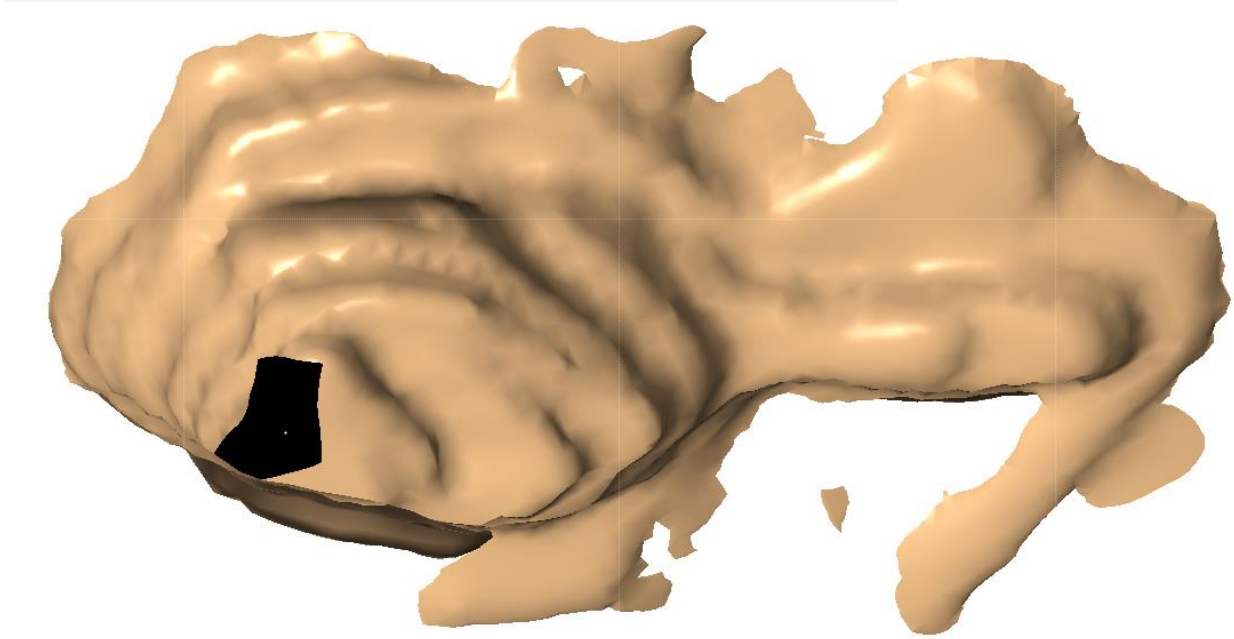

West vein 06 is a small NE trending vein located in the SW corner of the deposit. This vein acts primarily as a connector.

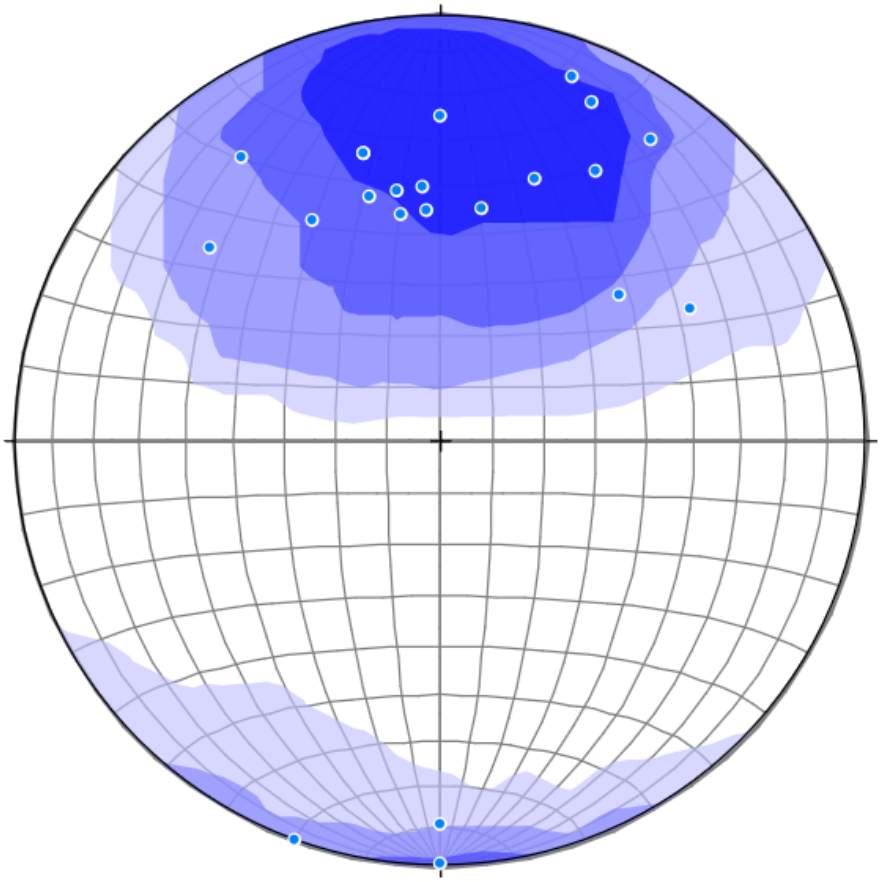

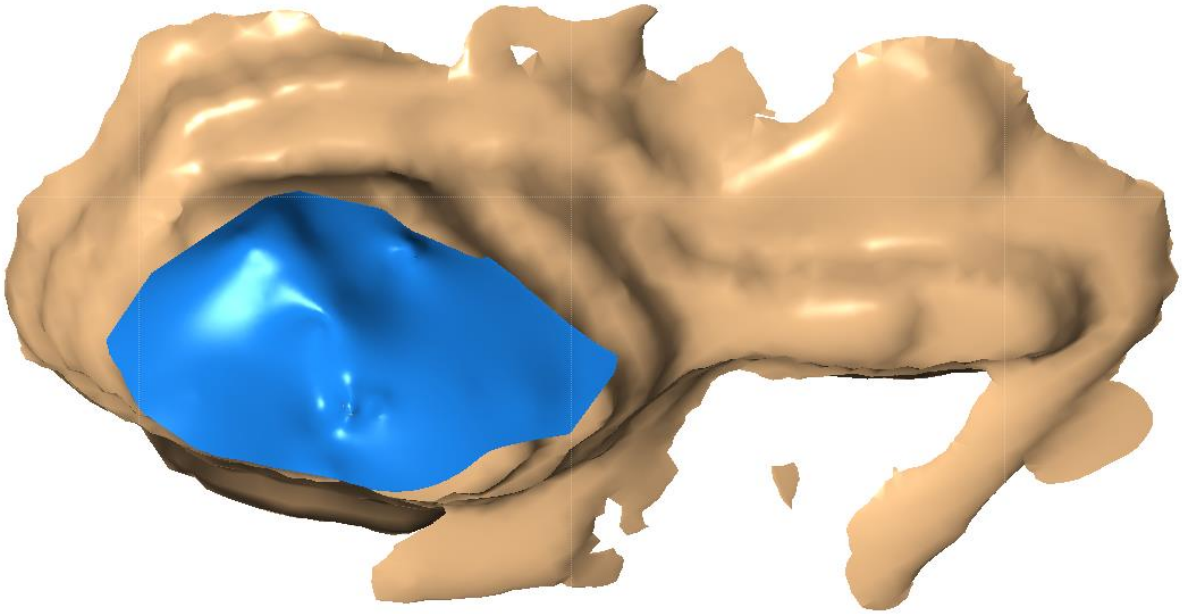

West vein 07 is the largest of the EW trending veins and forms almost a south dipping bowl shape towards the center of the deposit.

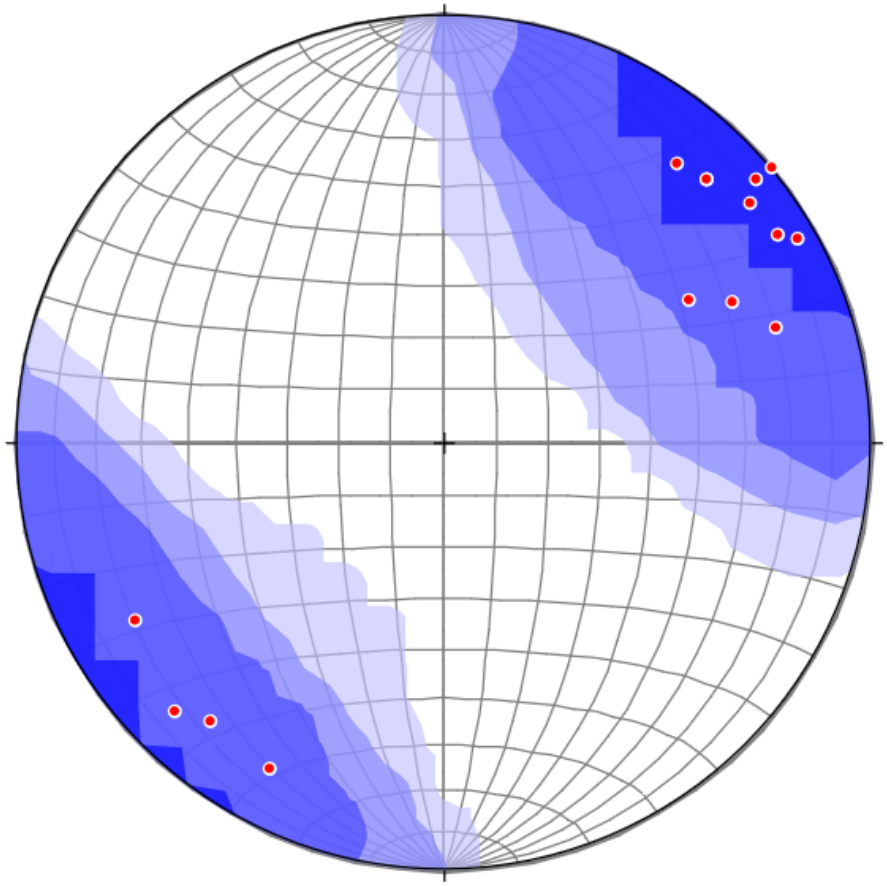

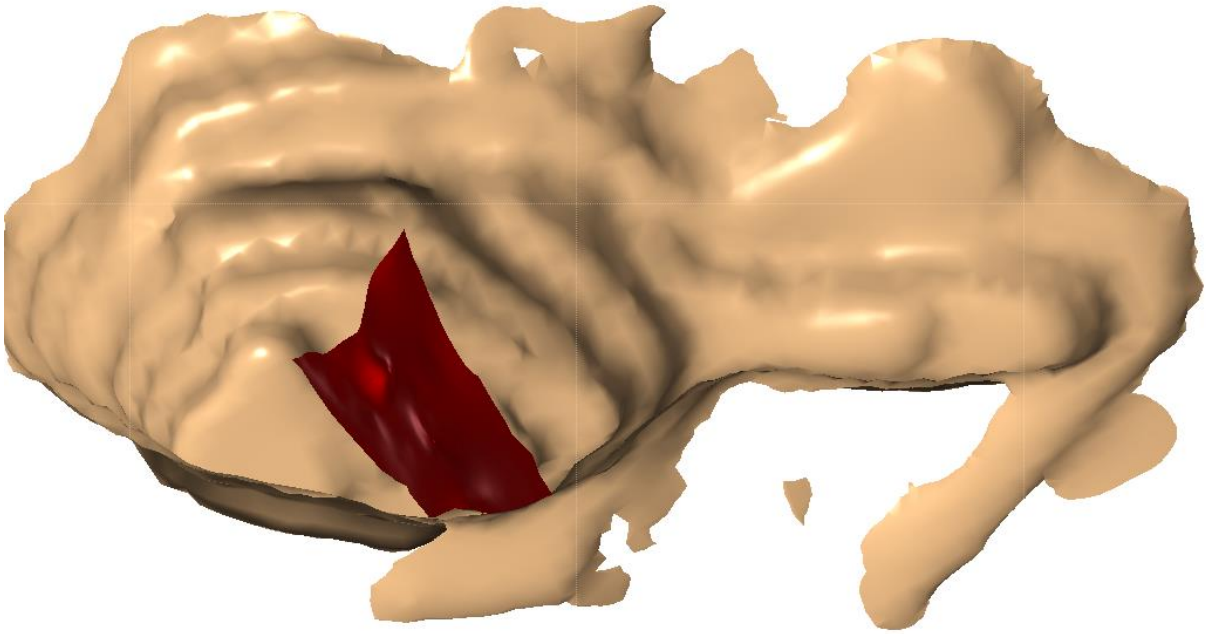

West vein 08 is a continuous SE trending vein in the SE corner of the deposit, was one of the most consistent veins in the deposit.

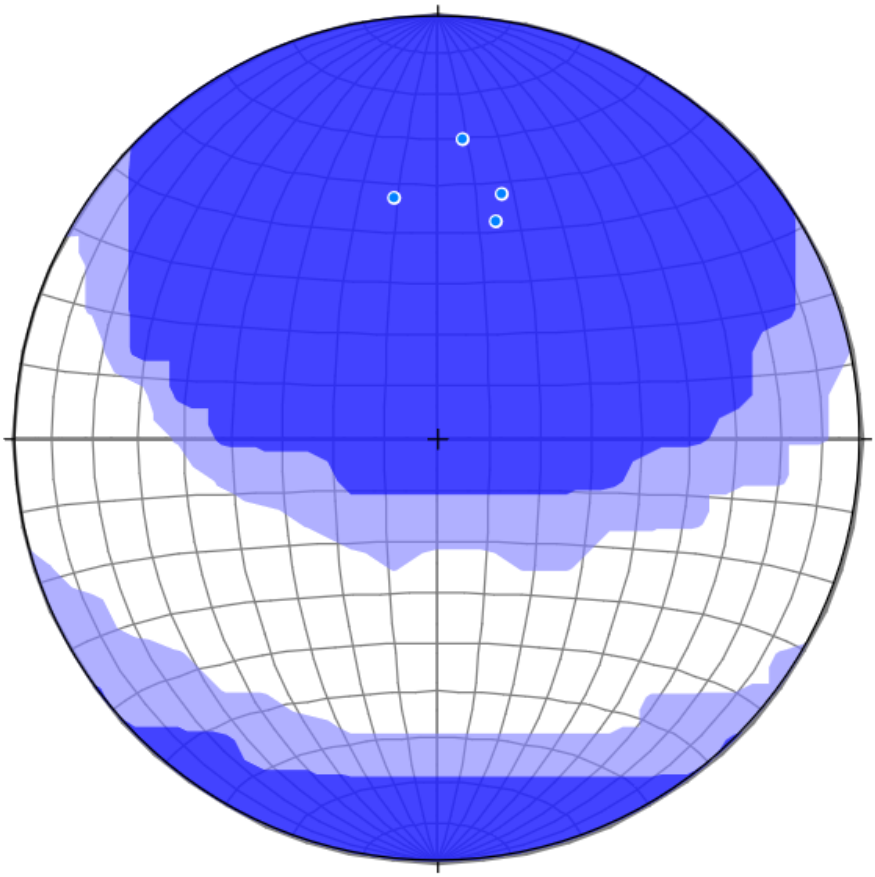

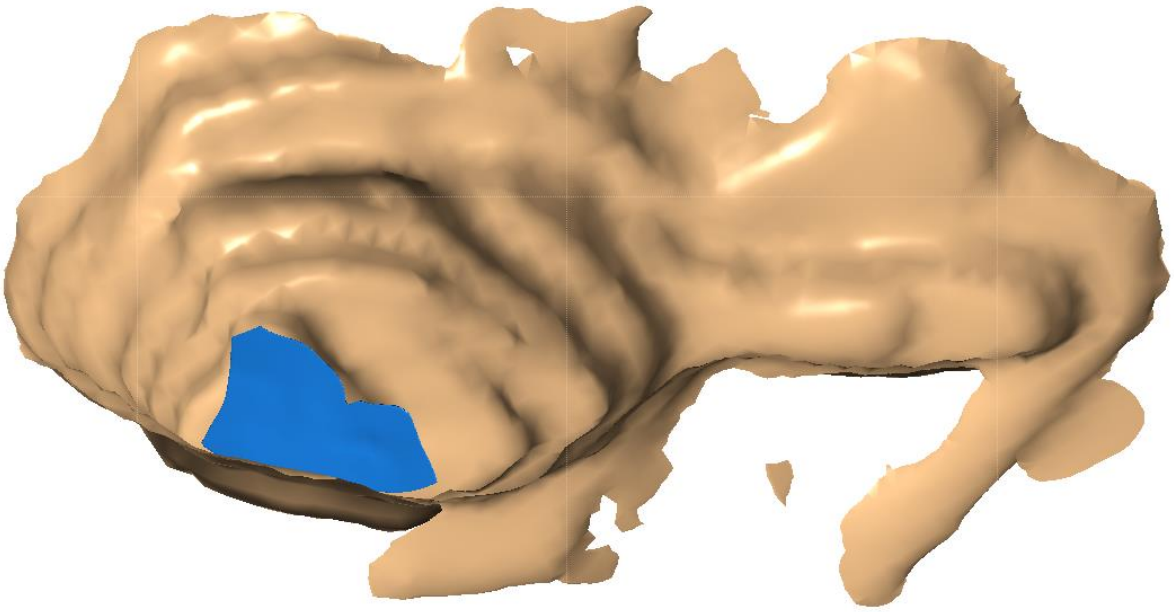

West vein 09 that is a small East trending, south dipping vein in the southern portion of the deposit.

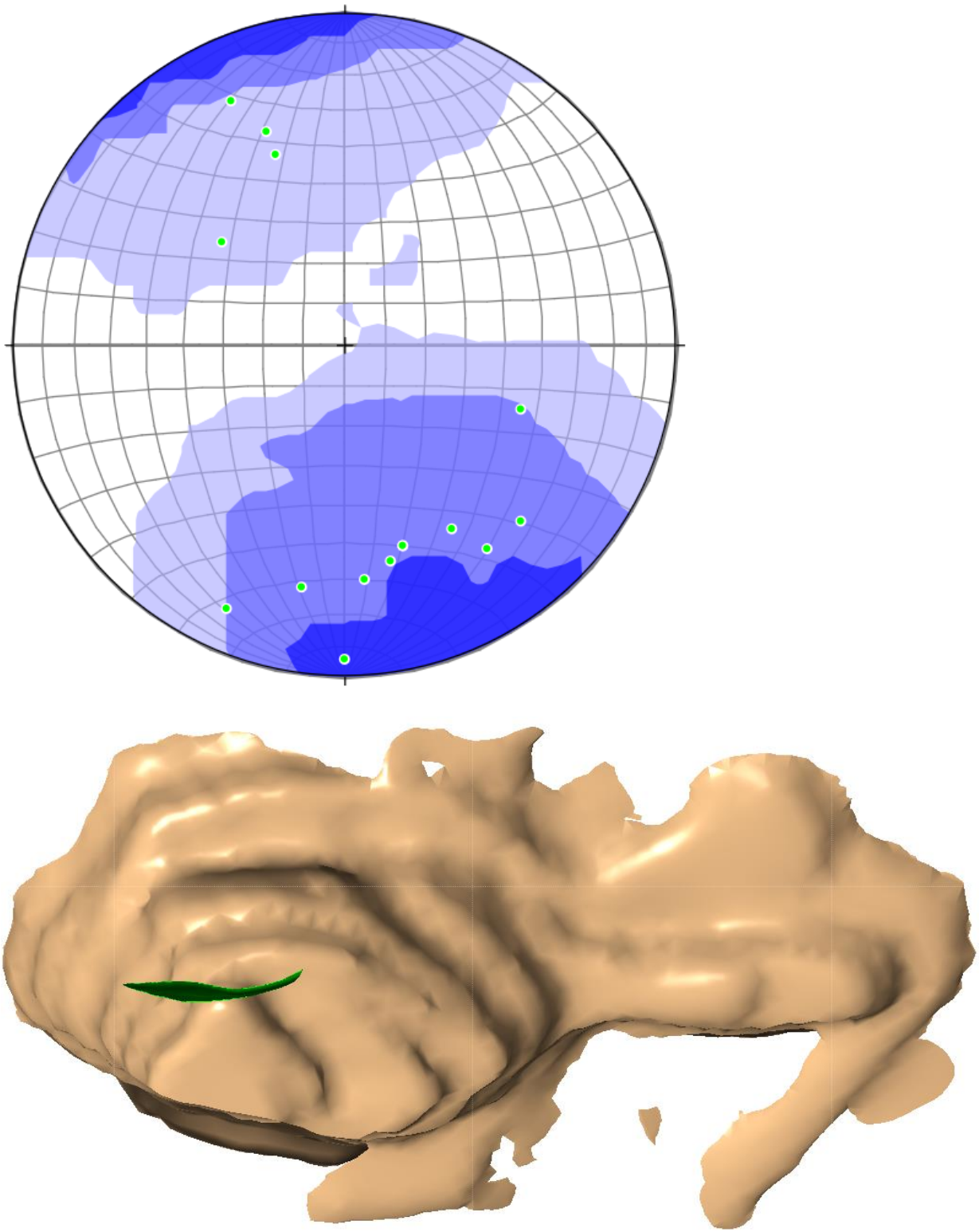

West vein 10 which is a small connector style vein in the central portion of the deposit.

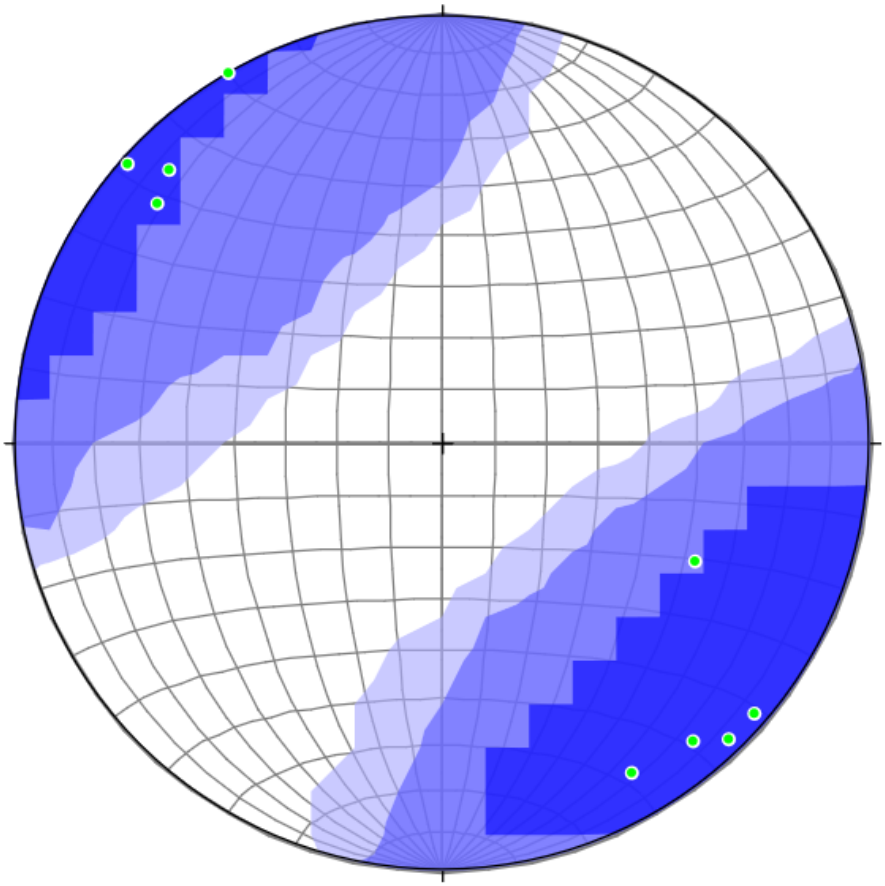

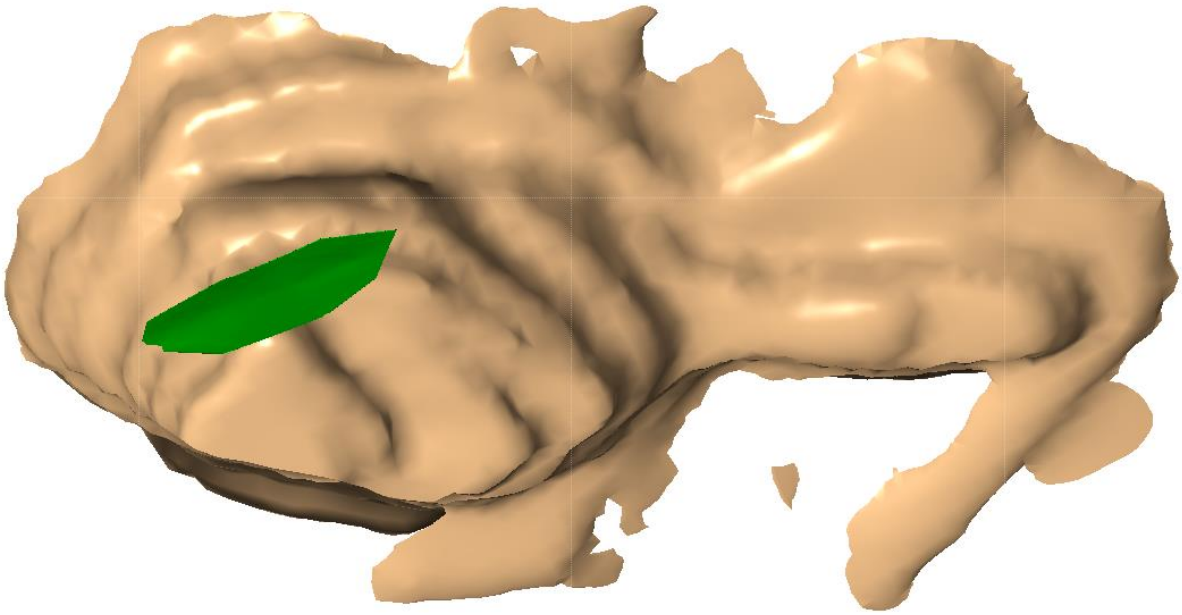

West vein 11 that is a straight and relatively small vein in the NW corner of the deposit.

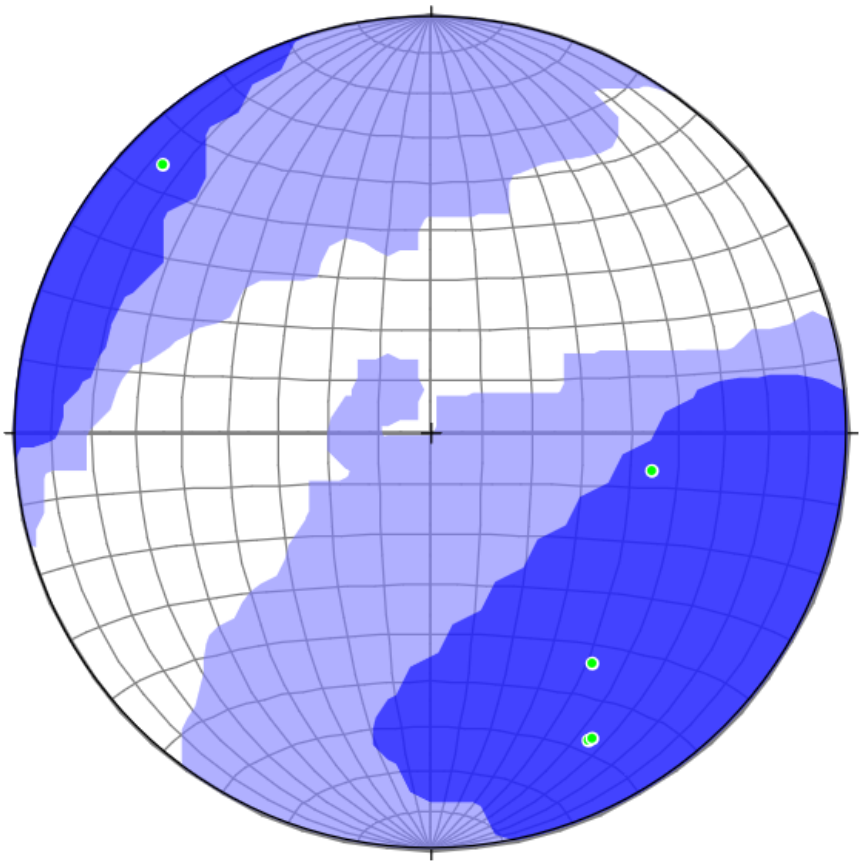

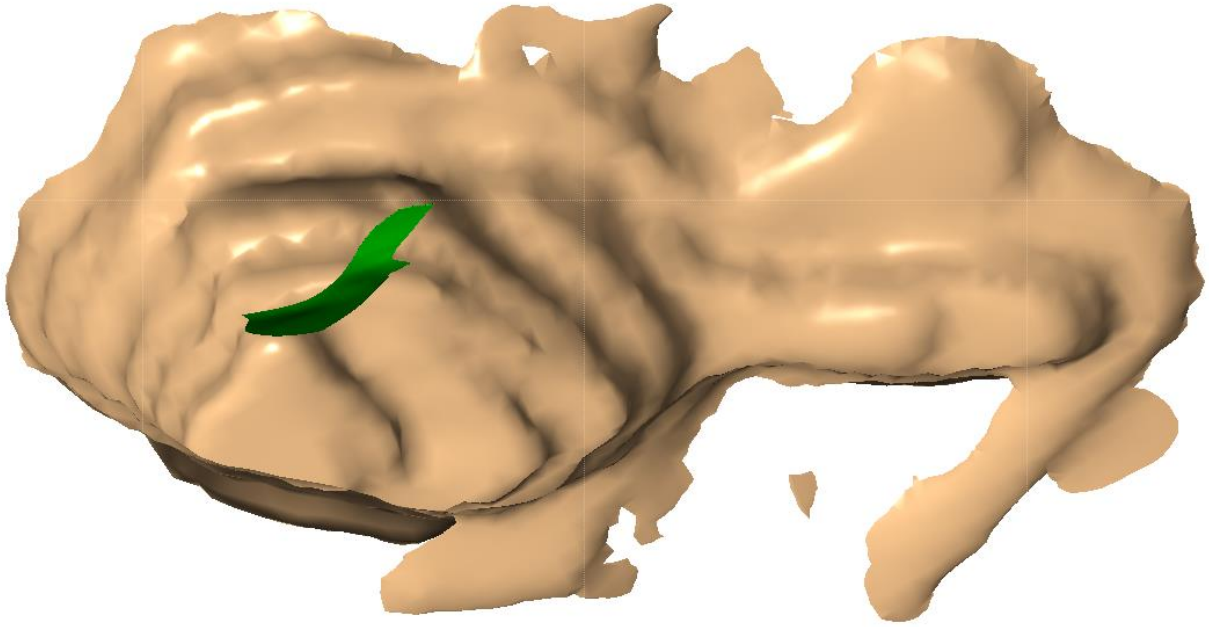

West vein 12, which is a small vein that acts as a bride between more continuous veins.

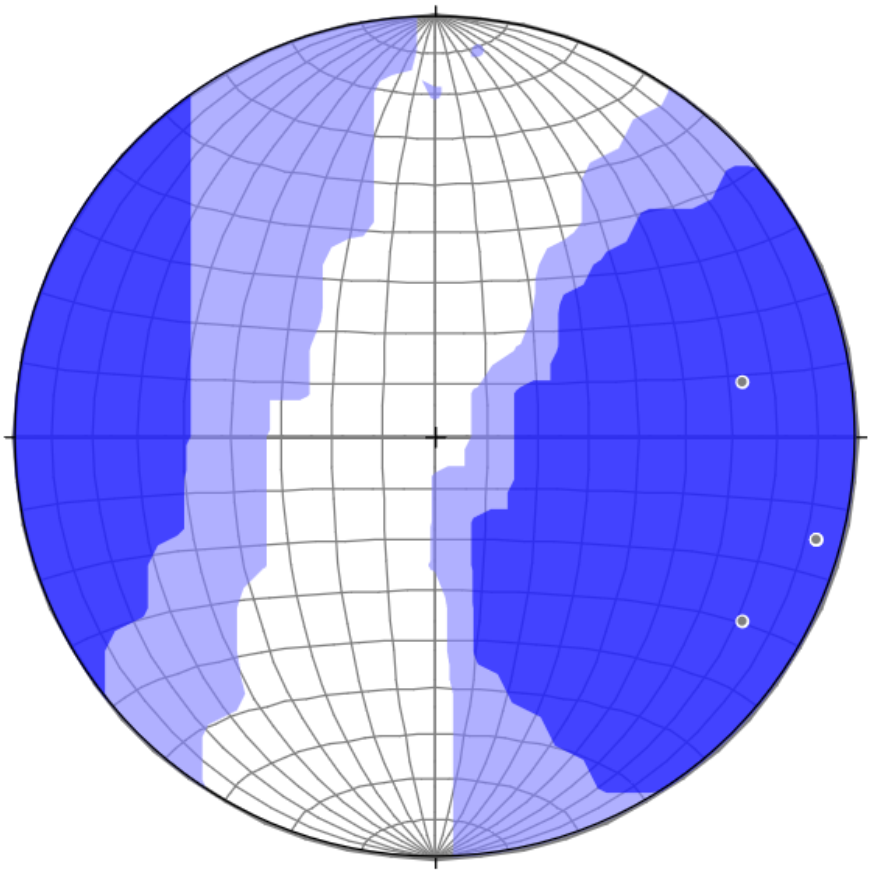

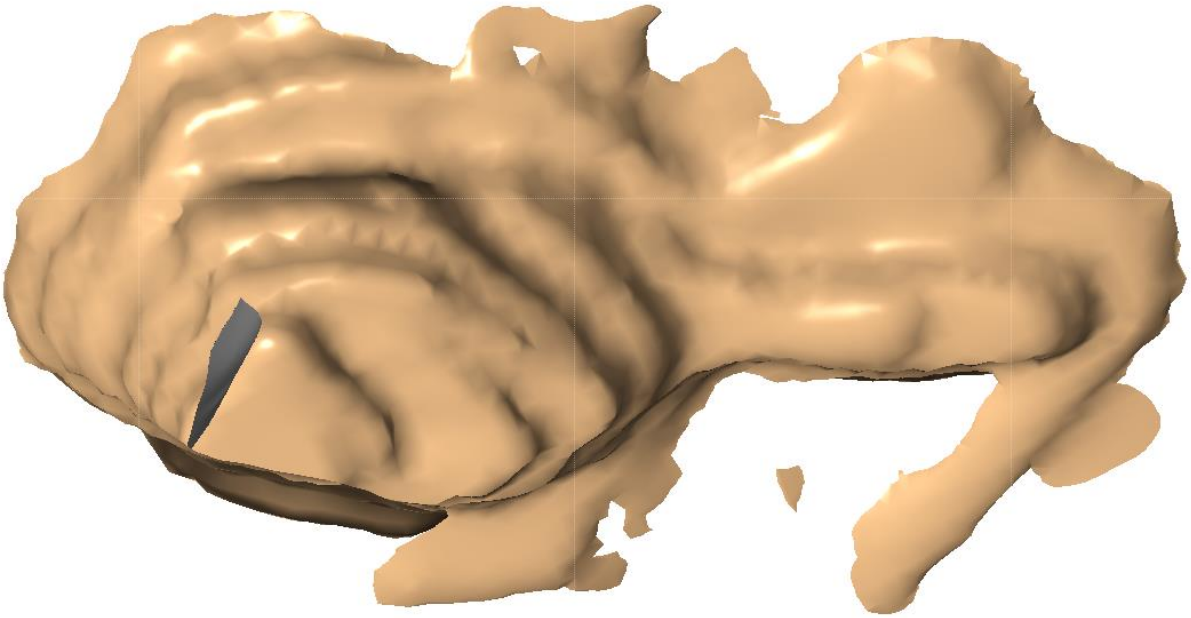

West vein 13, which is a small vein occurring in the SW corner of the deposit

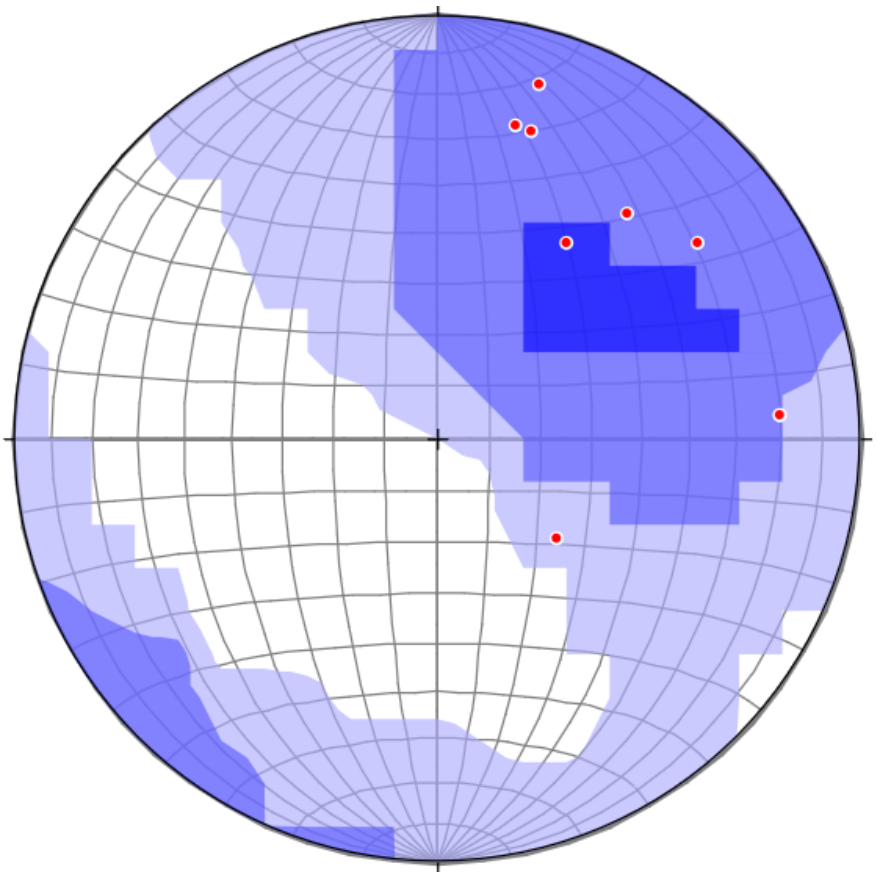

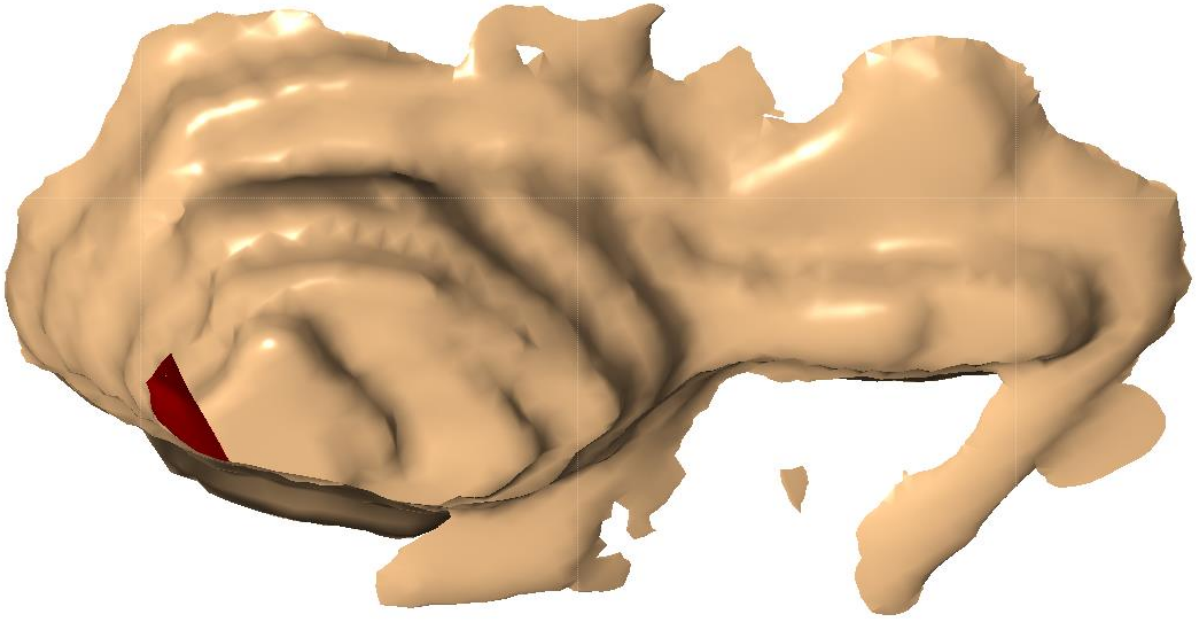

West vein 14, small vein occurring in the SW corner of the deposit

Appendix B – Sample Transects

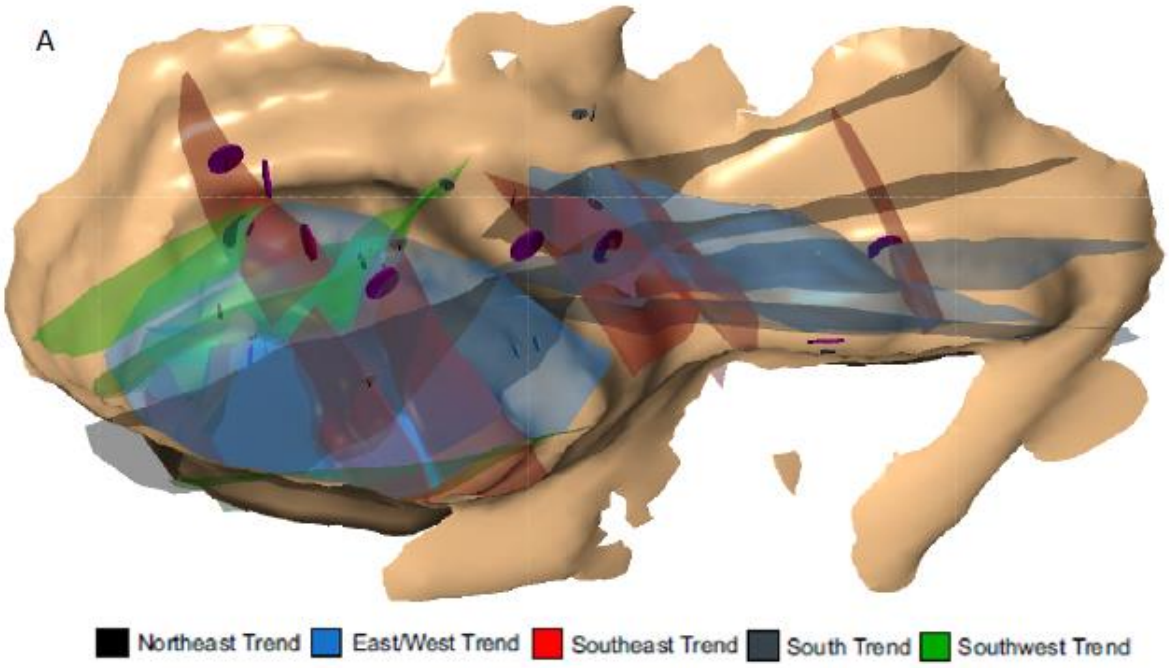

A) 3D model showing the location of sample sets (transects). Transects submitted for assay are represented by large purple disks while un-submitted transects are represented by smaller grey disks are transect locations. B) Is a photograph showing common layout for transect sampling.

Appendix C – Photographs of Characteristic Vein Features

Pinch and swell pattern of sulfide veins. A) Demonstrates pinching along dip from 50cm to <5cm. B) Demonstrates pinching in vein along strike.

Photographs vein orientation changes. A) Demonstrates ~110-degree deflection in dip with a bi-furcation as the vein wraps around a clast. B) Shows typical 90-degree deflection in vein along strike associated with a thickening of mineralization. C) Intersection between two veins with a local thickening of mineralization in two of the veins.

Photo of vein thickening associated with the junction of three smaller sulphide veins. Note the rounded nature of the clasts and irregular, wispy nature of the smaller veinlets. Magnetic pen (~10cm) for scale.

Appendix D – Select Plan Sections of Broken Hammer

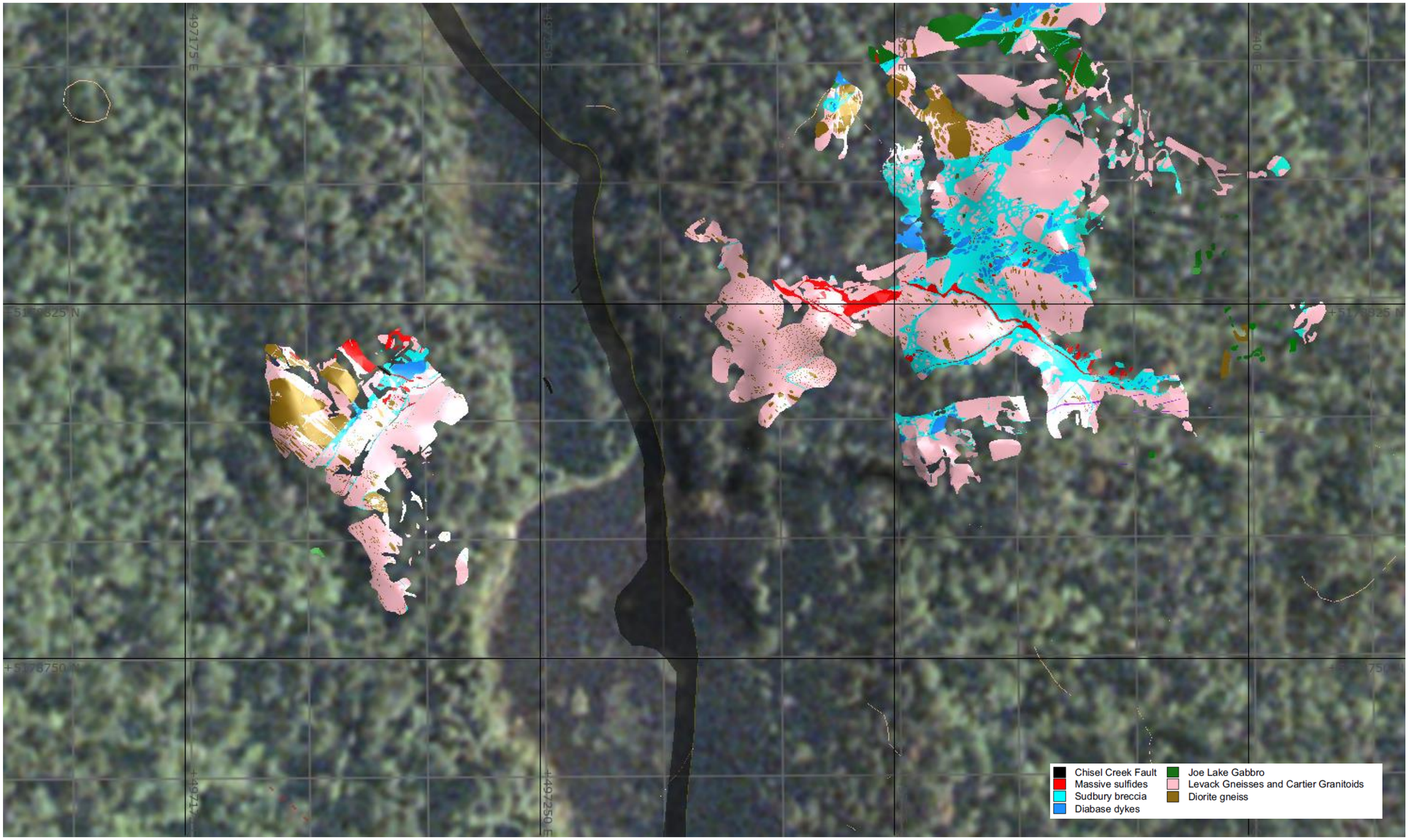

Plan Section 1: Surface showing detail mapping of Broken Hammer Trenches (modified from unpublished Wallbridge Mining map produced by D. Peterson. Elevation ranges from ~394 to 410 m.

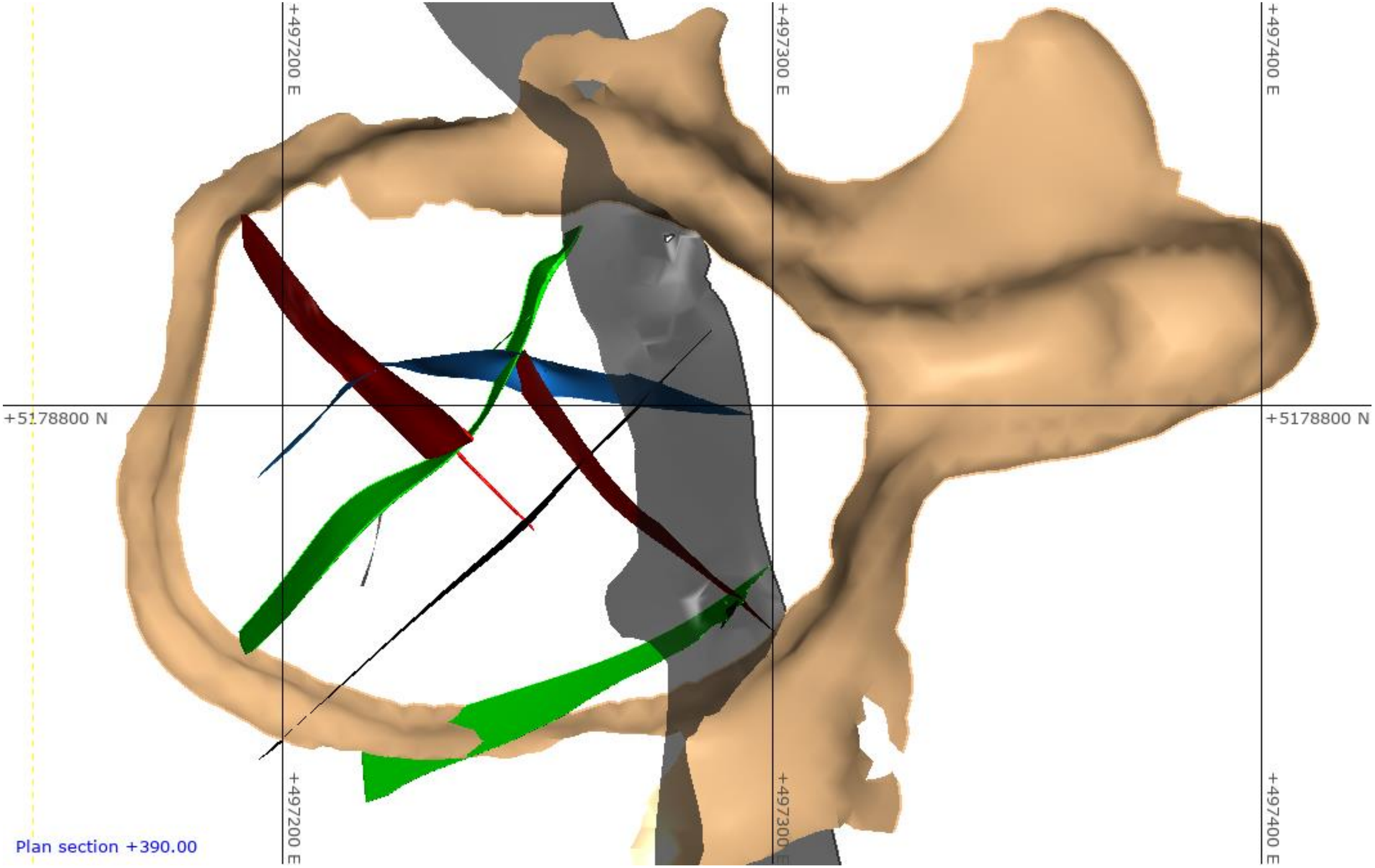

Plan Section 2: 390 m elevation showing the thickened East veins which have been thrust onto the West Pit by the Chisel Creek Fault. Note how much thinner the West Pit veins are at this elevation.

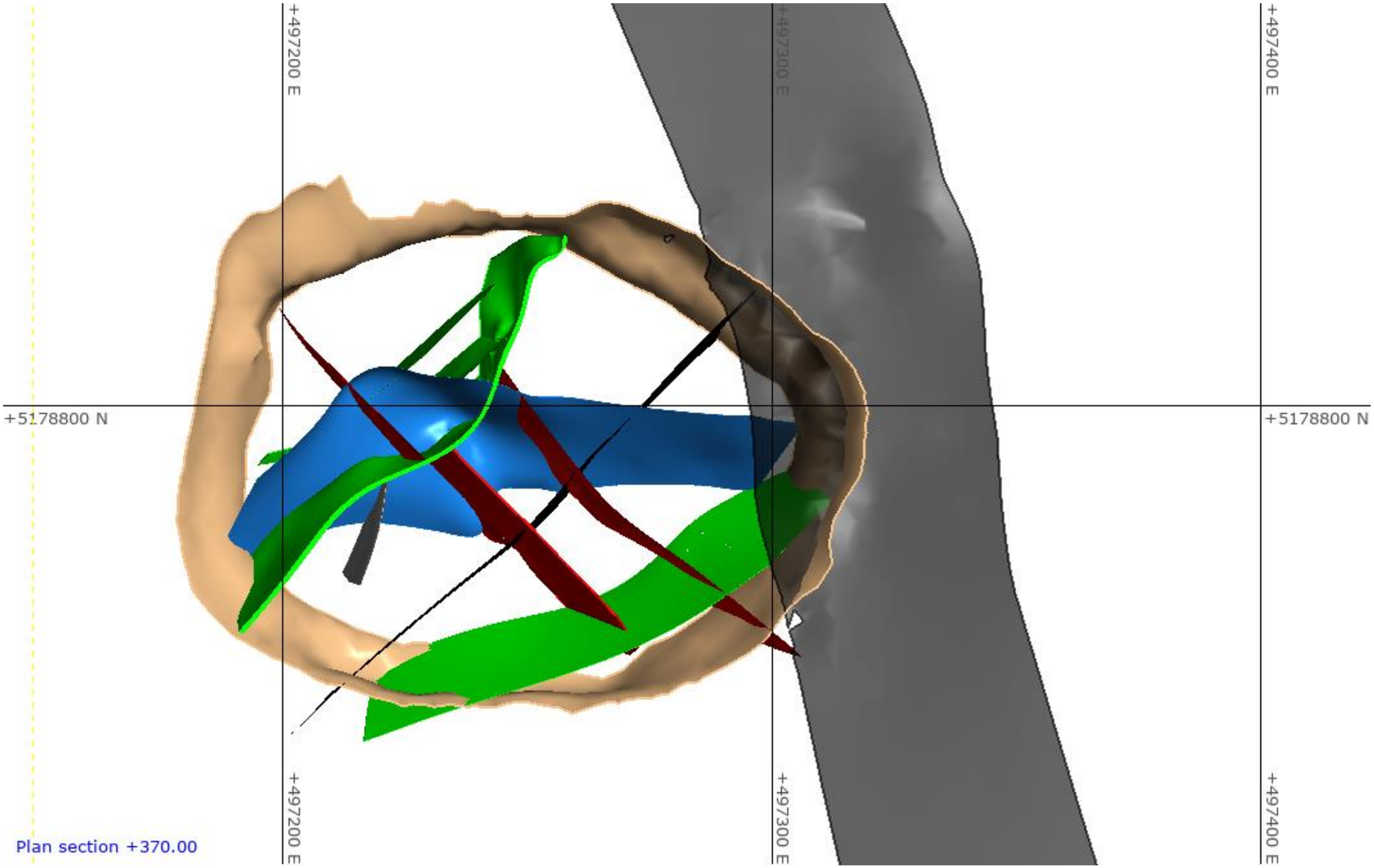

Plan Section 3: 370 m elevation (mid-elevation of deposit). Note the complexity as they wrap around large dasts of country rock (not shown) and the development of the bowl-shaped East trending-south dipping vein (central blue vein).

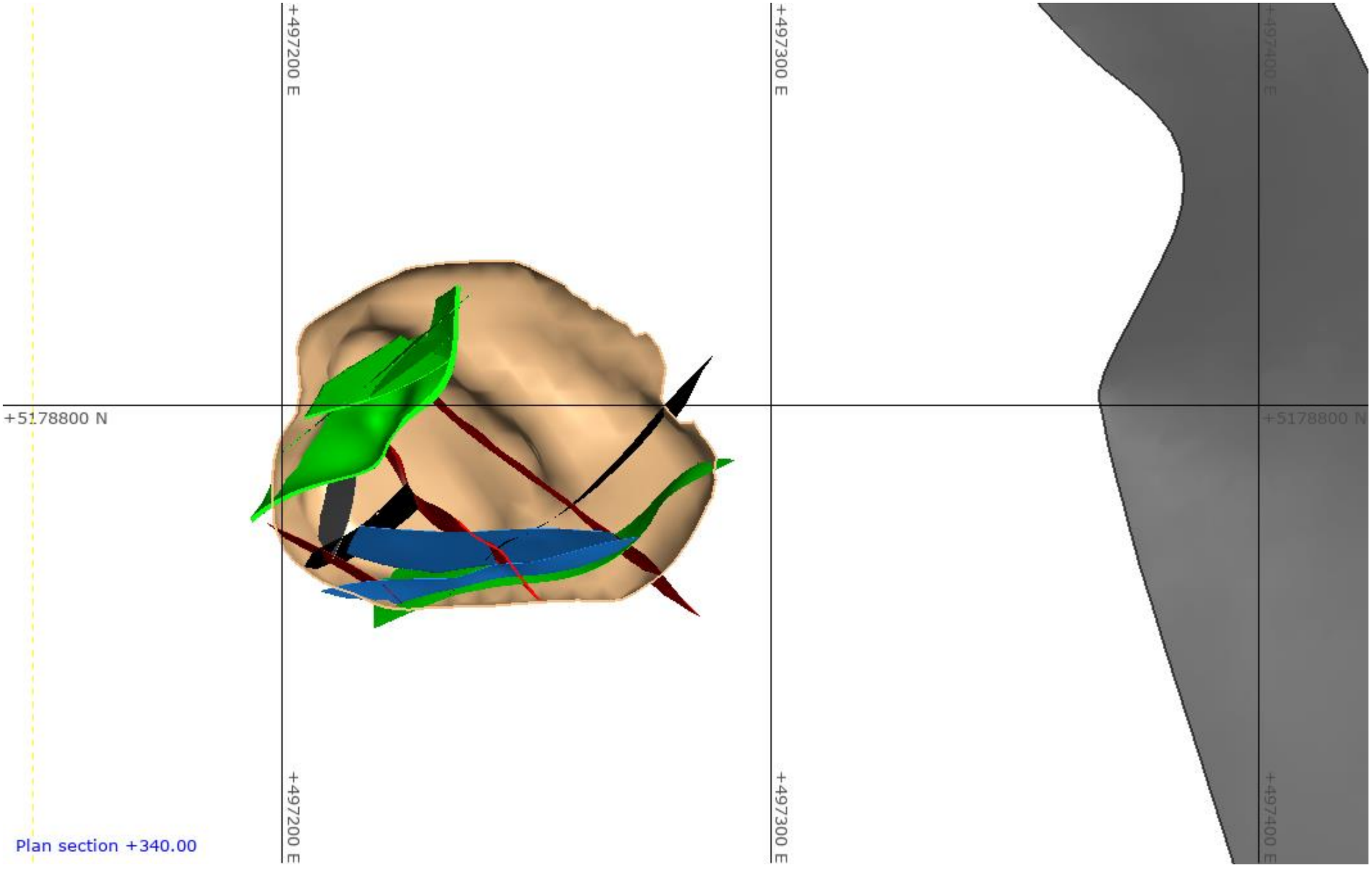

Plan Section 4: 340m elevation showing the bottom bench of the mine. Note how the veins have congregated towards the southern wall (following plunge of ore shoots/vein intersections). There is a local thickening of the green vein in the NW corner, which is associated with an increase in sperrylite crystals.

Appendix E – Assay Results, Sample Transects, and Mineralized Sample Photographs

Sample#	Sample Type	Distance	VnSet	Pit	Strike	Dip	Bench	Easting	Northing	Elevation	Date	Auppm	Ptppm	Pdppm	Agppm	Cu%	Ni%	S%
R232643	Grab		Low sulfide	East Pit			379	497355.95	5178802.836	384.0698	01-Dec-14	0.033	<0.005	0.004	0.56	1.54	0.0589	1.56
R232644	Grab		Low sulfide	East Pit			379				01-Dec-14	0.011	<0.005	0.003	0.18	0.176	0.0411	0.18
R232645	Grab		Low sulfide	East Pit			379				01-Dec-14	0.001	<0.005	0.002	0.07	0.121	0.0385	0.12
R232646	Grab		Low sulfide	East Pit			379				01-Dec-14	0.006	<0.005	0.002	0.14	0.115	0.0416	0.11
R232647	Grab		Low sulfide	East Pit			379				01-Dec-14	0.083	0.859	0.765	1.07	0.288	0.0205	0.29
R232648	Grab		Low sulfide	East Pit			379				01-Dec-14	0.374	1.78	1.2	5.02	0.311	0.037	0.32
R232649	*Standard*		*Low sulfide*	East Pit							*01-Dec-14*	0.176	0.316	0.375	2.15	0.347	0.296	1.48
R232650	*Blank*		*Low sulfide*	East Pit							*01-Dec-14*	<0.001	<0.005	0.002	0.02	0.00176	0.00068	<0.01
P448241	Channel	-1.9	Transect 1	West Pit			391				05-Sep-14	0.001	<0.005	0.001	0.65	0.0244	0.00472	0.42
P448243	Channel	-1.7	Transect 1	West Pit			391				05-Sep-14	0.126	0.031	0.176	1.69	0.731	0.104	0.96
P448246	Channel	-0.9	Transect 1	West Pit			391				05-Sep-14	<0.001	<0.005	0.001	0.21	0.01025	0.00621	0.35
P448248	Channel	-0.7	Transect 1	West Pit			391				05-Sep-14	<0.001	<0.005	0.001	0.08	0.00916	0.01325	0.37
P448250	Channel	-0.5	Transect 1	West Pit			391				05-Sep-14	<0.001	<0.005	0.002	0.15	0.0156	0.0484	0.43
P448251	Channel	-0.4	Transect 1	West Pit			391				05-Sep-14	0.001	<0.005	0.005	0.31	0.0474	0.0568	0.27
P448253	**Channel**	**-0.1**	Transect 1	West Pit			**391**	**497207.6725**	**5178819.785**	**391**	**05-Sep-14**	**2.66**	**1.23**	**23.7**	**2.1**	**15.85**	**0.1505**	**16.9**
P448254	**Channel**	**0**	Transect 1	West Pit	**140**	**86**	**391**	**497207.5508**	**5178819.27**	**391**	**05-Sep-14**	**2.76**	**7.55**	**23.5**	**3.63**	**29.3**	**0.0793**	**29.8**
P448255	**Channel**	**0.1**	Transect 1	West Pit	**140**	**86**	**391**	**497207.4767**	**5178819.695**	**391**	**05-Sep-14**	**1.145**	**5.15**	**3.44**	**1.57**	**0.818**	**0.114**	**0.87**
P448256	Channel	0.2	Transect 1	West Pit	140	86	391				05-Sep-14	0.394	2.56	1.38	3.22	0.185	0.01485	0.28
P448257	Channel	0.3	Transect 1	West Pit			391				05-Sep-14	0.004	0.173	0.025	0.4	0.0112	0.00777	0.1
P448259	*Standard*		*Transect 1*	*West Pit*							*05-Sep-14*	*0.126*	*0.306*	*4.97*	*0.19*	*0.0486*	*0.0756*	*0.18*
P448260	*Blank*		*Transect 1*	*West Pit*							*05-Sep-14*	*<0.001*	*0.007*	*0.008*	*0.02*	*0.0041*	*0.00069*	*0.01*
P448261	Channel	0.9	Transect 1	West Pit			391				05-Sep-14	0.001	<0.005	0.003	0.21	0.00986	0.0106	0.43
P448264	Channel	1.2	Transect 1	West Pit			391				05-Sep-14	0.001	<0.005	0.003	0.15	0.01005	0.00873	0.62
P448267	Channel	1.5	Transect 1	West Pit			391				05-Sep-14	0.01	<0.005	0.028	1.38	2.5		
P448269	Channel	1.7	Transect 1	West Pit			391				05-Sep-14	0.001	<0.005	0.003	0.15	0.0294	0.00448	0.23
P448271	Channel	1.9	Transect 1	West Pit			391				05-Sep-14	0.007	<0.005	0.001	0.11	0.0453	0.0039	0.22
R232686	Channel	2	Transect 2	West Pit			373				16-Jan-15	<0.001	<0.005	0.001	0.05	0.00262	0.00178	0.05
R232688	Channel	1.8	Transect 2	West Pit			373				16-Jan-15	<0.001	<0.005	0.001	0.06	0.00266	0.00194	0.06
R232691	Channel	1.5	Transect 2	West Pit			373				16-Jan-15	0.002	<0.005	0.002	0.05	0.041	0.00527	0.05
R232694	Channel	1.2	Transect 2	West Pit			373				16-Jan-15	<0.001	<0.005	<0.001	0.13	0.00739	0.00258	0.04
R232697	Channel	0.9	Transect 2	West Pit			373				16-Jan-15	<0.001	0.008	0.001	0.05	0.00273	0.00339	0.08
R232701	Channel	0.6	Transect 2	West Pit			373				16-Jan-15	<0.001	<0.005	<0.001	0.05	0.00257	0.0032	0.09
R232704	Channel	0.3	Transect 2	West Pit			373				16-Jan-15	0.033	<0.005	0.002	0.57	0.0155	0.0418	0.11
R232705	Channel	0.2	Transect 2	West Pit			373				16-Jan-15	0.017	0.085	0.114	1.87	0.0549	0.058	0.1
R232706	Channel	0.1	Transect 2	West Pit			373				16-Jan-15	0.175	0.759	0.726	3.44	0.1285	0.0748	0.15
R232707	**Channel**	**0**	Transect 2	West Pit	**190**	**45**	**373**	**497243.6057**	**5178808.681**	**376.23**	**16-Jan-15**	**1.515**	**0.84**	**21.6**	**53**	**13.55**	**0.1505**	**13.9**
R232711	*Standard (measured PGE)*		Transect 2	West Pit								0.119	0.327	5.06	0.23	0.0589	0.0761	0.19
R232712	*Blank*		Transect 2	West Pit								<0.001	<0.005	0.006	0.03	0.0052	0.00083	0.01
R232747	Channel	0.9	Transect 3	West Pit			364				29-May-15	0.005	<0.005	0.019	1.17	0.369	0.01715	0.48
R232748	Channel	0.8	Transect 3	West Pit			364				29-May-15	0.001	<0.005	0.002	0.32	0.0156	0.0216	0.61
R232749	Channel	0.7	Transect 3	West Pit			364				29-May-15	0.001	<0.005	0.002	0.39	0.01045	0.00669	0.49
R232750	Channel	0.6	Transect 3	West Pit			364				29-May-15	0.002	<0.005	0.002	1.07	0.0343	0.00872	0.46
R232751	Channel	0.5	Transect 3	West Pit			364				29-May-15	0.001	0.069	0.002	1.08	0.144	0.01445	0.45
R232752	Channel	0.4	Transect 3	West Pit			364				29-May-15	0.003	0.01	0.012	0.76	0.0277	0.00895	0.42

Sample #	Sample Type	Distance	Vn Set	Pit	Strike	Dip	Bench	Easting	Northing	Elevation	Date	Au ppm	Pt ppm	Pd ppm	Ag ppm	Cu %	Ni %	S %
R232753	Channel	0.3	Transect 3	West Pit			364				29-May-15	0.003	0.006	0.004	0.71	0.0425	0.0679	0.13
R232754	Channel	0.2	Transect 3	West Pit			364				29-May-15	0.106	0.42	0.495	1.82	0.1555	0.208	0.18
R232755	Channel	0.1	Transect 3	West Pit			364				29-May-15	2.41	10.05	17.95	25.2	1.745	0.224	1.85
R232756	**Channel**	**0**	Transect 3	West Pit	**220**	**70**	**364**	**497226.49**	**5178790.77**	**367.266**	**29-May-15**	**2.31**	**24.2**	**25.5**	**>100**	**22.2**	**10.1**	**27.2**
R232757	Channel	-0.1	Transect 3	West Pit			364				29-May-15	0.51	2.06	1.77	3.52	0.362	0.108	0.38
R232758	*Standard CFRM-100*		Transect 3	West Pit								0.173	0.333	0.362	2.2	0.354	0.315	1.58
R232759	*Blank*		Transect 3	West Pit								0.005	0.052	0.036	0.13	0.0214	0.00773	0.03
R230051	Grab	-1	Transect 4	West Pit			382				03-Nov-14	<0.001	<0.005	0.004	0.24	0.00731	0.0126	0.16
R230052	Grab	-0.9	Transect 4	West Pit			382				03-Nov-14	0.016	<0.005	0.002	0.3	0.149	0.117	0.17
R230053	Grab	-0.8	Transect 4	West Pit			382				03-Nov-14	0.414	2.3	1.895	3.43	0.674	0.191	0.69
R230054	Grab	-0.7	Transect 4	West Pit			382				03-Nov-14	0.073	0.247	0.423	0.96	0.131	0.0736	0.14
R230055	Grab	-0.5	Transect 4	West Pit			382				03-Nov-14	0.016	<0.005	0.024	0.52	0.0204	0.0494	0.04
R230056	Grab	-0.4	Transect 4	West Pit			382				03-Nov-14	0.472	0.498	4.61	4.73	2.7		
R230057	Grab	-0.3	Transect 4	West Pit			382				03-Nov-14	0.358	2.63	1.465	2.54	0.228	0.1255	0.23
R230058	Grab	-0.1	Transect 4	West Pit			382				03-Nov-14	0.004	<0.005	0.019	0.2	0.0271	0.0919	0.03
R230059	**Grab**	**0**	Transect 4	West Pit	**70**	**64**	**382**	**497230.3406**	**5178805.592**	**385.2774**	**03-Nov-14**	0.636	0.43	30.7	12.2	30.5	2.7	33
R230060	**Grab**	**0.1**	Transect 4	West Pit	**70**	**64**	**382**	**497230.4406**	**5178805.592**	**385.2774**	**03-Nov-14**	0.512	11.4	30.9	9.08	27.2	2.73	28.8
R230061	Grab	0.2	Transect 4	West Pit			382				03-Nov-14	0.29	2.17	1.605	4.2	0.393	0.106	0.4
R230062	Grab	0.4	Transect 4	West Pit			382				03-Nov-14	0.017	0.013	0.024	0.18	0.0461	0.0137	0.07
R230063	Grab	0.5	Transect 4	West Pit			382				03-Nov-14	0.053	0.184	0.278	0.63	0.107	0.01875	0.19
R230064	Grab	0.6	Transect 4	West Pit			382				03-Nov-14	0.045	0.091	0.13	0.93	0.0804	0.0165	0.1
R230067	*Standard*		Transect 4	West Pit							*03-Nov-14*	0.177	0.306	0.375	2.08	0.341	0.291	1.48
R230068	*Blank*		Transect 4	West Pit							*03-Nov-14*	<0.001	<0.005	0.003	0.02	0.00296	0.00093	<0.01
P448219	Grab	1.9	Transect 5	East Pit			391				22-Aug-14	<0.001	<0.005	0.003	0.09	0.0816	0.0076	0.14
P448220	Grab	1.8	Transect 5	East Pit			391				22-Aug-14	0.004	<0.005	0.007	0.07	0.198	0.0204	0.02
P448221	Grab	1.7	Transect 5	East Pit			391				22-Aug-14	<0.001	<0.005	0.008	0.1	0.137	0.024	0.08
P448222	Grab	1.6	Transect 5	East Pit			391				22-Aug-14	<0.001	<0.005	0.002	0.08	0.144	0.01605	0.09
P448223	Grab	1	Transect 5	East Pit			391				22-Aug-14	0.116	0.007	0.024	2.48	0.317	0.00558	0.35
P448224	Grab	0.6	Transect 5	East Pit			391				22-Aug-14	0.016	<0.005	0.006	0.46	0.121	0.0858	0.15
P448225	**Grab**	**0.1**	**Transect 5**	East Pit			**391**	**497293.69**	**5178826.413**	**392.428**	**22-Aug-14**	1.365	<0.005	0.094	0.51	0.15	0.428	0.04
P448226	**Grab**	**0**	**Transect 5**	East Pit	**68**	**56**	**391**	**497293.69**	**5178826.413**	**393.624**	**22-Aug-14**	0.802	0.15	33.5	1.48	31.2	2.81	35
P448227	**Grab**	**-0.1**	**Transect 5**	East Pit	**68**	**56**	**391**	**497293.69**	**5178826.413**	**392.428**	**22-Aug-14**	0.217	<0.005	0.462	0.26	0.137	0.399	0.11
P448228	Grab	-0.2	Transect 5	East Pit			391				22-Aug-14	<0.001	<0.005	0.01	0.1	0.01845	0.00658	0.04
P448229	Grab	-0.3	Transect 5	East Pit			391				22-Aug-14	0.302	<0.005	1.01	0.26	0.156	0.471	0.1
P448230	Grab	-0.4	Transect 5	East Pit			391				22-Aug-14	1.095	<0.005	2.5	1.8	0.497	0.245	0.46
P448231	Grab	-0.5	Transect 5	East Pit			391				22-Aug-14	0.077	<0.005	0.188	0.17	0.167	0.352	0.17
P448232	Grab	-0.6	Transect 5	East Pit			391				22-Aug-14	0.014	<0.005	0.036	0.39	0.0621	0.1495	0.07
P448233	Grab	-0.8	Transect 5	East Pit			391				22-Aug-14	0.155	<0.005	0.883	2.3	0.219	0.0221	0.23
P448234	Grab	-0.9	Transect 5	East Pit			391				22-Aug-14	0.175	0.022	1.24	4.72	0.212	0.0211	0.23
P448235	Grab	-1	Transect 5	East Pit			391				22-Aug-14	0.097	0.013	0.188	0.92	0.153	0.109	0.15
P448236	Grab	-1.1	Transect 5	East Pit			391				22-Aug-14	0.006	<0.005	0.023	0.85	0.0454	0.0154	0.06
P448237	Grab	-1.2	Transect 5	East Pit			391				22-Aug-14	0.052	0.289	0.266	1.25	0.0793	0.0117	0.19
P448238	Grab	-1.3	Transect 5	East Pit			391				22-Aug-14	<0.001	<0.005	0.002	0.14	0.0388	0.00602	0.11
P448239	*Standard*		Transect 5	East Pit								0.175	0.327	0.373	2.01	0.343	0.295	1.5
P448240	*Blank*		Transect 5	East Pit								<0.001	<0.005	0.001	0.01	0.00089	0.00036	<0.01
R232565	Channel	5	Transect 6	West Pit			385				20-Oct-14	0.002	<0.005	0.003	0.04	0.00183	0.00238	0.02

Sample #	Sample Type	Distance	Vn Set	Pit	Strike	Dip	Bench	Easting	Northing	Elevation	Date	Au ppm	Pt ppm	Pd ppm	Ag ppm	Cu %	Ni %	S %
R232566	Channel	3	Transect 6	West Pit			385				20-Oct-14	<0.001	<0.005	0.001	0.04	0.00061	0.00125	0.02
R232567	Channel	1	Transect 6	West Pit			385				20-Oct-14	<0.001	<0.005	0.001	0.05	0.00074	0.00085	0.01
R232568	**Channel**	**0**	Transect 6	West Pit			**385**				**20-Oct-14**	**<0.001**	**<0.005**	**0.001**	**0.05**	**0.00059**	**0.00097**	**0.01**
R232569	Channel	0.1	Transect 6	West Pit			385				20-Oct-14	<0.001	<0.005	0.001	0.08	0.00054	0.00048	0.01
R232570	Channel	0.2	Transect 6	West Pit			385				20-Oct-14	<0.001	<0.005	0.002	0.44	0.00101	0.00036	<0.01
R232571	Channel	0.3	Transect 6	West Pit			385				20-Oct-14	<0.001	<0.005	0.001	0.08	0.00354	0.00084	0.02
R232572	Channel	0.5	Transect 6	West Pit			385				20-Oct-14	<0.001	<0.005	0.002	0.08	0.00188	0.00103	0.01
R232573	Channel	0.8	Transect 6	West Pit			385				20-Oct-14	0.001	<0.005	0.001	0.08	0.00226	0.00231	0.01
R232574	Channel	1.5	Transect 6	West Pit			385				20-Oct-14	<0.001	<0.005	0.001	0.06	0.00278	0.00256	0.01
R232575	Channel	1.1	Transect 6	West Pit			385				20-Oct-14	<0.001	<0.005	0.001	0.12	0.00377	0.00571	0.03
R232576	Grab	-0.4	Transect 6	West Pit			385				20-Oct-14	0.18	0.501	0.528	1.19	0.122	0.0374	0.09
R232577	Grab	-0.5	Transect 6	West Pit			385				20-Oct-14	0.244	0.798	1.145	1.6	0.0636	0.0203	0.05
R232578	Grab	-0.6	Transect 6	West Pit			385				20-Oct-14	0.346	1.04	1.05	2.09	0.597	0.0202	0.56
R232579	Grab	-0.7	Transect 6	West Pit			385				20-Oct-14	0.001	<0.005	0.007	1.85	0.00287	0.00173	<0.01
R232580	Grab	-0.8	Transect 6	West Pit			385				20-Oct-14	0.002	0.024	0.027	0.62	0.00481	0.01325	0.01
R232581	*Standard*		Transect 6	West Pit							*20-Oct-14*	0.176	0.289	0.366	2.11	0.352	0.3	1.54
R232582	*Blank*		Transect 6	West Pit							*20-Oct-14*	<0.001	<0.005	0.001	0.02	0.00078	0.0007	<0.01
R232596	Channel	0.6	Transect 7	West Pit			382				12-Nov-14	0.876	0.012	0.104	0.33	0.0106	0.0208	0.01
R232597	Channel	0.5	Transect 7	West Pit			382				12-Nov-14	0.018	0.059	0.082	0.25	0.0216	0.079	0.05
R232598	Channel	0.4	Transect 7	West Pit			382				12-Nov-14	0.014	0.146	0.064	0.12	0.0137	0.0873	0.01
R232599	Channel	0.3	Transect 7	West Pit			382				12-Nov-14	0.015	<0.005	0.022	0.08	0.00923	0.101	<0.01
R232600	Channel	0.2	Transect 7	West Pit			382				12-Nov-14	0.065	0.011	0.075	0.17	0.128	0.149	0.13
R232601	**Channel**	**0**	**Transect 7**	**West Pit**	**320**	**30**	**382**	**497273.404**	**5178829.915**	**0**	**12-Nov-14**	**0.341**	**0.894**	**2.87**	**0.45**	**0.58**	**0.168**	**0.59**
R232602	Channel	-0.1	Transect 7	West Pit			382				12-Nov-14	0.765	1.53	1.775	0.49	0.232	0.13	0.24
R232760	Channel	1.8	Transect 8	West Pit			358				23-Jul-15	0.012	<0.005	0.012	0.37	0.918	0.292	0.58
R232761	Channel	1.7	Transect 8	West Pit			358				23-Jul-15	0.056	<0.005	0.009	0.56	0.486	0.0978	0.47
R232762	Channel	1.6	Transect 8	West Pit			358				23-Jul-15	0.031	<0.005	0.002	1.12	0.234	0.01565	0.24
R232763	Channel	1.5	Transect 8	West Pit			358				23-Jul-15	0.047	<0.005	0.002	2.37	0.342	0.01175	0.35
R232764	Channel	1.4	Transect 8	West Pit			358				23-Jul-15	0.302	<0.005	0.004	1.46	1.025	0.0241	0.98
R232765	Channel	1.3	Transect 8	West Pit			358				23-Jul-15	0.001	<0.005	0.001	0.33	0.0211	0.00854	0.14
R232766	Channel	1.2	Transect 8	West Pit			358				23-Jul-15	0.062	<0.005	0.003	0.38	0.154	0.00972	0.27
R232767	Channel	1.1	Transect 8	West Pit			358				23-Jul-15	0.021	<0.005	0.004	0.4	0.136	0.00875	0.18
R232768	Channel	1	Transect 8	West Pit			358				23-Jul-15	0.017	<0.005	0.029	0.23	0.127	0.246	0.14
R232769	Channel	0.9	Transect 8	West Pit			358				23-Jul-15	0.002	<0.005	0.009	0.32	0.01965	0.00846	0.03
R232770	Channel	0.8	Transect 8	West Pit			358				23-Jul-15	0.002	0.006	0.03	0.41	0.01995	0.00249	0.06
R232771	Channel	0.7	Transect 8	West Pit			358				23-Jul-15	<0.001	<0.005	0.013	0.14	0.0158	0.00502	0.14
R232772	Channel	0.6	Transect 8	West Pit			358				23-Jul-15	<0.001	<0.005	0.001	0.33	0.00893	0.00354	0.21
R232773	Channel	0.5	Transect 8	West Pit			358				23-Jul-15	<0.001	<0.005	0.001	0.37	0.0064	0.00349	0.12
R232774	Channel	0.4	Transect 8	West Pit			358				23-Jul-15	<0.001	<0.005	0.001	0.29	0.00888	0.0333	0.04
R232775	Channel	0.3	Transect 8	West Pit			358				23-Jul-15	<0.001	<0.005	0.004	0.14	0.00829	0.00473	0.01
R232776	Channel	0.2	Transect 8	West Pit			358				23-Jul-15	<0.001	<0.005	0.007	0.17	0.01845	0.0907	0.03
R232777	Channel	0.1	Transect 8	West Pit			358				23-Jul-15	1.01	0.006	0.245	0.38	0.01305	0.331	0.02
R232778	**Channel**	**0**	Transect 8	West Pit	**294**	**76**	**358**	**497222.7719**	**5178791.814**	**360.8485**	**23-Jul-15**	**1**	**84.8**	**57.5**	**17.9**	**32.3**	**0.0257**	**35.3**
R232779	**Channel**	**-0.1**	Transect 8	West Pit	**294**	**76**	**358**	**497222.8173**	**5178791.723**	**342.8061**	**23-Jul-15**	**1.11**	**24.7**	**40.8**	**57.9**	**33.1**	**0.017**	**33.3**
R232780	Channel	-0.2	Transect 8	West Pit			358				23-Jul-15	1.005	0.126	3.74	0.95	0.523	0.322	0.56
R232781	Channel	-0.3	Transect 8	West Pit			358				23-Jul-15	0.003	0.051	0.045	0.64	0.0432	0.024	0.06

Sample#	Sample Type	Distance	Vn Set	Pit	Strike	Dip	Bench	Easting	Northing	Elevation	Date	Auppm	Ptppm	Pdppm	Agppm	Cu%	Ni%	S%
R232782	Channel	-0.4	Transect 8	West Pit			358				23-Jul-15	0.001	0.021	0.014	0.27	0.00881	0.00462	0.09
R232783	Channel	-0.5	Transect 8	West Pit			358				23-Jul-15	0.001	0.008	0.003	0.14	0.00628	0.00086	0.08
R232784	Channel	-0.6	Transect 8	West Pit			358				23-Jul-15	<0.001	0.011	0.001	0.17	0.00512	0.00056	0.07
R232785	Channel	-0.7	Transect 8	West Pit			358				23-Jul-15	0.001	<0.005	0.001	0.17	0.00666	0.00087	0.11
R232786	Channel	-0.8	Transect 8	West Pit			358				23-Jul-15	0.005	0.018	0.051	0.35	0.0458	0.00102	0.11
R232787	Channel	-0.9	Transect 8	West Pit			358				23-Jul-15	0.004	0.011	0.003	0.35	0.0329	0.00394	0.18
R232788	Channel	-1	Transect 8	West Pit			358				23-Jul-15	0.03	<0.005	0.007	0.8	0.281	0.0131	0.3
R232789	Channel	-1.1	Transect 8	West Pit			358				23-Jul-15	0.005	<0.005	0.001	0.27	0.0461	0.01505	0.38
R232790	Channel	-1.2	Transect 8	West Pit			358				23-Jul-15	0.001	<0.005	0.004	0.24	0.00619	0.00421	0.16
R232791	Channel	-1.3	Transect 8	West Pit			358				23-Jul-15	0.002	<0.005	0.002	1.42	0.00469	0.00376	0.11
R232792	Channel	-1.4	Transect 8	West Pit			358				23-Jul-15	0.001	<0.005	<0.001	0.25	0.00705	0.014	0.22
R232793	Channel	-1.5	Transect 8	West Pit			358				23-Jul-15	0.001	<0.005	0.001	0.13	0.0078	0.0177	0.23
R232794	Channel	-1.6	Transect 8	West Pit			358				23-Jul-15	0.001	<0.005	<0.001	0.13	0.00784	0.00583	0.25
R232795	Channel	-1.7	Transect 8	West Pit			358				23-Jul-15	<0.001	<0.005	0.001	0.17	0.00803	0.00479	0.25
R232796	Channel	-1.8	Transect 8	West Pit			358				23-Jul-15	0.001	<0.005	<0.001	0.19	0.00736	0.00227	0.26
R232797	Channel	-1.9	Transect 8	West Pit			358				23-Jul-15	0.001	<0.005	<0.001	0.24	0.00456	0.00098	0.14
R232798	Channel	-2	Transect 8	West Pit			358				23-Jul-15	0.001	<0.005	<0.001	0.21	0.00493	0.00105	0.17
R232799	*Standard*		Transect 8	West Pit								0.182	0.313	0.363	2.09	0.346	0.308	1.63
R232800	*Blank*		Transect 8	West Pit								<0.001	<0.005	<0.001	0.01	0.0005	0.00029	<0.01
R232651	Channel	-1.6	Transect 9	East Pit			376				30-Dec-14	0.006	<0.005	0.011	0.23	0.114	0.0237	0.12
R232652	Channel	-1.5	Transect 9	East Pit			376				30-Dec-14	0.054	<0.005	0.083	1.67	0.222	0.0195	0.27
R232653	Channel	-1.4	Transect 9	East Pit			376				30-Dec-14	0.02	0.005	0.085	0.58	0.131	0.0299	0.16
R232654	Channel	-1.3	Transect 9	East Pit			376				30-Dec-14	0.119	0.005	0.963	0.83	0.4	0.0265	0.42
R232655	Channel	-1.2	Transect 9	East Pit			376				30-Dec-14	0.365	0.005	3.74	1.66	0.219	0.0196	0.24
R232656	Channel	-1.1	Transect 9	East Pit			376				30-Dec-14	0.012	<0.005	0.032	0.44	0.244	0.0179	0.27
R232657	Channel	-0.6	Transect 9	East Pit			376				30-Dec-14	0.032	<0.005	0.029	1.33	0.168	0.00959	0.19
R232658	Channel	-0.5	Transect 9	East Pit			376				30-Dec-14	0.072	0.006	0.24	0.77	0.276	0.0216	0.31
R232659	Channel	-0.4	Transect 9	East Pit			376				30-Dec-14	0.082	0.3	0.357	0.63	0.251	0.0297	0.27
R232660	Channel	-0.3	Transect 9	East Pit			376				30-Dec-14	0.098	0.437	0.561	0.37	0.558	0.0576	0.58
R232661	Channel	-0.2	Transect 9	East Pit			376				30-Dec-14	3.81	2.35	8.35	10.2	0.713	0.1075	0.76
R232662	Channel	-0.1	Transect 9	East Pit			376				30-Dec-14	0.434	0.462	0.99	1.46	0.1825	0.1115	0.19
R232663	**Channel**	**0**	Transect 9	**East Pit**	**165**	**80**	**376**	**497256.5785**	**5178827.918**	**379.169**	**30-Dec-14**	**3.21**	**2.74**	**12.15**	**10.4**	**9.48**	**0.113**	**10.2**
R232664	Channel	0.1	Transect 9	East Pit			376				30-Dec-14	0.295	0.419	1.965	1.34	0.286	0.0831	0.31
R232665	Channel	0.2	Transect 9	East Pit			376				30-Dec-14	0.042	0.005	0.117	0.41	0.0856	0.0644	0.11
R232666	Channel	0.3	Transect 9	East Pit			376				30-Dec-14	0.253	0.447	0.858	3.28	0.29	0.0334	0.37
R232667	Channel	0.4	Transect 9	East Pit			376				30-Dec-14	1.205	2.5	3.66	3	0.588	0.0793	0.66
R232668	Channel	0.5	Transect 9	East Pit			376				30-Dec-14	2.22	0.031	2.06	3.01	0.285	0.0293	0.33
R232669	*Standard*		*Transect 9*	*East Pit*							*30-Dec-14*	*0.174*	*0.31*	*0.362*	*2.05*	*0.333*	*0.293*	*1.55*
R232670	*Blank*		*Transect 9*	*East Pit*							*30-Dec-14*	*0.005*	*<0.005*	*0.013*	*0.03*	*0.00327*	*0.0011*	*0.01*
R232671		0.6	Transect 9	East Pit			376				30-Dec-14	0.046	0.036	0.242	0.5	0.247	0.0394	0.26
R232672		0.7	Transect 9	East Pit			376				30-Dec-14	0.151	0.716	0.61	1.52	0.167	0.0168	0.21
R232673		0.8	Transect 9	East Pit			376				30-Dec-14	0.192	<0.005	0.011	0.35	0.14	0.0226	0.16
R232674		0.9	Transect 9	East Pit			376				30-Dec-14	0.206	0.006	0.019	0.46	0.271	0.0239	0.29
R232713		-1.7	Transect 10	West Pit			364				29-May-15	0.035	<0.005	0.009	1.1	0.151	0.014	0.22
R232714		-1.6	Transect 10	West Pit			364				29-May-15	0.085	0.005	0.072	0.45	1.395	0.178	1.4
R232715		-1.5	Transect 10	West Pit			364				29-May-15	0.047	<0.005	0.061	0.49	0.677	0.0572	0.73

Sample #	Sample Type	Distance	Vn Set	Pit	Strike	Dip	Bench	Easting	Northing	Elevation	Date	Au ppm	Pt ppm	Pd ppm	Ag ppm	Cu %	Ni %	S %
R232716		-1.4	Transect 10	West Pit			364				29-May-15	0.118	<0.005	0.03	0.56	0.798	0.0488	0.87
R232717		-1.3	Transect 10	West Pit			364				29-May-15	0.516	<0.005	0.059	0.57	0.771	0.0709	0.82
R232718		-1.2	Transect 10	West Pit			364				29-May-15	0.301	<0.005	0.145	1.16	1.3	0.058	1.41
R232719		-1.1	Transect 10	West Pit			364				29-May-15	5.59	0.059	2.96	5.92	0.635	0.0444	0.69
R232721		-0.9	Transect 10	West Pit			364				29-May-15	0.644	3.53	5.52	1.1	1.27	0.362	1.26
R232722		-0.8	Transect 10	West Pit			364				29-May-15	1.15	2.99	5.31	4.26	0.882	0.248	0.89
R232723		-0.7	Transect 10	West Pit			364				29-May-15	0.156	0.045	0.448	1.05	0.632	0.1995	0.64
R232724		-0.6	Transect 10	West Pit			364				29-May-15	0.282	0.033	0.182	1.55	1.455	0.115	1.65
R232725		-0.5	Transect 10	West Pit			364				29-May-15	0.239	0.04	0.198	1.61	1.615	0.1115	1.7
R232726		**-0.4**	Transect 10	**West Pit**	**184**	**74**	**364**				**29-May-15**	**0.113**	**<0.005**	**0.031**	**0.99**	**1.54**	**0.139**	**1.57**
R232727		**-0.3**	Transect 10	**West Pit**	**184**	**74**	**364**				**29-May-15**	**0.113**	**<0.005**	**0.008**	**0.74**	**1.37**	**0.1215**	**1.4**
R232728		**-0.2**	Transect 10	**West Pit**	**184**	**74**	**364**				**29-May-15**	**0.187**	**0.033**	**0.111**	**0.81**	**1.165**	**0.123**	**1.2**
R232729		-0.1	Transect 10	West Pit			364				29-May-15	0.236	0.019	0.123	1.08	0.963	0.0798	1.01
R232730		**0**	Transect 10	**West Pit**	**184**	**74**	**364**	**497244.635**	**5178816.138**	**367.147**	**29-May-15**	**0.521**	**50.7**	**22.7**	**21.3**	**16**	**0.0697**	**16.9**
R232732		**0.2**	Transect 10	**West Pit**	**184**	**74**	**364**				**29-May-15**	**6.4**	**90.4**	**31.8**	**7.26**	**3.89**	**0.703**	**4.1**
R232733		0.3	Transect 10	West Pit			364				29-May-15	0.168	0.103	0.199	1.74	0.94	0.0868	1.06
R232734	*Standard*		*Transect 10*	*West Pit*			*364*				*29-May-15*	*0.17*	*0.32*	*0.357*	*2.05*	*0.345*	*0.298*	*1.56*
R232735	*Blank*		*Transect 10*	*West Pit*			*364*				*29-May-15*	*0.01*	*0.099*	*0.065*	*0.02*	*0.01075*	*0.00227*	*0.02*
R232737		0.4	Transect 10	West Pit			364				29-May-15	0.163	0.262	0.432	1.25	0.993	0.0925	1.09
R232738		0.5	Transect 10	West Pit			364				29-May-15	0.173	0.017	0.434	1.13	0.896	0.119	0.97
R232739		0.6	Transect 10	West Pit			364				29-May-15	0.854	0.754	2.96	3.83	1.22	0.0976	1.3
R232740		0.7	Transect 10	West Pit			364				29-May-15	0.051	0.025	0.079	1.86	0.262	0.029	0.3
R232741		0.8	Transect 10	West Pit			364				29-May-15	0.322	1.05	1.48	2.35	0.575	0.0579	0.57
R232742		0.9	Transect 10	West Pit			364				29-May-15	0.097	0.162	0.314	1.23	0.795	0.1395	0.81
R232743		1	Transect 10	West Pit			364				29-May-15	0.166	0.121	0.592	1.66	1.52	0.157	1.61
R232744		1.1	Transect 10	West Pit			364				29-May-15	0.181	0.382	0.863	4.01	0.877	0.0774	0.99
R232745		1.2	Transect 10	West Pit			364				29-May-15	0.442	1.975	2.41	2.72	2.17	0.1635	1.99
R232746		1.3	Transect 10	West Pit			364				29-May-15	0.177	0.009	0.502	1.44	1.475	0.0958	1.5

Distance Plots Showing All Samples

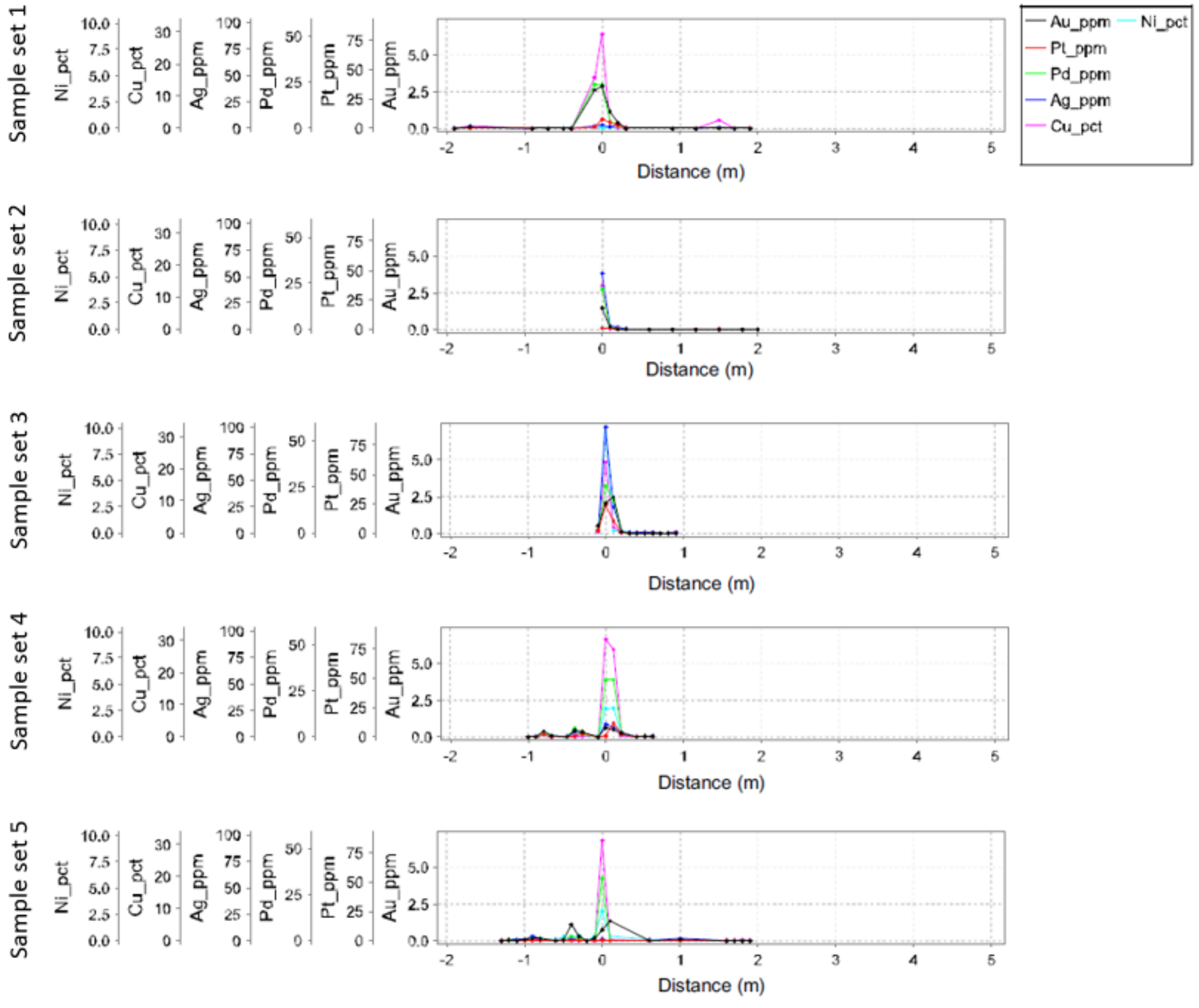

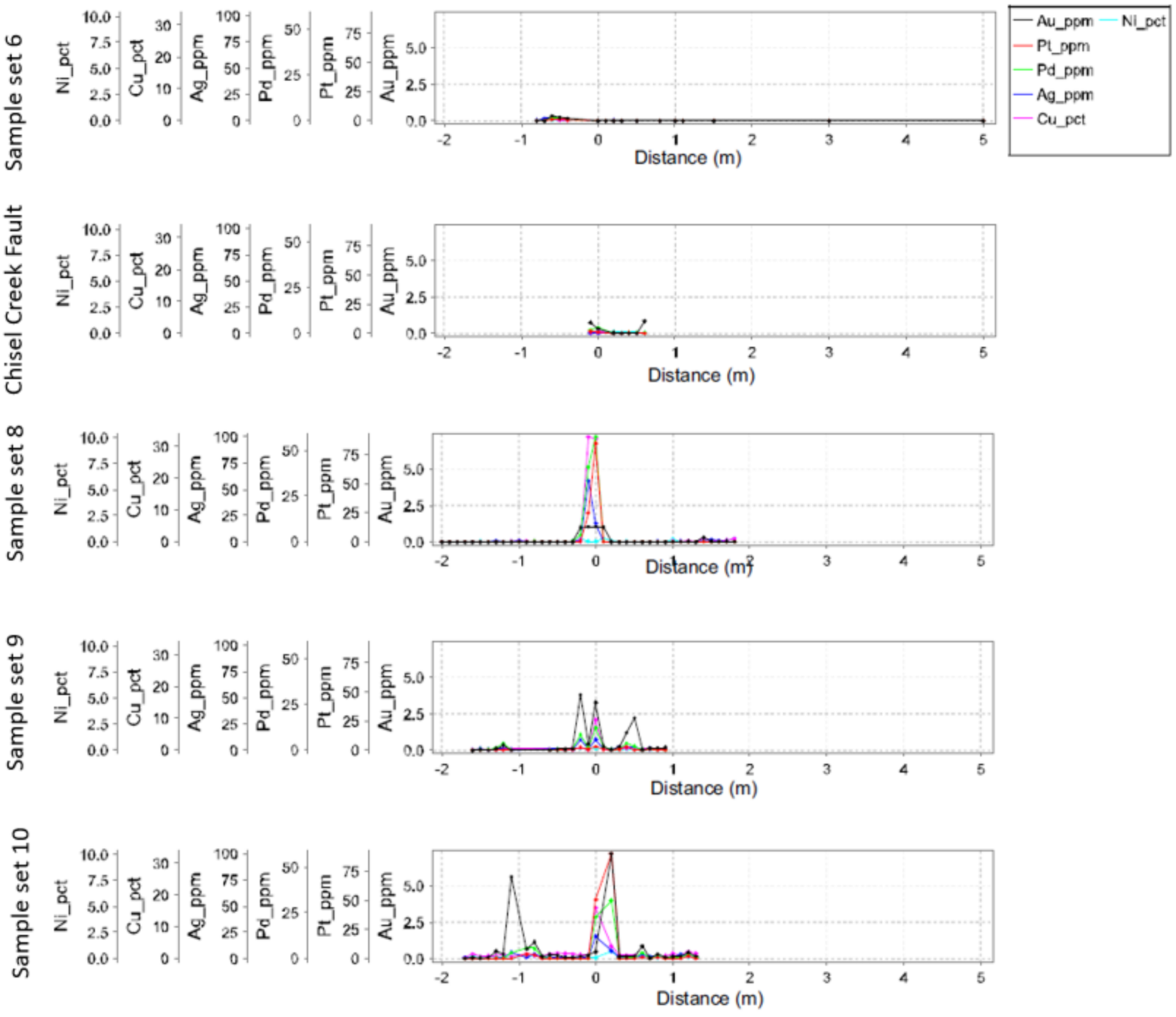
Sample set 6
Chisel Creek Fault
Sample set 8
Sample set 9
Sample set 10
Ni_pct
Cu_pct
Ag_ppm
Pd_ppm
Pt_ppm
Au_ppm
Distance (m)
Au_ppm
Ni_pct
Pt_ppm
Pd_ppm
Ag_ppm
Cu_pct

Distance Plots Showing All Samples with Massive Sulfides Rem

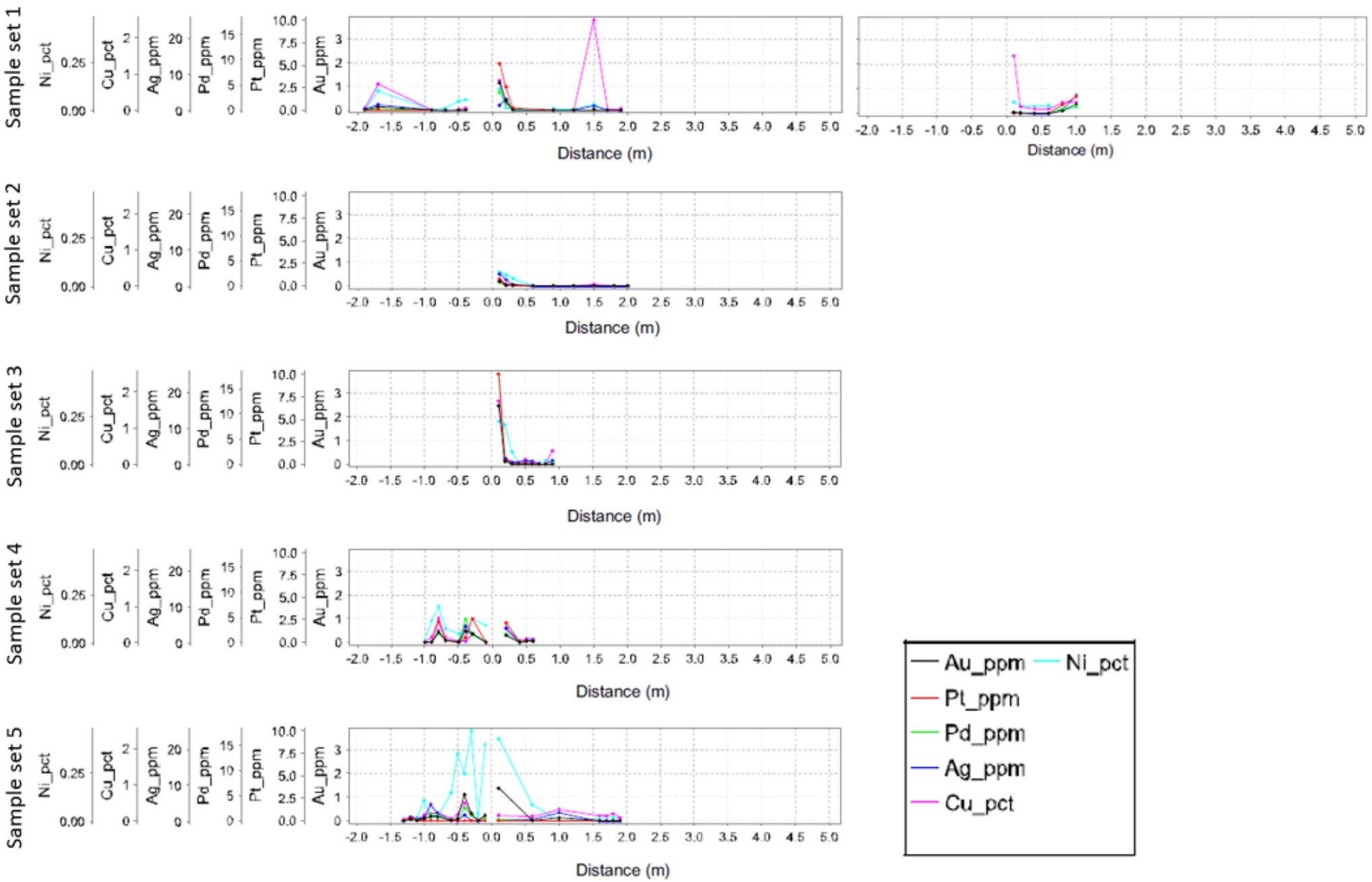

Chisel Creek Fault Sample set 6

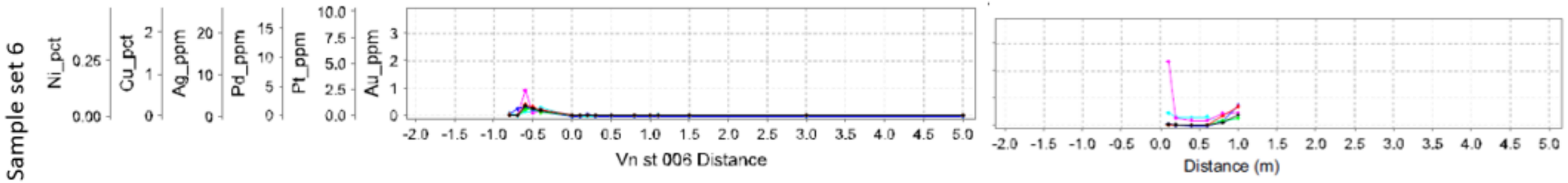

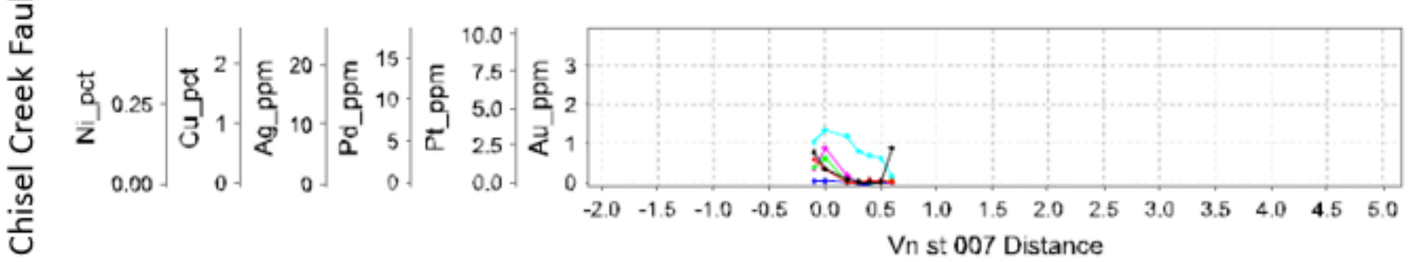

Sample set 8

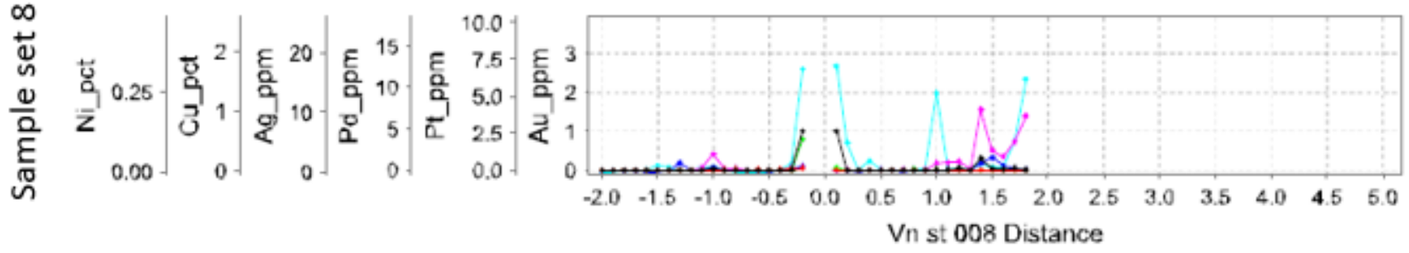

Sample set 9

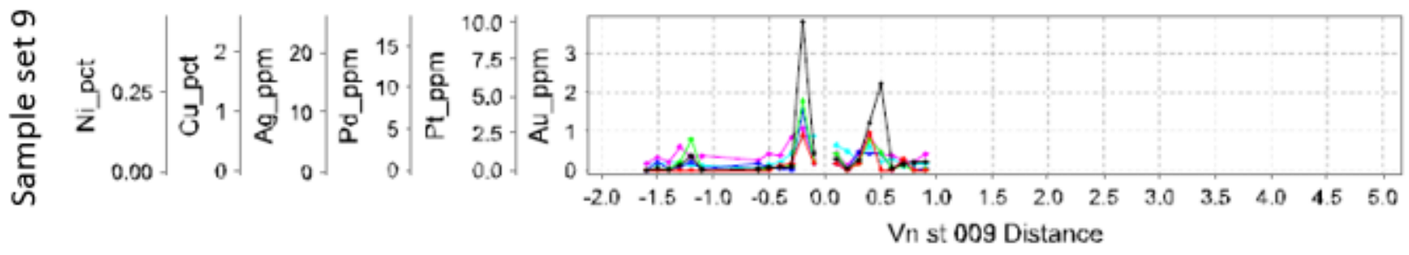

Sample set 10

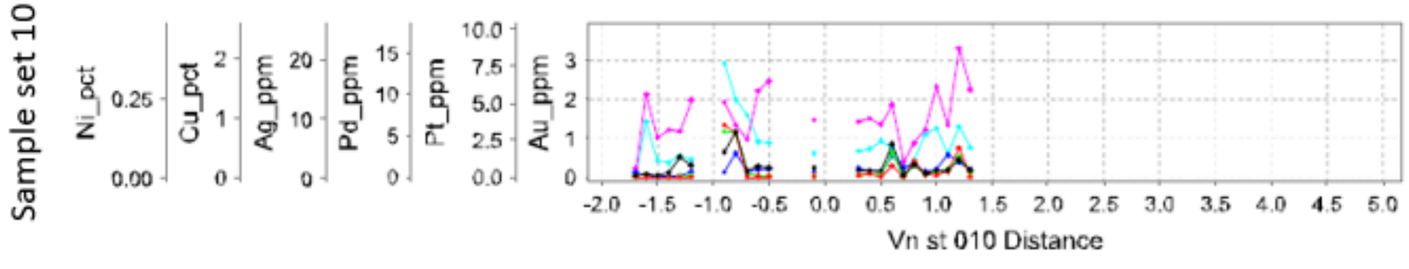

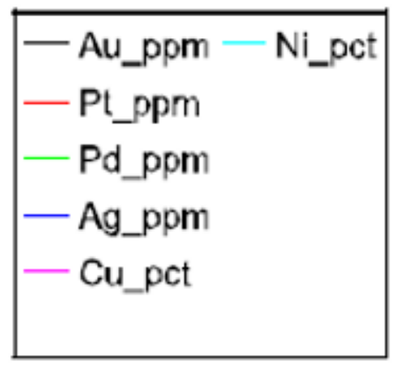

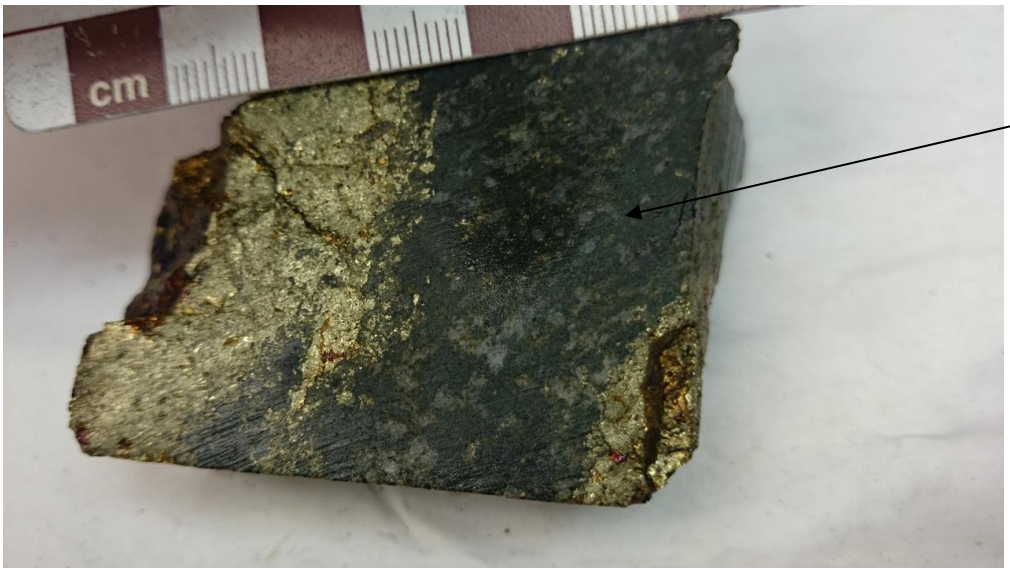

Transect 1: Sample P448252 taken from the vein's footwall. Displays strong chloritization within mafic gneiss

Transect 2: Sample R232707 showing irregular, wispy chalcopyrite stringers between two sulfide veins

Transect 3: Sample R232755 of mineralization along a 220 trending sulfide vein. Note the disseminated sulfides within the chloritized matrix

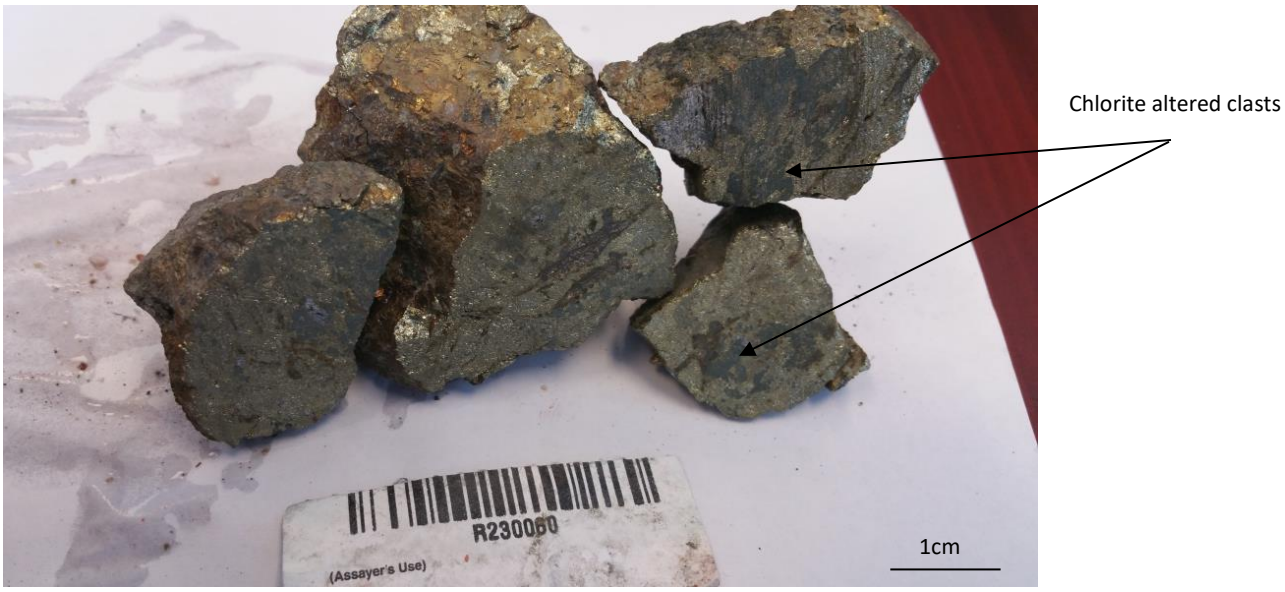

Transect 4: Sample R230060 of massive chalcopyrite. Note how chlorite replaces clasts within the sulfide

Transect 5: Sample P448226 of semi-massive sulfide bounding a core of highly altered Sudbury breccia

Transect 6: Sample R232578 of finely disseminated chalcopyrite along quartz intergrowth planes with potassium feldspar.

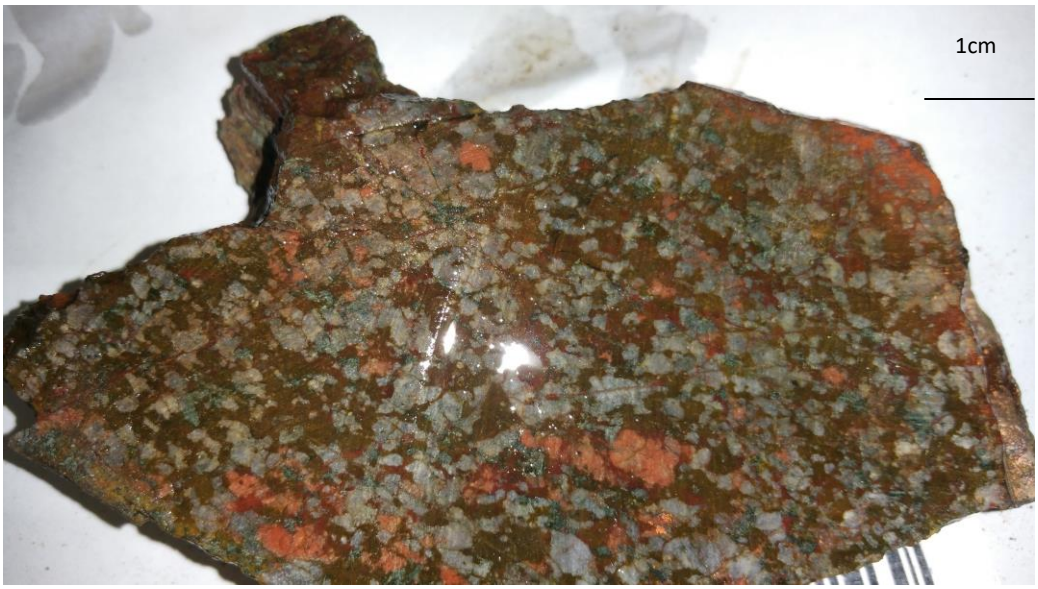

Transect 7: Sample R232599 of highly altered host rock. Taken from above the damage zone of the Chisel Creek Fault

Vein set 08: Sample R232778 of massive sulfide.

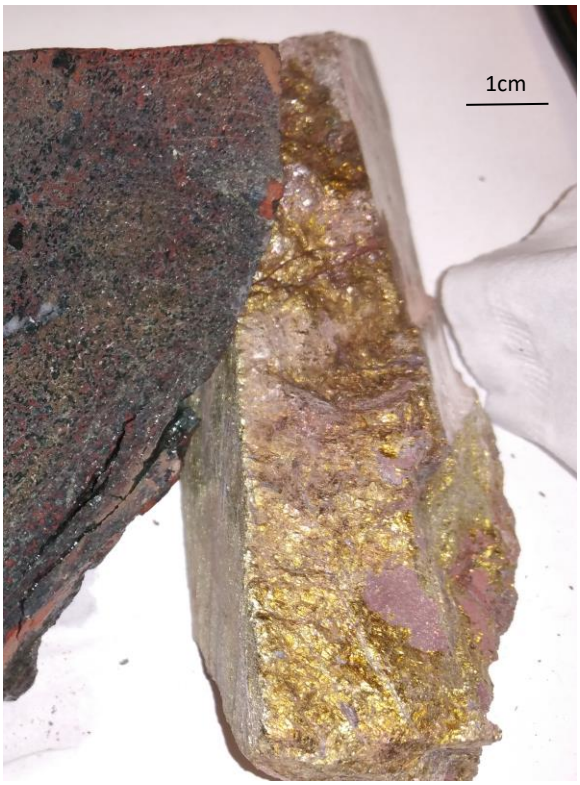

Transect 9: Sample R232663 showing the mix of massive chalcopyrite and altered country rock

Transect 10: Sample R232732 of semi-massive sulfide cutting thermally altered pegmatitic granite

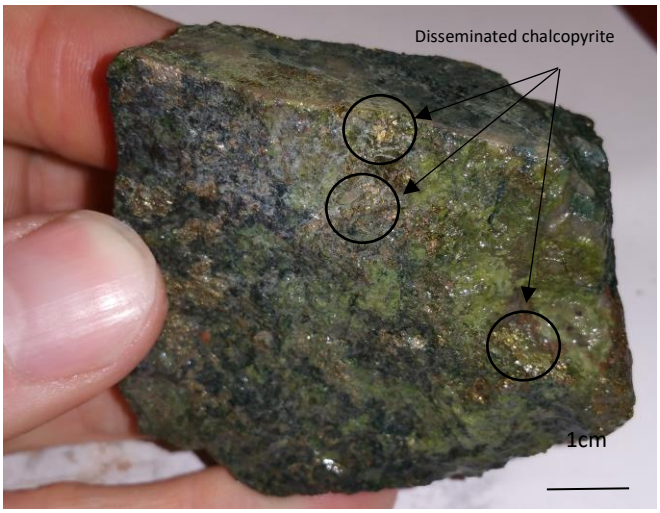

Low sulfide: Sample R232643 showing disseminated chalcopyrite within chlorite overprinting epidote

Appendix F – Emplacement Model for Mineralization and Paragenetic Diagram for Broken Hammer

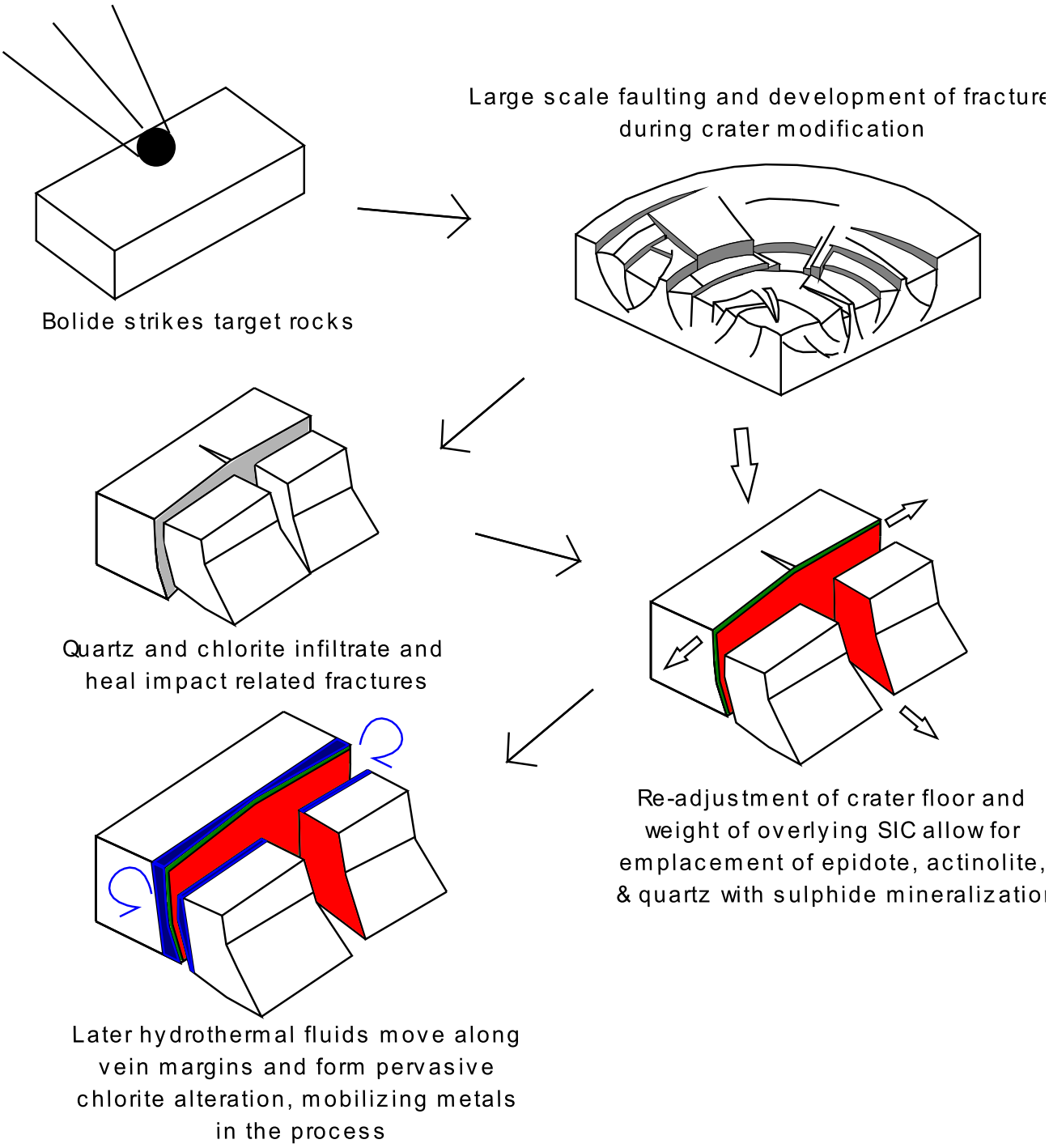

Idealized schematic outlining fracture formation during impact processes, emplacement of quartz and chlorite, reactivation of fractures and emplacement of epidote-actinolite-quartz and sulphide mineralization, with final hydrothermal overprint resulting in pervasive chlorite formation

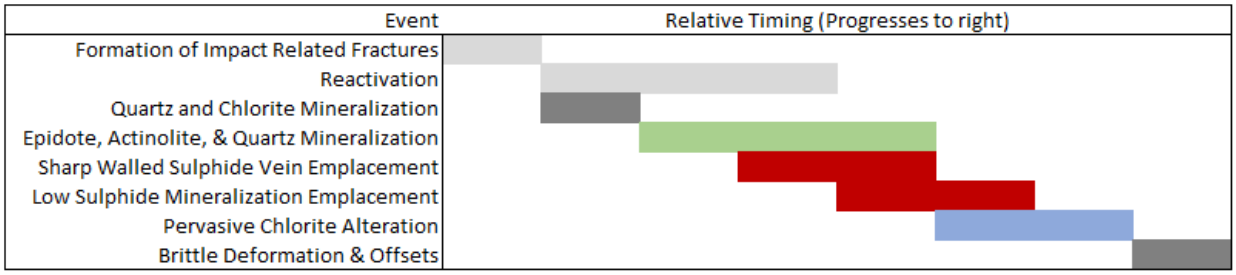

Paragenetic sequence outlining the relative age of events as evidenced at Broken Hammer